



Michigan Technological University
Create the Future Digital Commons @ Michigan Tech

Dissertations, Master's Theses and Master's
Reports - Open

Dissertations, Master's Theses and Master's
Reports

2013

ACETYL RADICAL IN TOBACCO SMOKE: DETECTION, QUANTIFICATION AND SIMULATION

Na Hu

Michigan Technological University

Follow this and additional works at: <https://digitalcommons.mtu.edu/etds>


 Part of the [Chemistry Commons](#)

Copyright 2013 Na Hu

Recommended Citation

Hu, Na, "ACETYL RADICAL IN TOBACCO SMOKE: DETECTION, QUANTIFICATION AND SIMULATION",
Dissertation, Michigan Technological University, 2013.
<https://doi.org/10.37099/mtu.dc.etds/453>

Follow this and additional works at: <https://digitalcommons.mtu.edu/etds>

 Part of the [Chemistry Commons](#)

ACETYL RADICAL IN TOBACCO SMOKE: DETECTION,
QUANTIFICATION AND SIMULATION

By
NA HU

A DISSERTATION
Submitted in partial fulfillment of the requirements for the degree of
DOCTOR OF PHILOSOPHY
In Chemistry

MICHIGAN TECHNOLOGICAL UNIVERSITY
2013

This dissertation has been approved in partial fulfillment of the requirements for the Degree of DOCTOR OF PHILOSOPHY in Chemistry.

Department of Chemistry

Dissertation Advisor: *Dr. Sarah A. Green*

Committee Member: *Dr. Haiying Liu*

Committee Member: *Dr. Shiyue Fang*

Committee Member: *Dr. Shiliang Wu*

Department Chair: *Dr. Sarah A. Green*

Table of Contents

| | |
|---|-------------|
| List of Figures..... | v |
| List of Schemes..... | viii |
| List of Tables | x |
| Preface..... | xi |
| Acknowledgements | xii |
| Abstract..... | xiv |
| Chapter 1: Introduction | 1 |
| 1.1 Free Radicals..... | 1 |
| 1.1.1 Fundamental Chemistry | 1 |
| 1.1.2 Sources of Radicals in the Atmosphere | 5 |
| 1.1.3 Photochemical NO _x Cycling..... | 6 |
| 1.1.4 Scavengers and Fates | 7 |
| 1.2 Tobacco Composition and Chemistry..... | 8 |
| 1.2.1 Tobacco Types and Composition..... | 8 |
| 1.2.2 Tobacco Smoke Composition and Chemistry..... | 11 |
| 1.3 Significance of Free Radicals | 22 |
| 1.3.1 Atmospheric Chemistry | 22 |
| 1.3.2 Human Health Concern..... | 24 |
| 1.4 References..... | 26 |
| Chapter 2: Radical Trapping and Analysis Methods | 31 |
| 2.1 Previous Methods and Results | 31 |
| 2.1.1 Radicals Detection by Direct Electron Paramagnetic Resonance (EPR) from the Particulate Phase of Cigarette Smoke | 31 |
| 2.1.2 Radical Detection by EPR Spin Trapping Methods from Gas Phase Smoke | 33 |
| 2.1.3 Fluorescence Probes for Short-lived Radical Detection | 36 |
| 2.1.4 Nitroxide Spin Trapped Radicals Analysis by Mass Spectrometry | 40 |
| 2.2 Trapping and Analysis Methods in This Study..... | 41 |
| 2.3 References..... | 43 |
| Chapter 3: Structural Identifications of Gas Phase Tobacco Smoke Radicals by Mass Spectrometry..... | 45 |
| 3.1 Introduction..... | 46 |
| 3.1.1 Principles of Electrospray Ionization Mass Spectrometry | 46 |
| 3.1.2 Principles of Liquid Chromatography Mass Spectrometry | 48 |
| 3.1.3 The Application of Liquid Chromatography Mass Spectrometry in Identification of Radicals..... | 51 |
| 3.2 Experimental and Methods Development..... | 53 |
| 3.2.1 Sample Preparation | 53 |
| 3.2.2 Instrumentation | 57 |

| | |
|---|-----|
| 3.3 Results..... | 58 |
| 3.3.1 3AP Standard Analysis | 58 |
| 3.3.2 Acetone Photolysis Standard Analysis | 60 |
| 3.3.3 Smoke Samples..... | 62 |
| 3.3.4 NO/air/CH ₃ CHO Model..... | 70 |
| 3.3.5 LC-MS Spectrum..... | 71 |
| 3.4 Discussion..... | 75 |
| 3.5 Conclusion | 77 |
| 3.6 References..... | 78 |
| Chapter 4: Comparisons and Quantitative analysis of acetyl radical in smoke, standard, and model samples by HPLC-FL | 79 |
| 4.1 Introduction..... | 80 |
| 4.2 Experimental Methods | 82 |
| 4.3 Results..... | 87 |
| 4.3.1 Marlboro Cigarette Smoke Sample with the Continuously Drawn Method | 87 |
| 4.3.2 Marlboro Cigarette Smoke Sample with the FTC Puff-based Method..... | 89 |
| 4.3.3 Marlboro Cigarette Smoke Sample with the FTC Puff-based Method with GF/F | 90 |
| 4.3.4 3R4F Cigarette Smoke Sample with Continuously Drawn Method..... | 91 |
| 4.3.5 3R4F Cigarette Smoke Sample with FTC Puff-based Method..... | 92 |
| 4.3.6 3R4F Cigarette Smoke Sample with FTC Puff-based Method with GF/F | 93 |
| 4.3.7 Model Mixture | 94 |
| 4.3.8 Acetone Photolysis Sample..... | 95 |
| 4.3.9 Fluorescence Calibration Curve..... | 96 |
| 4.4 Discussion | 97 |
| 4.5 Conclusion | 104 |
| 4.6 References..... | 105 |
| Chapter 5: Models and Computational Simulations on Acetyl Radical Generation in Cigarette smoke | 108 |
| 5.1 Introduction..... | 109 |
| 5.2 Experiment and Method..... | 112 |
| 5.2 Result | 115 |
| 5.3 Discussion..... | 117 |
| 5.3.1. Simplified NO-NO ₂ -CH ₃ CHO Mechanism Investigation by Matlab | 117 |
| 5.3.2. Atmospheric Chain Reactions Model Investigation by Master of Chemical Mechanisms | 123 |
| 5.3.3. Atmospheric Chain Reactions Model with Isoprene Addition Investigation by Master of Chemical Mechanisms..... | 138 |
| 5.4 Conclusion and Future Work..... | 147 |
| 5.5 References..... | 149 |
| Appendix..... | 153 |

List of Figures

Chapter 1

| | |
|---|----|
| Figure 1.1. Research cigarettes manufactured by Reference Cigarette Program, College of Agriculture from Kentucky University. | 10 |
| Figure 1.2. Chemical and physical processes in burning cigarette. | 13 |
| Figure 1.3. The configuration of Cambridge filter and holder. | 18 |
| Figure 1.4. A model of general processes occurring during condensation of mainstream smoke precursor vapor leaving the burning zone..... | 19 |

Chapter 2

| | |
|---|----|
| Figure 2.1. Analysis flow diagram for the radicals in mainstream smoke.. | 42 |
|---|----|

Chapter 3

| | |
|---|----|
| Figure 3.1. Schematic of the electrospray ionization process..... | 47 |
| Figure 3.2. The LC-MS components. | 49 |
| Figure 3.3. Apparatus used to trap carbon-centered radicals from the burning cigarette..... | 54 |
| Figure 3.4. Diagram of gas mixture model reaction apparatus..... | 56 |
| Figure 3.5. The full mass spectrum for 3AP solution in 50/50 MeOH/H ₂ O with <i>m/z</i> range of 50-200 acquired in profile mode..... | 59 |
| Figure 3.6. The full mass spectrum for the acetone photolysis standard sample with <i>m/z</i> range of 50-500 acquired in profile mode..... | 60 |
| Figure 3.7. ESI-MS spectrum of R-3AP-NDA adduct of the acetone photolysis sample with <i>m/z</i> range of 300-380. | 61 |
| Figure 3.8. ESI-MS full spectrum of smoke sample from Marlboro continuous drawn method with <i>m/z</i> range of 50-300. | 63 |
| Figure 3.9. ESI-MS analysis of nicotine with <i>m/z</i> range of 50-210 acquired in profile mode..... | 64 |
| Figure 3.10. ESI-MS/MS spectrum of R-3AP adduct of the Marlboro continuous drawn smoke sample with <i>m/z</i> range of 50-270..... | 65 |
| Figure 3.11. ESI-MS full spectrum of R-3AP-NDA adduct of the Marlboro continuous drawn smoke sample with <i>m/z</i> range of 100-600. | 66 |
| Figure 3.12. ESI-MS/MS spectrum of R-3AP-NDA adduct of the Marlboro continuous drawn smoke sample with <i>m/z</i> range of 200-400..... | 67 |
| Figure 3.13. ESI-MS/MS spectrum of R-3AP adducts of the 3R4F reference cigarette smoke sample under FTC smoking conditions with <i>m/z</i> range of 50-250..... | 68 |
| Figure 3.14. ESI-MS/MS spectrum of R-3AP-NDA adducts of the 3R4F reference cigarette smoke sample under FTC smoking conditions with <i>m/z</i> range of 100- 500..... | 69 |

| | |
|---|----|
| Figure 3.15. ESI-MS/MS spectrum of R-3AP-NDA adducts of NO/air/ CH ₃ CHO model with <i>m/z</i> range of 150-500. | 70 |
| Figure 3.16. 3D LC-MS for acetone irradiation standard. | 71 |
| Figure 3.17. (a) 3D LC-MS for smoke sample for <i>m/z</i> range [80-400] from 0 to 30 min. (b) 3D LC-MS for smoke sample for <i>m/z</i> range [170-230] from 2.0 to 6.0 min. | 72 |
| Figure 3.18. Representative LC-MS chromatograms selected ion monitoring (SIM) of 200.60-201.60 of 3AP adducts from fresh Marlboro cigarette smoke, gas phase model, and aqueous acetone photolysis sample. | 74 |

Chapter 4

| | |
|---|-----|
| Figure 4.1. Apparatus used to trap carbon-centered radicals from the burning cigarette. | 84 |
| Figure 4.2. Diagram of gas mixture model reaction apparatus. | 86 |
| Figure 4.3. Representative fluorescence chromatogram of the carbon-centered radical suite collected from Marlboro cigarette smoke sample with the continuous drawn method. | 88 |
| Figure 4.4. Representative fluorescence chromatogram of the carbon-centered radical suite collected from Marlboro cigarette smoke sample with FTC puff-based method. | 89 |
| Figure 4.5. Representative fluorescence chromatogram of the carbon-centered radical suite collected from Marlboro cigarette smoke sample with FTC puff-based method with GF/F. | 90 |
| Figure 4.6. Representative fluorescence chromatogram of the carbon-centered radical suite collected from 3R4F cigarette smoke sample with continuous drawn method. | 91 |
| Figure 4.7. Representative fluorescence chromatogram of the carbon-centered radical suite collected from 3R4F cigarette smoke sample with FTC puff-based method. | 92 |
| Figure 4.8. Representative fluorescence chromatogram of the carbon-centered radical suite collected from 3R4F cigarette smoke sample with FTC puff-based method with GF/F. | 93 |
| Figure 4.9. Representative fluorescence chromatogram of the carbon-centered radical suite collected from model mixture. | 94 |
| Figure 4.10. Representative fluorescence chromatogram of the carbon-centered radical suite collected from acetone photolysis standards. | 95 |
| Figure 4.11. CPA-NDA calibration curve. | 96 |
| Figure 4.12. Representative HPLC/FLD chromatograms of radicals trapped from fresh cigarette smokes, model gas mixture, and aqueous acetone photolysis sample. | 98 |
| Figure 4.13. Acetyl radical concentrations compared for different cigarettes types, smoking conditions and particle filter set up. | 102 |

Chapter 5

| | |
|---|-----|
| Figure 5.1. Diagram of gas mixture model reaction apparatus..... | 113 |
| Figure 5.2. Comparison of the representative chromatograms resulting from NO/air/CH ₃ CHO model and NO/air/CH ₃ CHO/isoprene model..... | 116 |
| Figure 5.3. Matlab computational simulation of generation of CH ₃ C(O)· from our experimental gas mixture..... | 120 |
| Figure 5.4. Matlab-based kinetic calculation of production of CH ₃ C(O)· from the 3R4F Kentucky Reference cigarette smoke based on literature reported initial concentrations of CH ₃ CHO and NO in the smoke..... | 122 |
| Figure 5.5. MCM simulation by NO/air/CH ₃ CHO model on the generation of CH ₃ C(O)-3AP from the 3R4F Kentucky Reference cigarette smoke at 25 s when $k_{3AP}[3AP]/k_{O_2}[O_2]$ equals to 10^{-8} | 130 |
| Figure 5.6. MCM simulation by NO/air/CH ₃ CHO model on the generation of CH ₃ C(O)-3AP from the 3R4F Kentucky Reference cigarette smoke at 25 s when $k_{3AP}[3AP]/k_{O_2}[O_2]$ equals to 10^{-4} | 131 |
| Figure 5.7. MCM simulation by NO/air/CH ₃ CHO model on the generation of CH ₃ C(O)-3AP from the 3R4F Kentucky Reference cigarette smoke at 25 s when $k_{3AP}[3AP]/k_{O_2}[O_2]$ equals to 100..... | 132 |
| Figure 5.8. MCM simulation by NO/air/CH ₃ CHO model on the generation of CH ₃ C(O)-3AP at different $k_{3AP}[3AP]/k_{O_2}[O_2]$ | 133 |
| Figure 5.9. MCM simulation by NO/air/CH ₃ CHO model on the generation of CH ₃ C(O)-3AP from the 3R4F Kentucky Reference cigarette smoke at 25 s at different $k_{3AP}[3AP]/k_{O_2}[O_2]$ ratios..... | 134 |
| Figure 5.10. Matlab-based kinetic calculation of the production of CH ₃ C(O)· from the 3R4F Kentucky Reference cigarette smoke based on literature reported initial concentrations of CH ₃ CHO and NO in the smoke..... | 136 |
| Figure 5.11. MCM simulation by NO/air/CH ₃ CHO model on the generation of CH ₃ C(O)-3AP from the 3R4F Kentucky Reference cigarette smoke at 250 s when $k_{3AP}[3AP]/k_{O_2}[O_2]$ equals to 10..... | 137 |
| Figure 5.12. MCM simulation by NO/air/CH ₃ CHO/isoprene model on the generation of CH ₃ C(O)-3AP from the 3R4F Kentucky Reference cigarette smoke at 250 s when $k_{3AP}[3AP]/k_{O_2}[O_2]$ equals to 10..... | 142 |
| Figure 5.13. MCM simulation by NO/air/CH ₃ CHO/isoprene model on the generation of CH ₃ C(O)-3AP from the 3R4F Kentucky Reference cigarette smoke at 25 s at different $k_{3AP}[3AP]/k_{O_2}[O_2]$ ratios..... | 143 |
| Figure 5.14. Comparison of the competitive effects of 3AP and O ₂ on acetyl radical trapping by NO/air/CH ₃ CHO and NO/air/CH ₃ CHO/isoprene models..... | 144 |

List of Schemes

Chapter 1

| | |
|--|----|
| Scheme 1.1. The Pathway of Radicals Damage to DNA..... | 4 |
| Scheme 1.2. Chain cycling reactions of radicals in the troposphere. | 7 |
| Scheme 1.3. Diprotonated, monoprotated and free base form nicotine at different pHs. | 15 |
| Scheme 1.4. Ozone generation in the stratosphere. | 22 |
| Scheme 1.5. Ozone depletion reactions by chloride radical resulted from photolysis chlorofluorocarbons. | 22 |
| Scheme 1.6. Photochemical air pollution formation in Los Angeles | 23 |

Chapter 2

| | |
|--|----|
| Scheme 2.1. The structure of PBN and carbon-centered and oxygen-center radicals trapping reactions..... | 34 |
| Scheme 2.2. The structures of nitroxides..... | 37 |
| Scheme 2.3. Fluorescence trap for free radicals detection..... | 37 |
| Scheme 2.4. Trapping of carbon-centered radical ($\cdot R$) by 3AP, followed by solution-phase derivatization with NDA to produce the fluorescent radical-adduct. | 39 |

Chapter 3

| | |
|---|----|
| Scheme 3.1. Acetyl radical and methyl radical are generated by acetone photolysis reaction..... | 54 |
| Scheme 3.2. 3AP oxidization reaction and adducts..... | 59 |

Chapter 4

| | |
|--|-----|
| Scheme 4.1. Trapping of carbon-centered radical ($\cdot R$) by 3AP, followed by solution-phase derivatization with NDA to produce the fluorescent radical-adduct. | 82 |
| Scheme 4.2. Acetyl radical and methyl radical are generated by acetone photolysis reaction..... | 84 |
| Scheme 4.3. 3AP oxidization reactions and adducts. | 99 |
| Scheme 4.4. The partition coefficient for CH_3 -3AP-NDA, CH_3CO -3AP-NDA, 3AP'-NDA and 3AP''-NDA..... | 100 |

Chapter 5

| | |
|---|-----|
| Scheme 5.1. Possible sources and sinks for NO_2 in cigarette smoke and other possible radicals generated by NO_x chemistry..... | 109 |
| Scheme 5.2. Acetaldehyde-based chain reactions of acetyl radical generation in tobacco smoke..... | 124 |

| | |
|--|-----|
| Scheme 5.3. The flowchart of acetyl radical cycling and sinks in gas phase. | 126 |
| Scheme 5.4. Isoprene chain reactions to generate HO ₂ radical in gas phase smoke. | 138 |

List of Tables

Chapter 1

| | |
|---|----|
| Table 1.1. Tobacco components and percentages..... | 9 |
| Table 1.2. Selected Organic compounds in different types of tobacco. | 10 |
| Table 1.3. Reference Cigarette composition and specifications. | 11 |
| Table 1.4. Approximate number and classes of compounds identified in fresh tobacco smoke. | 17 |
| Table 1.5. A summarized table of major constituents of the Particulate Matter in the mainstream smoke by Hoffmann et al. | 20 |

Chapter 3

| | |
|---|----|
| Table 3.1. Thermo Finnigan LCQTM Advantage LC-MS conditions | 58 |
| Table 3.2. Fragmentation pattern from different samples in ESI-MS spectrum..... | 75 |

Chapter 4

| | |
|---|-----|
| Table 4.1. Retention time of peaks from acetone photolysis standard, gas phase model and smoke samples | 97 |
| Table 4.2. Comparison of acetyl radical concentrations in different cigarettes types, smoking conditions and particle filter set up | 101 |

Chapter 5

| | |
|---|-----|
| Table 5.1. Mechanisms proposed by Pryor and coworkers for radical generation in gas phase smoke..... | 110 |
| Table 5.2. Several abundant compounds and their concentrations in gas phase cigarette smoke | 111 |
| Table 5.3. Compounds and initial concentrations for MCM simulation on 3AP sensitivity by NO/air/CH ₃ CHO model..... | 127 |
| Table 5.4. Reactions from mcm_subset for MCM simulation on 3AP sensitivity by NO/air/CH ₃ CHO model..... | 128 |
| Table 5.5. Compounds and initial concentrations for MCM simulation on 3AP sensitivity by NO/air/CH ₃ CHO/isoprene model..... | 139 |
| Table 5.6. Proposed reactions for acetyl radical generation in cigarette smoke by NO/air/CH ₃ CHO/isoprene model | 140 |

Preface

This dissertation is submitted for the degree of Doctor of Philosophy at Michigan Technological University. The research described in this dissertation was conducted by Na Hu under the supervision of Dr. Sarah A. Green in the Department of Chemistry at Michigan Technological University from September 2007 to June 2013.

The original research in this dissertation including experimental work and computational simulations was performed entirely by Na Hu. Neither this or similar works have been submitted for any other degree or diploma at any other university. Portions of Chapters 3, 4, and 5 in this dissertation will be submitted to peer-reviewed journals in 2013. The contribution of Na Hu includes all experimental work, computational simulations, data analysis, and manuscripts preparation. Na Hu and Dr. Sarah A. Green will be the only authors on the papers.

Acknowledgements

I found the acknowledgments to be the most difficult part of my dissertation to write, since I have so many people to thank. My PhD dissertation will not be completely finished until I properly recognize these great people.

First of all, I'd like to give special thanks to my advisor, Dr. Sarah A. Green, for her guidance, support, and love through the last six years. Not only has she been an incredible advisor in my research, but she has also been an influential mentor in my life. Every time I felt frustrated in my experiment and didn't really know if there was an answer, she was always able to show me a way forward. In addition to continuously inspiring me in pursuit of the truth in science, she has never been reluctant in offering me the strongest support in my career development. I am very grateful to her for supporting me to work in industry two times as an intern in California in 2011 and Wisconsin in 2012. These were valuable experiences that helped pave the way for my future.

Second, I'd like to thank my committee members: Dr. Haiying Liu, Dr. Shiyue Fang and Dr. Shiliang Wu for being in my committee and helping me with my dissertation.

Third, I'd like to thank the Chemistry department at Michigan Tech for the financial support and help in various ways. I would especially like to thank Dean W. Seppala for fixing the HPLC during my first year; Jerry L. Lutz for the liquid chromatography mass spectrometry training; Shane Christ, who is not in the Chemistry department anymore, for computer techniques support; and Celine E.

Grace, Denise J. Laux and Margaret Dunstan for office assistance. Also, as a teaching assistant, I'd like to thank my supervisors and coordinators, Lorri A. Reilly, Aparna Pandey, Dr. Sarah Hill and Lois A. Blau for the first year chemistry lab and recitation classes. I also need to give my deepest gratitude to several professors and staff for insightful discussions and meaningful activities, including Dr. Dallas K. Bates for the mass spectrum analysis discussion; Dr. Bahne C. Cornilsen for physical chemistry class; Dr. David J. Chesney for the instrumental analysis class; Dr. Lynn R. Mazzoleni for the mass spectrum class; Special thanks to the late Dr. Richard E. Honrath in the Department of Civil and Environmental Engineering, for the atmospheric class, during which I learned the most for the gas phase radical reactions; Kelley M. Smith, for teaching me how to play racquet ball and forming a team by "Sodium" and "Potassium"; and Dr. Rudy Luck, although you beat me 11-2 in table tennis, I still like you.

Fourth, I'd like to thank my friends for their support, especially during the difficulties: Dr. Ming Ning, Dr. Xiang Zhang and Dr. Zezhou Wang for taking good care of me after my two knee injuries; Keith Anderson for doing proofreading for me during the last few years; and Dr. Qili Hu, Dr. Martha J. B. Meneses, May E. Y. Kim and Alex Bruns, for their company and friendship. Thank Amei Cheung for inspiring me to chase the dreams.

Last but not least, I would like to thank my parents, Qin Hu and Rong Cheng, for their constant love and support. It was a long journey for me to finish my PhD degree in the United States and I could not have done this without you!

Abstract

Free radicals are present in cigarette smoke and can have a negative effect on human health by attacking lipids, nucleic acids, proteins and other biologically important species. However, because of the complexity of the tobacco smoke system and the dynamic nature of radicals, little is known about the identity of the radicals, and debate continues on the mechanisms by which those radicals are produced. In this study, acetyl radicals were trapped from the gas phase using 3-amino-2, 2, 5, 5-tetramethyl-proxyl (3AP) on solid support to form stable 3AP adducts for later analysis by high performance liquid chromatography (HPLC), mass spectrometry/tandem mass spectrometry (MS-MS/MS) and liquid chromatography–mass spectrometry (LC-MS). Simulations of acetyl radical generation were performed using Matlab and the Master Chemical Mechanism (MCM) programs.

A range of 10-150 nmol/cigarette of acetyl radical was measured from gas phase tobacco smoke of both commercial and research cigarettes under several different smoking conditions. More radicals were detected from the puff smoking method compared to continuous flow sampling. Approximately twice as many acetyl radicals were trapped when a GF/F particle filter was placed before the trapping zone. Computational simulations show that NO/NO₂ reacts with isoprene, initiating chain reactions to produce a hydroxyl radical, which abstracts hydrogen from acetaldehyde to generate acetyl radical. With initial concentrations of NO, acetaldehyde, and isoprene in a real-world cigarette smoke scenario, these mechanisms can account for

the full amount of acetyl radical detected experimentally. This study contributes to the overall understanding of the free radical generation in gas phase cigarette smoke.

Chapter 1: Introduction

1.1 Free Radicals

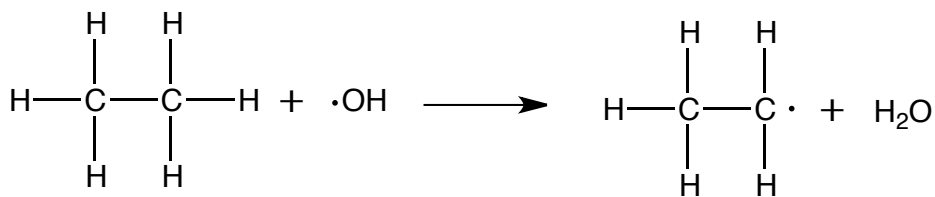
Free radicals are atoms, molecules, or ions that have an unpaired electron in the outer valence shell. Organic free radicals are exceptionally chemically reactive because of the drive to form more stable compounds by pairing off their lone electron. The high reactivity and short lifetime makes free radical detection and identification extremely difficult.

1.1.1 Fundamental Chemistry

Because of their exceptional reactivity, free radicals play an important role in atmospheric chemistry, the combustion processes, polymerization, biological aspects, and other areas. Free radicals can participate in a wide range of reactions, including abstractions, additions, oxidations and reductions, rearrangements, and electron transfer. In this chapter, hydroxyl radical ($\bullet\text{OH}$) is used as an example to review some fundamental free radical chemistry.

1.1.1.1 H Abstraction

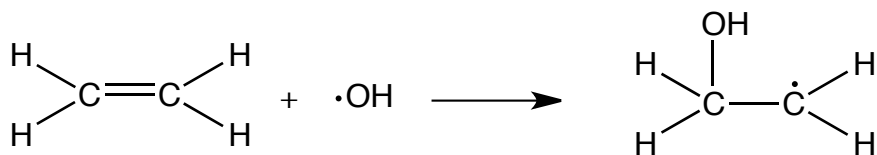
OH can attack on saturated hydrocarbon compounds such as alkanes to abstract a hydrogen atom to form a water molecule and an alkyl radical. For example, OH can abstract a hydrogen atom from ethane to form an ethane radical and H_2O with a reaction rate constant of $2.44 \times 10^{-13} \text{ cm}^2/\text{molecules}\cdot\text{s}$ as shown in Reaction 1.1.



Reaction 1.1. Hydroxyl radical abstraction reaction with an alkane (ethane) to produce carbon-centered radical.

1.1.1.2 Double Bond Addition

Rather than abstracting hydrogen, OH adds to the double bond when alkenes are present. The OH double bond addition reaction is faster than its hydrogen abstraction reaction, with a reaction rate constant of $8.51 \times 10^{-12} \text{ cm}^2/\text{molecules}\cdot\text{s}$ for ethane.



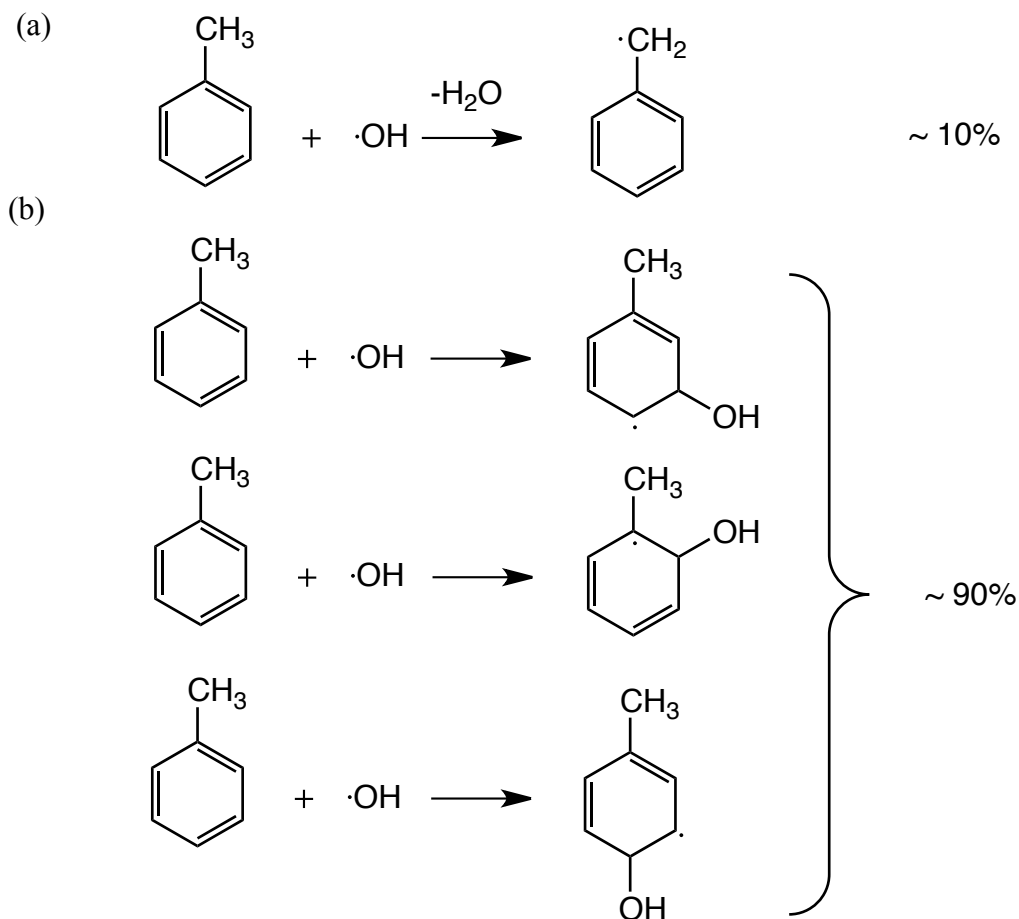
Reaction 1.2. Hydroxyl radical double bond addition reaction with an alkene (ethene) to produce carbon-centered radicals.

Reaction 1.2 shows an example of a double bond addition reaction of a hydroxyl radical to an alkene to produce a carbon-centered radical.

1.1.1.3 Aromatics Hydrogen Abstraction and Addition Reactions

The reaction with the hydroxyl radical is the major sink for aromatic compounds in the atmosphere. Aromatics can undergo a combination of hydrogen abstraction and addition reactions. For example, for the reaction of toluene with hydroxyl radical, the major reaction pathway (~90%) is via OH radical addition to the aromatic ring while

the minor pathway (~10%) is via hydrogen atom abstraction from C-H bond of the methyl group as shown below in Reaction 1.3.



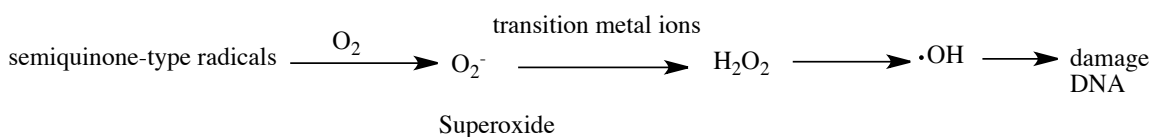
Reaction 1.3. (a) Hydroxyl radical hydrogen abstraction reactions with aromatic compounds (~10% of pathway); (b) addition reactions with aromatic compounds (~90% of pathway).

1.1.1.4 Biological Effects

Free radicals play an important role in the life process of plants and animals by acting as signaling molecules in plant biochemistry and physiology. For example, the radical nitric oxide (NO) is an important messenger molecule involved in many physiological and pathological processes in mammals including humans (Hou et al. 1999). By a

broad definition, transition metals containing unpaired electrons can also be defined as free radicals. These d-block elements such as Cu, Mn and Fe are essential in human diet and metabolism (Halliwell and Gutteridge 1999) .

Reactive oxygen species (ROS) such as OH, H₂O₂, and O₂⁻ are produced during normal cell metabolism (Halliwell and Cross 1994). These accidental free radicals from metabolism can induce oxidative effects, which result in lipid peroxidation, oxidation of proteins, and damage to certain organs, mainly lung and other tissues (Ozguner et al. 2005). Free radicals can also oxidize unsaturated lipids (Porter et al. 1995). There are three stages involved in carcinogenesis: initiation, promotion, and progression. It is believed that free radicals are involved in the initiation step by activating a procarcinogen to its carcinogenic form, or binding the carcinogenic species to NDA (Pryor 1997). Hydroxyl radicals are especially reactive and can damage or modify any biomolecule such as lipids, proteins and DNA. For example, hydroxyl radicals can react with DNA to break the DNA strand or form hydroxylated DNA bases, which leads to gene mutation. The general pathway of radical damage to DNA is shown in Scheme 1.1.



Scheme 1.1. The pathway of radical damage to DNA.

Environmental free radical sources such as ozone, nitrogen oxides, and cigarette smoke can also cause oxidative damage. Cigarette smoke is a cancer initiator and promoter and contains a large number of carcinogenic and mutagenic compounds such as polycyclic aromatic hydrocarbons (PAHs), N-nitrosamines,

aldehydes and various other organic compounds (Swauger et al. 2002). Although the mechanisms for cigarette smoke-induced carcinogenesis have not been completely elucidated, many studies have established the central role of free radicals in tobacco smoke carcinogenesis and in the last two decades (Halliwell and Cross 1994; Leanderson et al. 1993; Ozguner et al. 2005; Pryor 1997; Randerath et al. 1986; Valavanidis et al. 2009).

1.1.2 Sources of Radicals in the Atmosphere

Radical chemistry in the atmosphere has been well studied and can provide basic principles to radical generation in cigarette smoke. In this study, the hydroxyl radical is used to illustrate radical chemistry in the atmosphere. As shown in Reaction 1.4-1.7, the major sources for hydroxyl radicals in the troposphere are from ozone photolysis reactions.



Ozone photolysis produces excited singlet oxygen atom ($O(^1D)$) at wavelength smaller than 319 nm (Reaction 1.4). Excited singlet oxygen collides with atmospheric molecules such as N_2 or O_2 (M) to remove excess energy, producing ground state oxygen atom ($O(^3P)$) (Reaction 1.5). In some cases, an excited singlet oxygen atom collides with H_2O and produces two hydroxyl radicals (Reaction 1.6).

The ground state O atom combines rapidly with O₂ to reform O₃, resulting in a null cycle (Reaction 1.7).

1.1.3 Photochemical NO_x Cycling

NO, NO₂ and O₃ are major compounds involved in the basic photochemical cycle in the troposphere. NO₂ is decomposed at wavelengths < 424 nm to give NO and O (Reaction 1.8) and regenerated as a result of reactions of NO and O₃, HO₂, and NO₂ (Reaction 1.9).



In analyzing these chain reactions above, we can apply the pseudo-steady state approximation (PSSA) to O₃. In atmospheric chemistry, the pseudo-steady-state approximation is a method to calculate low concentrations of reactive intermediate species such as free radicals by assuming that they are consumed as rapidly as they are formed. For example, at steady state for O₃, ozone is formed from the photolysis of NO₂ at the same rate at which it is consumed by NO, which is shown in Equation 1.1. Hence, the ozone concentration at steady state is $J_8 [NO_2]/k_9 [NO]$, as shown in Equation 1.2.

$$0 \cong \frac{d[O_3]}{dt} = r_8 - r_9 = J_8[NO_2] - k_9[NO][O_3] \quad (\text{Equation 1.1})$$

$$[O_3] = \frac{J_8[NO_2]}{k_9[NO]} \quad (\text{Equation 1.2})$$

Equation 1.2 is also called the photostationary state relation, which shows that the ozone concentration at steady state is proportional to the [NO₂]/[NO] ratio.

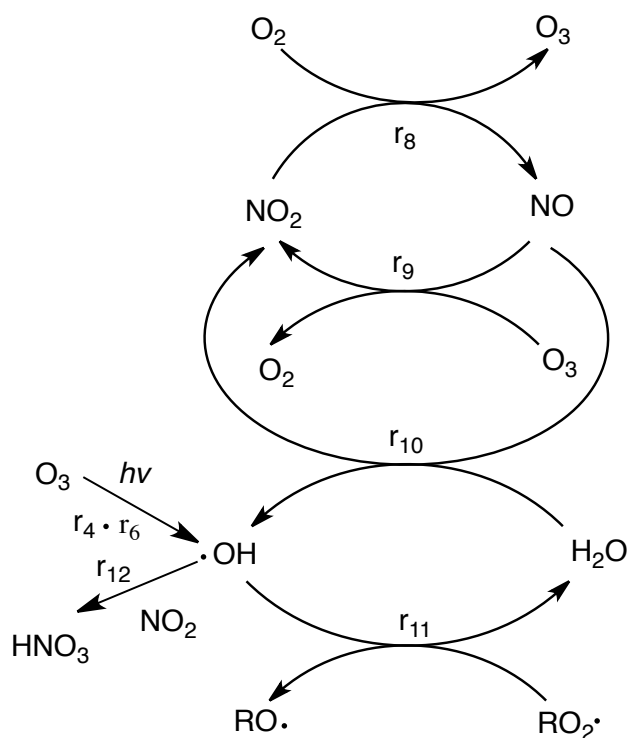


Reaction 1.10-1.11 shows that NO can also react with peroxides including HO₂ and RO₂ to regenerate NO₂ and produce OH and RO radicals. As one of the major components in cigarette smoke, NO_x can also play an important role in radical generation and cycling in the tobacco smoke.

1.1.4 Scavengers and Fates



When a hydroxyl radical and nitrogen dioxide collide, the chain reactions shown in Scheme 1.2 come to a termination by producing HNO₃ as shown in Reaction 1.12.



Scheme 1.2. Chain cycling reactions of radicals in the troposphere.

Steady-state for OH is shown in Equation 1.3- 1.4.

$$0 \cong \frac{d[OH]}{dt} = r_4 \cdot r_6 + r_{10} - r_{12} = J_4 k_6 [O_3][H_2O] + k_{10}[NO][H_2O] - k_{12}[OH][NO_2]$$

(Equation 1.3)

$$[OH] = \frac{J_4 k_6 [O_3][H_2O] + k_{10}[NO][H_2O]}{k_{12}[NO_2]} = \frac{J_4 J_8 k_6 [H_2O][NO_2] + k_9 k_{10} [NO]^2 [HO_2]}{k_9 k_{12} [NO][NO_2]}$$

(Equation 1.4)

It is logical to compare the sources, cycling, and fate of radicals in the atmosphere and in tobacco smoke because they have the same chemical nature. However, there are several key differences between reactions in the atmosphere and those in tobacco smoke. First, smoke has a much higher volatile organic compounds (VOCs) level than the atmosphere does (Hoffmann et al. 2001); second, there is little or no O₃ present in cigarette smoke compared to the atmosphere; Third, photolysis reactions are not very important in cigarette smoke, due to its lack of exposure to strong ultraviolet lights. Fourth, the reaction time for free radicals in cigarette smoke is much shorter than that in the atmosphere, which usually lasts for hours, or even days. Hence, a modified atmospheric model is required to investigate free radical chemistry in cigarette smoke.

1.2 Tobacco Composition and Chemistry

1.2.1 Tobacco Types and Composition

Tobacco is a complex plant member of the *Solanaceae* or *Nightshade* family, with most of the commercial tobacco being of the *Nicotiana tabacum* species. Research has shown that the smoke delivery and smoke constituents greatly depend

on the tobacco leaf characteristics (Borgerding and Klus 2005). It is estimated that there are more than 4000 different chemical constituents in the tobacco leaf, as shown in Table 1.1 (Weeks 1985).

Table 1.1. Tobacco components and percentages.

| Compounds | Percentages % |
|-----------------------|---------------|
| Waxes and wax esters | 0.66-1.20 |
| Solanesol and esters | 0.80-2.00 |
| Organic acids | 3.00-7.67 |
| Polyphenols | 0.75-5.70 |
| Reducing sugars | 0.80-25.00 |
| Non reducing sugars | 1.00-5.00 |
| Starch and pectins | 0-8.00 |
| Nicotine | 0.28-4.00 |
| Amino acids | 0.25-3.00 |
| Cellulose and lignin | 25.00-28.50 |
| Volatile oils | 0.25-1.00 |
| Protein | 1.00-3.00 |
| Water (free and bond) | 11.00-24.00 |

Tobacco components and their percentages are affected by genetics, agricultural practices, weather conditions, and harvesting, resulting in different smoke components or smoking quality (Leffingwell 1999). For example, the formation of proteins, amino acids and nicotine is based on the abundance of the nitrogen supplies in the different tobacco plants. Mainly based on the production locations, three types of tobacco, including Virginia, Burley and Oriental, are used for cigarette manufacturing worldwide (Thielen et al. 2008). In addition, the curing procedure, which allows for the slow oxidation and degradation in the tobacco leaf before consumption, can also affect the amount of nicotine and VOCs in cigarette smoke as well. Generally speaking, there are three types of curing: air, flue- and sun-curing. Burley tobacco is a light air-cured tobacco, which contains little sugar. Flue-cured tobacco usually contains more sugar and a medium to high level of nicotine. Turkish

tobacco, which is sometimes called Oriental tobacco, is a sun-cured tobacco, which contains less nicotine and fewer carcinogens than other varieties. Smoke composition details of Burley, Flue-cured and Turkish tobacco are shown in Table 1.2 (Borgerding and Klus 2005).

Table 1.2. Selected Organic compounds in different tobacco types

| Smoke constituent | Tobacco Type | | |
|-------------------------|--------------|------------|---------|
| | Burley | Flue-cured | Turkish |
| Tar, mg/cig | 16.7 | 20.6 | 20.7 |
| Nicotine, mg/cig | 1.5 | 2.1 | 0.7 |
| Carbon monoxide, mg/cig | 17.1 | 15.7 | 15.1 |
| Phenol, µg/cig | 27.2 | 34.1 | 25.9 |
| Catechol, µg/cig | 49.4 | 120.2 | 110.3 |
| Hydroquinone, µg/cig | 41.0 | 131.7 | 81.9 |
| Nitric oxide, µg/cig | 442 | 91 | 83 |
| Formaldehyde, µg/cig | 12.9 | 66.0 | 75.3 |
| Acetaldehyde, µg/cig | 866 | 1124 | 911 |

Reference Cigarettes

To allow for replication and comparison in different laboratories and experiments, several types of reference cigarettes were manufactured by Reference Cigarette Program, College of Agriculture from Kentucky University as standard cigarettes as shown in Figure 1.1 (RCP 2011).



Figure 1.1. Research cigarettes manufactured by Reference Cigarette Program, College of Agriculture from Kentucky University.

The first reference cigarette 1R1 was manufactured in 1968 to serve as an international standard. Other series of reference cigarettes including 1R3F, 2R4F, and 1R5F were manufactured later for different research purposes. For example, 2R4F is a low nicotine research cigarette and 1R5F is an ultra low nicotine research cigarette. More specifications for various reference cigarettes are shown in Table 1.3.

Table 1.3. Reference Cigarette composition and specifications.

| Composition | 1R3F | 2R4F | 1R5F |
|---------------|--------|--------|--------|
| Flue-cured | 32.54% | 32.51% | 5.75% |
| Burley | 20.04% | 19.94% | 42.25% |
| Turkish | 11.09% | 11.08% | 7.00% |
| Maryland | 1.06% | 1.24% | / |
| Reconstituted | 27.17% | 27.13% | 15.00% |
| Invert Sugar | 5.30% | 5.30% | 5.30% |
| Glycerin | 2.80% | 2.80% | 2.80% |

1.2.2 Tobacco Smoke Composition and Chemistry

Tobacco smoke is a very complex and dynamic system, consisting of more than 4,800 compounds partitioned between gas and particulate phases. Most of these compounds can be found in the particulate phase and some are classified as semivolatiles. As defined by the Federal Trade Commission (FTC), tar is the total particulate matter (TPM) minus nicotine and water (Pillsbury 1996). There is a dynamic equilibrium between both phases, which can be affected by concentration, pressure, and chemical reactions. Owing to the complexity of the cigarette system, smoke from different cigarettes or under different smoking conditions could produce different components.

Federal Trade Commission (FTC) Conditions

In addition to the variations in cigarette types, the measured composition of

cigarette smoke is also greatly affected by the smoking methods for the complex chemical reactions taking place in the smoking process. To allow for replication and comparison in different laboratories and experiments, the American Federal Trade Commission (FTC) introduced a standard smoking method for cigarette smoke scientific research in 1966 (FTC 1966). The FTC puff-resolved method draws 35 mL of smoke for each puff over a 2-second duration; one puff is sampled every minute.

Mainstream Smoke and Sidestream Smoke

Mainstream smoke (MS), sometimes called whole smoke (WS), is the aerosol and gas mixture generated during a puff from the burning site drawn through the cigarette rod, and inhaled by the smoker. Instead of reaching the rod, sidestream smoke (SS) is primarily formed between puffs during the smoldering process at lower temperatures. A picture of mainstream smoke and sidestream smoke is shown in Figure 1.2. Although there are a lot of similarities in chemical composition between mainstream and sidestream smoke, there are also some differences in combustion temperature, pH and the degree of dilution with air. The dilution with air in sidestream smoke results in a rapid temperature decrease and smaller particle size distribution compared to its counterpart in mainstream smoke (Thielen et al. 2008).

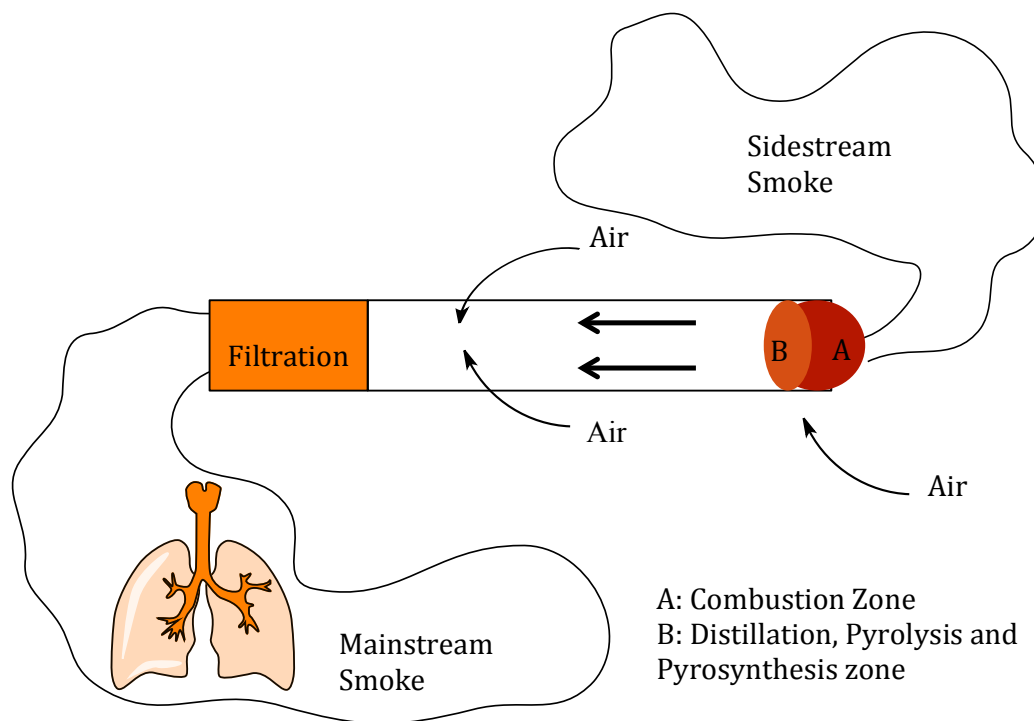


Figure 1.2. Chemical and physical processes in burning cigarette adapted from Thielen et al. 2008.

The burning of a cigarette can be divided into two processes by different temperatures and oxygen concentrations: exothermic oxidation/combustion zones and endothermic pyrolysis/distillation zones as shown in Figure 1.2. The combustion zone is at or near the burning tip, with a temperature as high as 950 °C and the sufficient oxygen concentration of 20.4% (Thielen et al. 2008). In this exothermic oxidation / combustion zone, the major products are water, carbon dioxide, and carbon monoxide, because of the high temperature and sufficient oxygen. A zone of distillation, pyrolysis and pyrosynthesis is behind the burning tip with lower temperature (200-600°C) and oxygen level (20.4%-0%). This endothermic pyrolysis/distillation zone can produce a variety of organic compounds, which can have

multiple reactions in the gas phase.

The chemical species in tobacco leaves are the precursors to the smoke constituents by a variety of mechanisms. First, volatile and thermally stable compounds in tobacco can be easily transferred directly to the gas phase smoke. For example, methanol transfers efficiently from tobacco leaf to the smoke because of its volatility and heat stability. Various saturated and unsaturated hydrocarbons, and other stable VOCs are distilled out of the tobacco during the combustion process. Even some less volatile compounds such as nicotine can be transferred into the gas phase smoke at a higher temperature or pH. Second, some tobacco constituents undergo oxidation and pyrolysis reactions to produce partially oxidized species or even nearly completely degrade into smaller molecules. For example, polysaccharides, sugars, proteins, cellulose, pectin, lignin, and amino acids can thermally decompose into a wide variety of small organic compounds in tobacco smoke. Previous study shows that formaldehyde in mainstream smoke can be generated by saccharides such as sugars and cellulose in burning cigarettes. Third, many reactions happen at the distillation, pyrolysis and pyrosynthesis zone and new compounds are pyrosynthesized by protein and carbohydrates or their degradation compounds (Green 1977).

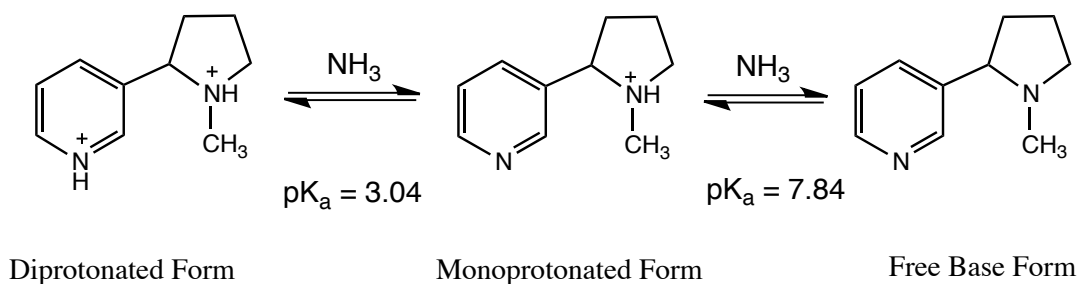
Variables on Combustion and Pyrolysis Outcome

Many variables can affect the outcome of the combination of the combustion and pyrolysis processes, such as temperature, oxygen concentration, pH, and additives present.

Baker et al. showed that the generation of formaldehyde is dependent on the burning temperature and other components such as amino compounds, which can suppress the yield of formaldehyde by reacting with it to produce a complex (Baker et al. 2006).

The level of peroxides in cigarette smoke is greatly dependent on the oxygen concentration. In the presence of sufficient oxygen, carbon-centered radicals can be rapidly oxidized into oxygen-centered radicals, which can convert NO into NO₂ (Atkinson et al. 1997; Atkinson 2001).

As mentioned in the last paragraph, nicotine can be easily transferred to the gas phase smoke during the combustion process at a higher pH. It is also often questioned whether the tobacco manufacturers deliberately add base ammonium to make the smoke more basic, which releases more nicotine in free base form, and improves nicotine delivery to the respiratory system, thus making it more addictive.



Scheme 1.3. Diprotonated, monoprotonated and free base form nicotine at different pHs.

When ammonia is present in tobacco, it increases the pH, which drives the reaction to the right and produces more free-based nicotine as shown in Scheme 1.3. Since the tobacco in cigarettes is naturally acidic (Brunnemann and Hoffmann 1974),

the change in pH by adding ammonia not only affects nicotine delivery but also has a decisive influence on the chemical nature of the smoke.

During the processing, manufacturing, and packing processes of the cigarette, a wide range of additives is introduced to tobacco. According to the United States Department of Health and Human Services, there are 599 additives in cigarettes, including cocoa, sugars, methanol, glycerin, water and other ingredients. The main purposes for adding additives are to enhance aroma, to create a special flavor, to make it easier to inhale, and to preserve moisture levels (Geiss and Kotzias 2007).

Approximate numbers and classes of inorganic and organic compounds in fresh cigarette smoke are shown in Table 1.4. Inorganic species, such as N_2 , O_2 , CO, and CO_2 , and water account for 80-98% of total effluent of the fresh vapor phase cigarette. Among these major inorganic species in the vapor phase smoke, nitrogen oxides (NO_x , or NO and NO_2) play a crucial role in radical generation in gas phase smoke not only because they are major constituents of the vapor phase of the mainstream smoke of non-filter cigarette (100-600 $\mu\text{g}/\text{cigarette}$) (Hoffmann et al. 2001) but also because NO_2 can react with a wide range of organic compounds in cigarette smoke to produce radicals. In addition, approximately 760 of the major organic compounds in vapor-phase tobacco, including methane, volatile alkenes, isoprene, butadiene, acetylene, benzene, toluene, styrene and other volatile aromatic hydrocarbons are also present in the vapor phase smoke. Notably, approximately 110 different aldehydes are present in fresh tobacco smoke (Borgerding and Klus 2005), which can be possible precursors of radicals in tobacco smoke.

Table 1.4. Approximate number and classes of compounds identified in fresh tobacco smoke. (Borgerding and Klus 2005; Hoffmann et al. 2001)

| Class | Number | Major Compounds | Concentration/cigarette (% of total effluent) |
|--------------|--------|--|---|
| Inorganic | ~12 | Nitrogen Oxygen Carbon dioxide Carbon monoxide Water Argon Hydrogen Ammonia Nitrogen oxides (NO _x) Hydrogen cyanide Hydrogen sulfide | 280-320 mg (56-64%) 50-70 mg (11-14%) 45-65 mg (9-13%) 14-23 mg (2.8-4.6%) 7-12 mg (1.4-2.4%) 5 mg (1.0%) 0.5-1.0 mg 10-130 µg 100-600 µg 400-500 µg 20-90 µg |
| Hydrocarbons | ~760 | Methane Other volatile alkanes Volatile alkenes Isoprene Butadiene Acetylene Benzene Toluene Styrene Other volatile aromatic hydrocarbons | 1.0-2.0 mg 1.0-1.6 mg 0.4-0.5 mg 0.2-0.4 mg 25-40 µg 20-35 µg 6-70 µg 5-90 µg 10 µg 15-30 µg |
| Acids | ~230 | Formic acid Acetic acid Propionic acid Methyl formate Other volatile acids | 200-600 µg 300-1700 µg 100-300 µg 20-30 µg 5-10 µg |
| Aldehyde | ~110 | Formaldehyde Acetaldehyde Acrolein | 20-100 µg 400-1400 µg 60-240 µg |
| Nitriles | ~100 | Acetonitrile Other volatile nitriles | 100-150 µg 50-80 µg |
| Alcohols | ~380 | Methanol Other volatile alcohols | 80-650 µg 10-100 µg |

The complexity of the inorganic and organic species, and their high concentrations in cigarette smoke make tobacco smoke a unique atmospheric model.

Cigarette Tar and Total Particulate Matter (TPM)

The commonly used “Cambridge filter” is a glass fiber filter used for the collection of the particulate phase of cigarette smoke. The configuration of the Cambridge filter and its holder is shown in Figure 1.3.

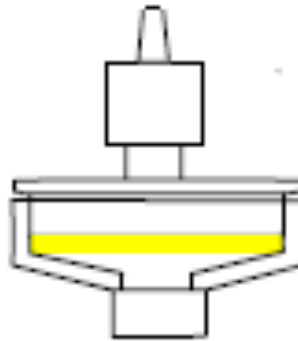
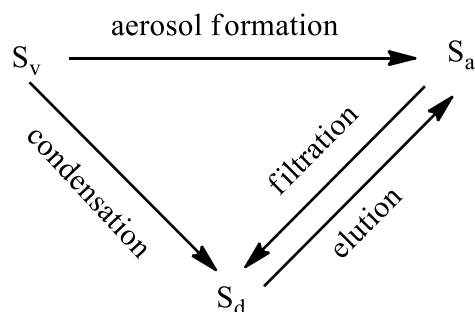


Figure 1.3. The configuration of Cambridge filter and holder.

When whole smoke passes through a Cambridge filter pad, the fraction collected on the filter is known as tar, or more specifically, nicotine free dry particulate matter (NFDPM)(Cech and Enke 2001), which is total particle matter (TPM) minus water and nicotine. The fraction passing through the filter is defined as the gas phase (GP) (Baker 1999).



S_v = vapor phase or gas phase smoke

S_a = particulate phase

S_d = tar deposited on the tobacco rod

Figure 1.4. A model of general processes occurring during condensation of mainstream smoke precursor vapor leaving the burning zone.

Figure 1.4 illustrates the dynamic balance between vapor phase, particulate phase, and tar. Semi-volatile compounds such as phenol are partitioned between vapor phase and particulate phase (Townsend 1983).

The tar content of a cigarette is not well defined. It contains thousands of different substances, which vary in different cigarettes and in different smoking regimes.

The particle phase of cigarette smoke consists of a distinctly different suite of compounds from that in the vapor phase. A higher molecular weight fraction of organic compounds such as nicotine, naphthalene and pyrenes are prone to condense into tar when the smoke cools. Large amounts of carcinogenic polynuclear aromatic hydrocarbons, including phenols, catechols, quinones, oleic acid, quinolines and other aza-arenes, are also present in the particulate phase. The distribution of ionizable

species, such as amines and nicotine, between gas phase and particulate phase is very sensitive to the pH of the aerosol liquid, which may be controlled by additives in tobacco (Pankow 2001).

A summary of major constituents of the Particulate Matter in the mainstream smoke is shown in Table 1.5 below.

Table 1.5. A summarized table of major constituents of the Particulate Matter in the mainstream smoke by Hoffmann et al.

| Compound | µg / cigarette |
|--|----------------|
| Nicotine | 100-3000 |
| Total nonvolatile hydrocarbons (45) ^{a,b} | 300-400 |
| Carcinogenic polynuclear aromatic hydrocarbons | 80-160 |
| Phenol | 60-180 |
| Other phenols (45) ^b | 200-400 |
| Catechols (4) | 100-200 |
| Other catechols (4) | 200-400 |
| Quinones (7) | 600-1000 |
| Linoleic acid | 150-250 |
| Linolenic acid | 150-250 |
| Lactic acid | 60-80 |
| Benzofurans (4) | 200-300 |

^a Parentheses show the number of individual compounds identified in a given group.

^b Estimate. (Hoffmann et al. 2001)

Free Radicals in Tobacco Smoke

It has previously been reported that the burning of tobacco produces semiquinone-type free radicals, which can induce oxidative stress and DNA damage. There are two distinctly different populations of radicals in cigarette smoke: short-lived radicals in gas-phase and relatively persistent long-lived quinone and hydroquinone radicals in the tar (Pryor et al. 1983b).

Primary free radicals are generated during the tobacco components pyrolysis and direct thermo decomposition. When TPM is exposed to air at room temperature, it can generate secondary free radicals, which strongly depend on the constituent,

temperature range, and atmospheric exposure time. Many studies have shown that tar contains a variety of environmentally persistent radicals, such as quinones and semiquinones, which can reduce O_2 to produce QH radical and eventually OH radical (Pryor 1985; Pryor et al. 1983a; Maskos et al. 2008; Pryor et al. 1983a).

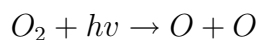
Persistent radicals have been found from the pyrolysis of tobacco (Adam et al. 2009). Persistent free radicals are usually associated with free radicals present in the structural biomass of the plant (polyphenols, carbohydrates, and lignin). ESR results show that the free or chemically TPM bound hydroquinone/catechol-type species are oxidized by ambient air to produce semiquinone-type radicals (Maskos et al. 2005).

Surprisingly, inconsistent with their highly reactive nature, free radicals are also detected well beyond the burning site, even as long as 10 minutes post combustion (Cueto and Pryor 1994; Flicker and Green 1998, 2001; Pryor et al. 1993). To explain this paradox, Pryor et al. (Pryor et al. 1993) proposed that radicals are continuously formed and destroyed in the gas phase by a steady state mechanism based on the addition of NO_2 to alkyl dienes. However, recent studies have raised questions about this steady state mechanism because of the lack of evidence for NO_2 -containing radicals and the discovery of apparently unrelated radicals, such as alkylaminocarbonyl and acyl radicals in mainstream smoke (Bartalis et al. 2007; Bartalis et al. 2009). In addition, several studies have indicated that the Cambridge filter, which separates gas phase smoke from total particulate matter (TPM), substantially influences the generation of radicals in smoke (Wooten 2011).

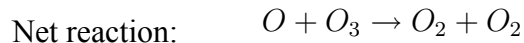
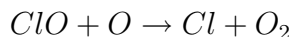
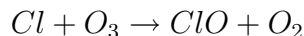
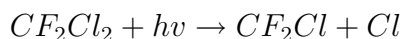
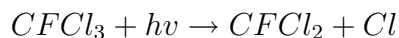
1.3 Significance of Free Radicals

1.3.1 Atmospheric Chemistry

Free radicals play a vital role in the atmospheric chemistry of both the stratosphere and the troposphere. For example, ozone is the most important trace constituent in the stratosphere, where it is generated by photolytic decomposition of O_2 as shown in Scheme 1.4. However, radicals such as bromine and chlorine radicals resulting from photolysis of many industrial gases, including chlorofluorocarbons (CFCs) and hydrochlorofluorocarbons (HCFCs), can attack ozone molecules, initiating catalytic cycles that deplete ozone as shown in Scheme 1.5.



Scheme 1.4. Ozone generation in the stratosphere.



Scheme 1.5. Ozone depletion reactions by chloride radical resulting from photolysis of chlorofluorocarbons.

The chloride radical is very destructive to ozone in the stratosphere because of the reaction loop which regenerates chloride radical, as shown in Scheme 1.5 (Pandis 1998). On average, one chlorine radical can destroy 10^5 ozone molecules before it is

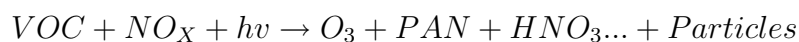
removed by other agents, which results in the phenomenon termed as the “Ozone Hole” over Antarctica.

As the primary oxidizing species in the troposphere, hydroxyl radicals play a key role by reacting with almost all atmospheric trace species.

In Jack G. Calvert’s early work on Hydrocarbon Involvement in Photochemical Smog Formation in the Los Angeles Atmosphere, he noted the importance of radical reaction in smog generation:

“Even though the compounds such as CH₄ and C₂H₄ are usually considered to be relatively unimportant reactants in smog development in the lower atmosphere, the rates of HO attack on them are not insignificant...Note that of the HO-radicals reacting in the chain-carrying steps, about 33% react with alkanes, 35% with alkenes, 20% with aromatics, and 12% with CO... The nature of the primary interaction of HO with olefinic and aromatic hydrocarbons remains uncertain; both radical abstraction of H-atoms and addition to the olefinic bond have been suggested to occur with the alkenes, although the importance of each is obscure at this time. The secondary steps of radical oxidation are also uncertain in most cases.” (Calvert 1976)

In addition, emissions of NO_x or mono-nitrogen oxides NO and NO₂ from urban transportation could result in serious pollution via photochemical reactions such as the “Los Angeles Smog”. The reactions are shown in Scheme 1.6.



Scheme 1.6. Photochemical air pollution formation in Los Angeles.

1.3.2 Human Health Concern

In the World Health Organization (WHO) website, the tobacco-related epidemic is listed as one of the leading causes of death, illness, and impoverishment and one of the biggest public health threats the world has ever faced. In WHO's website, it says:

“It kills nearly 6 million people a year, of whom more than 5 million are from direct tobacco use and more than 600,000 are nonsmokers exposed to second-hand smoke. Approximately one person dies every six seconds due to tobacco and this accounts for one in 10 adult deaths. Up to half of current users will eventually die of a tobacco-related disease.

Nearly 80% of the more than one billion smokers worldwide live in low- and middle-income countries, where the burden of tobacco-related illness and death is heaviest.”(WHO 2013)

Although there is increasing awareness of the harmfulness of tobacco smoke, according to the State of State Health website (CDC 2007), there are still about 48 million regular smokers in the U.S., which means one in five U.S. adults smoke. 47.70% of smokers have tried at least once to quit. The attributed costs to smoking in the United States are as high as \$194.45 billion in 2004.

As one of the leading causes of preventable deaths in the United States, smoking causes approximately 438,000 deaths annually by increasing the risk of heart disease, cancer, stroke, and chronic lung disease.

Of the 5000 compounds identified in tobacco smoke, 69 species are recognized as carcinogens, partitioned in both mainstream and sidestream smoke. Over the last sixty years, extensive efforts have been made to understand the correlations between cigarette smoking and diseases. Free radicals in tobacco smoke play an important role in these smoking-related diseases by causing DNA damage, lipid peroxidation, and protein oxidation (Ozguner et al. 2005; Porter et al. 1995). However, because of the complexity of free radicals in tobacco smoke, there are still many unanswered questions concerning the involvement of free radicals in the toxicology of tobacco smoke.

1.4 References

- Adam T, McAughey J, McGrath C, Mocker C, Zimmermann R. 2009. Simultaneous on-line size and chemical analysis of gas phase and particulate phase of cigarette mainstream smoke. *Analytical and bioanalytical chemistry* 394(4): 1193-1203.
- Atkinson R, Baulch DL, Cox RA, Hampson RF, Kerr JA, Rossi MJ, et al. 1997. Evaluated kinetic, photochemical and heterogeneous data for atmospheric chemistry .5. IUPAC Subcommittee on Gas Kinetic Data Evaluation for Atmospheric Chemistry. *J Phys Chem Ref Data* 26(3): 521-1011.
- Atkinson RB, D.L.; Cox, R.A.; Crowley, J.N.; Hampson, R.F, Jr.; Kerr, J.A.; Rossi, M.J.; Troe, J. 2001. Summary of Evaluated Kinetic and Photochemical Data for Atmospheric Chemistry.
- Baker R. 1999. Tobacco: production, chemistry, and technology. Blackwell Science: 398-439.
- Baker RR, Coburn S, Liu C. 2006. The pyrolytic formation of formaldehyde from sugars and tobacco. *J Anal Appl Pyrol* 77(1): 12-21.
- Bartalis J, Chan WG, Wooten JB. 2007. A new look at radicals in cigarette smoke. *Anal Chem* 79(13): 5103-5106.
- Bartalis J, Zhao YL, Flora JW, Paine JB, Wooten JB. 2009. Carbon-centered radicals in cigarette smoke: acyl and alkylaminocarbonyl radicals. *Anal Chem* 81(2): 631-641.
- Borgerding M, Klus H. 2005. Analysis of complex mixtures - Cigarette smoke. *Experimental and Toxicologic Pathology* 57: 43-73.
- Brunnemann KD, Hoffmann D. 1974. The pH of tobacco smoke. *Food Cosmet Toxicol* 12(1): 115-124.

Calvert JG. 1976. Hydrocarbon involvement in photochemical smog formation in Los Angeles atmosphere. *Environmental science & technology* 10(3): 256-262.

CDC CfDCaP. 2007. Behavior Risk Factor Surveillance System Survey Data. <http://appsncddcdc.gov/brfss/listasp?cat=TU&yr=2007&qkey=4396&state=All>.

Cech NB, Enke CG. 2001. Practical implications of some recent studies in electrospray ionization fundamentals. *Mass Spectrom Rev* 20(6): 362-387.

Cueto R, Pryor WA. 1994. Cigarette-Smoke Chemistry - Conversion of Nitric-Oxide to Nitrogen-Dioxide and Reactions of Nitrogen-Oxides with Other Smoke Components as Studied by Fourier-Transform Infrared-Spectroscopy. *Vib Spectrosc* 7(1): 97-111.

Flicker TM, Green SA. 1998. Detection and separation of gas-phase carbon-centered radicals from cigarette smoke and diesel exhaust. *Analytical Chemistry* 70(9): 2008-2012.

Flicker TM, Green SA. 2001. Comparison of gas-phase free-radical populations in tobacco smoke and model systems by HPLC. *Environ Health Perspect* 109(8): 765-771.

FTC. 1966. FTC Rescinds Guidance from 1966 on Statements Concerning Tar and Nicotine Yields. <http://www.ftc.gov/opa/2008/11/cigarettestestingshtm>.

Geiss O, Kotzias D. 2007. Tobacco, Cigarettes and Cigarette Smoke. Institute for Health and Consumer Protection.

Green CR. 1977. Some relationships between tobacco leaf and composition. *Proceedings of 173rd American Chemical Society Symposium*: 426-470.

Halliwell B, Cross CE. 1994. Oxygen-Derived Species - Their Relation to Human-Disease and Environmental-Stress. *Environ Health Persp* 102: 5-12.

Halliwell B, Gutteridge MC, John. 1999. Free Radicals in Biology and Medicine.

Hoffmann D, Hoffmann I, El-Bayoumy K. 2001. The less harmful cigarette: a controversial issue. a tribute to Ernst L. Wynder. *Chem Res Toxicol* 14(7): 767-790.

Hou YC, Janczuk A, Wang PG. 1999. Current trends in the development of nitric oxide donors. *Curr Pharm Design* 5(6): 417-441.

Leanderson P, Pryor W, Krinsky N, Lake R, Castonguay A, Zhao BL, et al. 1993. Cigarette Smoke-Induced DNA-Damage in Cultured Human Lung-Cells. *Ann Ny Acad Sci* 686: 249-261.

Leffingwell JC. 1999. Tobacco: Production, Chemistry, and Technology.

Maskos Z, Khachatryan L, Dellinger B. 2005. Precursors of radicals in tobacco smoke and the role of particulate matter in forming and stabilizing radicals. *Energ Fuel* 19(6): 2466-2473.

Maskos Z, Khachatryan L, Dellinger B. 2008. Formation of the persistent primary radicals from the pyrolysis of tobacco. *Energ Fuel* 22(2): 1027-1033.

Ozguner F, Koyu A, Cesur G. 2005. Active smoking causes oxidative stress and decreases blood melatonin levels. *Toxicol Ind Health* 21(1-2): 21-26.

Pandis JHSSN. 1998. Atmospheric Chemistry and Physics.

Pankow JF. 2001. A consideration of the role of gas/particle partitioning in the deposition of nicotine and other tobacco smoke compounds in the respiratory tract. *Chemical research in toxicology* 14(11): 1465-1481.

Pillsbury HC. 1996. Review of the Federal Trade Commission Method for Determining Cigarette Tar and Nicotine Yield. National Cancer Institute, NIH Publication 96-4028(9-14).

Porter NA, Caldwell SE, Mills KA. 1995. Mechanisms of Free-Radical Oxidation of Unsaturated Lipids. *Lipids* 30(4): 277-290.

Pryor DFCaWA. 1985. Free-Radical Chemistry of Cigarette Smoke and Its Toxicological Implications. *Environ Health Perspectives* 64: 111-126.

Pryor WA. 1997. Cigarette smoke radicals and the role of free radicals in chemical carcinogenicity. *Environ Health Perspect* 105 Suppl 4: 875-882.

Pryor WA, Hales BJ, Premovic PI, Church DF. 1983a. The radicals in cigarette tar: their nature and suggested physiological implications. *Science* 220(4595): 425-427.

Pryor WA, Stone K, Stone K, Cross CE, Machlin L, Packer L. 1993. Oxidants in Cigarette-Smoke - Radicals, Hydrogen-Peroxide, Peroxynitrate, and Peroxynitrite. *Ann NY Acad Sci* 686: 12-28.

Pryor WA, Tamura M, Church DF. 1983b. Spin Trapping Study of the Radicals Produced in Nox Olefin Reactions - a Model for Cigarette-Smoke. *Abstr Pap Am Chem S* 186(Aug): 221-ORGN.

Randerath E, Avitts TA, Reddy MV, Miller RH, Everson RB, Randerath K. 1986. Comparative P-32 Analysis of Cigarette Smoke-Induced DNA Damage in Human-Tissues and Mouse Skin. *Cancer Res* 46(11): 5869-5877.

RCP. 2011. Reference Cigarette Program, College of Agriculture, University of Kentucky Homepage. Available: <http://www.ca.uky.edu/refcig/>.

Swauger JE, Steichen TJ, Murphy PA, Kinsler S. 2002. An analysis of the mainstream smoke chemistry of samples of the US cigarette market acquired between 1995 and 2000. *Regul Toxicol Pharm* 35(2): 142-156.

Thielen A, Klus H, Muller L. 2008. Tobacco smoke: unraveling a controversial subject. *Experimental and toxicologic pathology : official journal of the Gesellschaft fur Toxikologische Pathologie* 60(2-3): 141-156.

Townsend DK. 1983. The effect of Tobacco moisture on the removal of cigarette smoke by the tobacco rod. 37th Tobacco Chemist's Research Conference: Number 31.

Valavanidis A, Vlachogianni T, Fiotakis K. 2009. Tobacco smoke: involvement of reactive oxygen species and stable free radicals in mechanisms of oxidative damage, carcinogenesis and synergistic effects with other respirable particles. *Int J Environ Res Public Health* 6(2): 445-462.

Weeks W. 1985. Chemistry of tobacco constituents influencing flavor and aroma. *Recent Advances in Tobacco Science* 11: 175-200.

WHO. 2013. <http://www.who.int/mediacentre/factsheets/fs339/en/>.

Wooten JB. 2011. Gas-phase Radicals in Cigarette Smoke: A Re-evaluation of the Steady-State Model and the Cambridge Filter Pad. *Organic Chemistry*.

Chapter 2: Radical Trapping and Analysis Methods

2.1 Previous Methods and Results

Although the existence of free radicals in tobacco smoke has been recognized for decades, it is very difficult to identify and quantify these radicals in smoke because of the complexity of the smoke system and the dynamic nature of the reactive radicals. Many efforts have been made to measure the radicals in both particulate phase and gas phase smoke. Historically, the most commonly used magnetic technique for radical detection in particulate smoke is Electron Paramagnetic Resonance (EPR) spectroscopy, also known as Electron Spin Resonance (ESR) spectroscopy. Spin trapping techniques were employed to stabilize the short-lived radicals in the gas phase for later analysis. In recent years, mass spectrometry has become the main instrument to identify the structures of radicals in cigarette smoke. In this chapter, the direct detection by EPR, spin-trapping methods, liquid chromatography and mass spectrometry (MS) analysis are briefly reviewed.

2.1.1 Radicals Detection by Direct Electron Paramagnetic Resonance (EPR) from the Particulate Phase of Cigarette Smoke

Electron Paramagnetic Resonance (EPR) has been one of the most frequently used methods to directly detect radicals from the particulate phase of cigarette smoke and tar since 1958 (Lyons et al. 1958). EPR is a widely used technique to analyze unpaired electron substances such as some transitional metals and free radicals. As paramagnetic centers, free radicals resonate at fixed frequencies, at which the unpaired electrons can move between their two spin states $m_s=+\frac{1}{2}$ and $m_s=-\frac{1}{2}$ by either

absorbing or emitting electromagnetic radiation, which is recorded and converted into a spectrum. Based on the equation $h\nu = g_e \mu_B B_0$, the frequency is directly proportional to the magnetic field strength, B_0 , the Bohr magneton, μ_B , and g-factor, g_e . When the Bohr magneton μ_B is a physical constant, and the magnetic field's strength B_0 is fixed, the g-factor g_e can provide information about a paramagnetic center's electronic structure. In addition to the g-factor, multi-lined spectra from hyperfine coupling, which results from the interaction of an unpaired electron with nearby nuclear spins, can be species-sensitive and reveal structural information about the radicals.

Several works on free radicals in the particulate phase of cigarette smoke by direct EPR methods have quantified the number of spins, which is proportional to the concentration, ranging from $6 \times 10^{15} \sim 2 \times 10^{19}$ spins/cigarette (Lyons et al. 1958).

Pryor et al. found that cigarette condensation contains at least four types of paramagnetic species including an inorganic phosphorus radical, a graphitic carbon radical, a polyaromatic hydrocarbon (PAH) radical and a quinone-hydroquinone system with 6×10^{14} spins per cigarette and 3×10^{16} spins per gram of tar. The half-life of the quinone-hydroquinone system is about 12 days with a g factor of 2.0025 to 2.0029 (Pryor et al. 1983a).

Maskos et al. observed two types of primary radicals in the total particulate matter (TMP) of Bright tobacco by the direct EPR analysis. One displaying a five-line EPR spectrum with an apparent g factor of 2.0064 was assigned to an immobilized tyrosyl radical and the other displaying a single-line EPR spectrum with a g factor of 2.0035-2.0040 was assigned to a delocalized radical of a partially oxygenated polymeric species (Maskos et al. 2008).

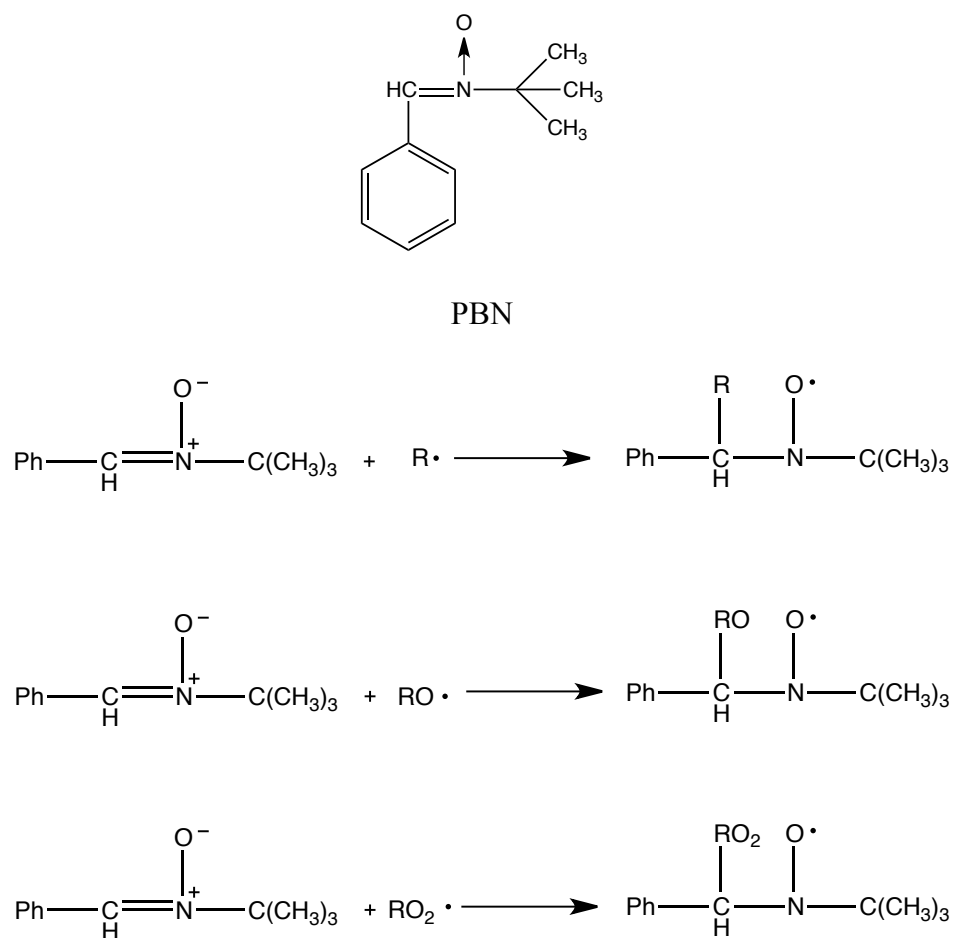
Although direct EPR was the first widely used method for radical detection, it has many disadvantages that have discouraged further applications in detection and quantification of free radicals in cigarette smoke. First, EPR cannot identify the exact structure, as it provides only minimal structural information of slight changes in hyperfine splitting constants and similar g factors. Second, direct EPR cannot detect short-lived free radicals in gas phase cigarette smoke; instead, it only allows detection of long-lived radicals in the particulate phase with a lifetime of minutes minute-long. Third, EPR doesn't separate the radicals and cannot provide information about specific molecular weights of the radicals detected.

Since the direct EPR method cannot provide unambiguous identification of free radicals, other trapping and analysis methods are required to better understand the radical populations in the gas phase cigarette smoke.

2.1.2 Radical Detection by EPR Spin Trapping Methods from Gas Phase Smoke

Free radicals in gas phase smoke are unstable transient species that have very short life times. It is very difficult to identify these radicals in the gas phase smoke by direct EPR detection without stabilization. During the last 50 years, many efforts have been made to overcome this problem by employing several spin trapping reagents and methods to trap the short-lived radicals in cigarette smoke for EPR analysis. Nitroso compounds and nitrones are the most commonly used species for the design of spin trapping reagents. Among all the variously substituted nitrones and nitroxides, α -

phenyl-N-tert-butylnitrone (PBN) was determined to be the best spin trap for quantifying free radicals from cigarette smoke (Bluhm et al. 1971; Pryor et al. 1983a).



Scheme 2.1. Structure of PBN and carbon-centered and oxygen-center radicals trapping reactions.

As shown in Scheme 2.1, carbon-centered and oxygen-centered radicals can be trapped by PBN by adding to the double bond of PBN, resulting in stable nitroxide radical, which can be detected by EPR.

In 1971, Bluhm et al. applied PBN spin trapping reagent in a benzene solution to trap the short-lived radicals in cigarette smoke, and found an alkoxyl radical;

however, no specific structure was identified by the EPR spectrum (Bluhm et al. 1971).

Pryor et al. used 0.1 M PBN in tertbutylbenzene solution to trap radicals ($R\bullet$) from both mainstream and sidestream gas phase smoke, and found 1×10^{16} spins per cigarette radicals in gas phase smoke (Pryor et al. 1983b). Surprisingly, they also found that the half-lives of these short lived-radicals were much longer than originally expected. Clearly inconsistent with their highly reactive nature, it was found that oxygen- and carbon-centered radicals can still be spin trapped from gas phase smoke after 5 min. To explain this discrepancy, they proposed a steady state mechanism in which free radicals in the gas phase are constantly generated and scavenged by NO_x reactions (Pryor et al. 1983c).

Since the spin adduct spectrum results depend greatly on the experimental conditions employed, it is crucial to develop a rigorous standard experimental protocol to compare results from different experiments. For optimization of the trapping conditions and better quantification of free radicals in cigarette smoke, Baum et al conducted a series of experiments including spin trap, EPR parameters, analysis and collection volume studies (Baum et al. 2003).

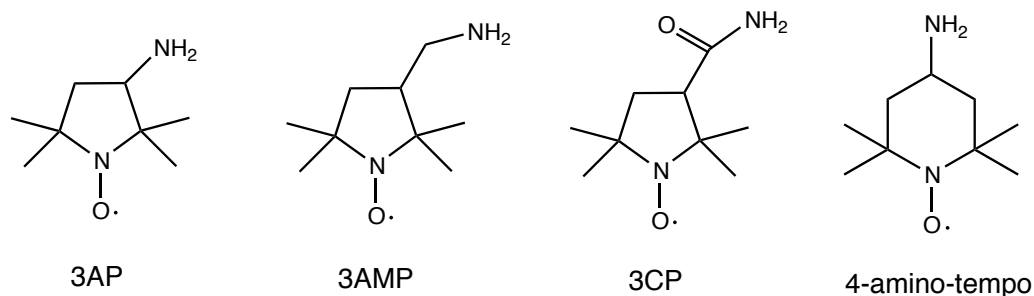
The development of spin trapping techniques has allowed researchers to convert highly reactive short-lived free radicals into more stable species for later analysis. The EPR spectrum can elucidate the functional groups for some categories of free radicals in cigarette smoke from the patterns and magnitude of the hyperfine splitting (Pryor et al. 1983c). However, the structure identification by EPR is very general, and doesn't allow for the unambiguous structural identification of the

individual free radical that is trapped. The indistinguishable g values and hyperfine splitting constants for the structurally similar spin adducts presents a major hurdle to accurate structure identification. In addition, due to the low rate constants of the trapping reaction, it only detects radicals in high concentration.

2.1.3 Fluorescence Probes for Short-lived Radical Detection

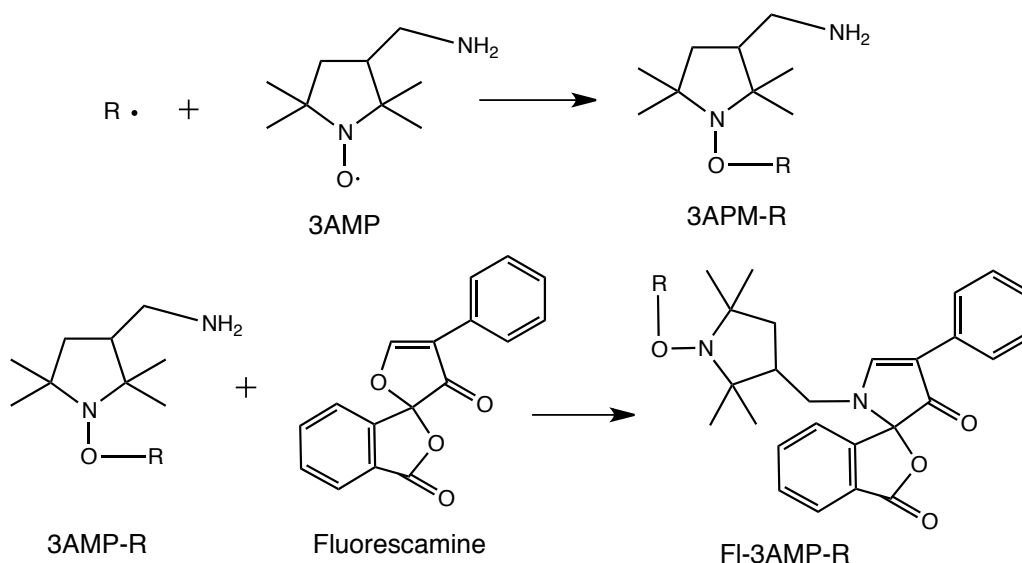
The limitations of EPR analysis in individual radical structural identification make it important to find alternative methods for better analysis of the free radicals in tobacco smoke.

During the late 1980's and early 1990's, Blough's group developed a highly sensitive fluorescence probe by employing di-tert-alkyl nitroxides as free radical trap (Green et al. 1990; Johnson et al. 1996; Kieber and Blough 1990). Yu Tang investigated a series of pyrrolidinyloxy nitroxides including 3-amino-2, 2, 5, 5-tetramethyl-1-pyrrolidinyloxy (3AP), 3-aminomethyl-2, 2, 5, 5-tetramethyl-1-pyrrolydinyloxy (3AMP) and 3-carbamoxyl-2, 2, 5, 5-tetramethyl-1-piperidinyloxy (4AT), as carbon-centered and oxygen centered radical traps. Structures of the investigated nitroxides are shown in Scheme 2.2. It shows that peroxy radicals oxidize 3AP to its corresponding oxoammonium cation, which rapidly decomposes to diamagnetic products.



Scheme 2.2. The structures of nitroxides.

The sensitivity of radical detection was greatly improved by covalently coupling the trapped radical adducts with a fluorescent tag to form diamagnetic products, which could then be detected optically by fluorescence detection.

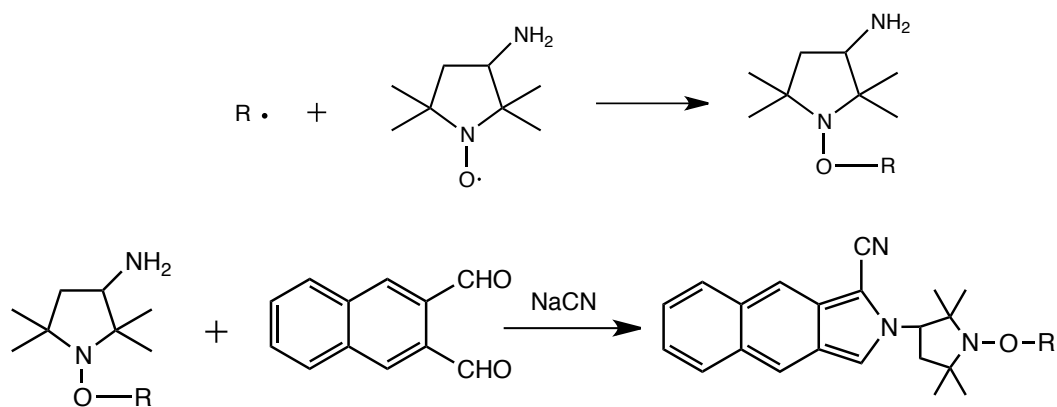


Scheme 2.3. Fluorescence trap for free radicals detection.

As shown in Scheme 2.3, 3AMP traps carbon-centered radicals and forms stable 3AMP-R adducts because of the robustness of the di-tert-alkyl structure. The resulting 3AMP-R adducts were derivatized with fluorescamine to produce highly fluorescent FI-3AMP-R adducts for quantitative analysis. The parent 3AMP-FI, however, doesn't exhibit fluorescence, owing to the efficient intermolecular

quenching of the excited singlet by 3AMP. When 3AMP traps carbon-centered radicals, it forms diamagnetic products and eliminates the intermolecular quenching pathway, producing intensive fluorescence signals that can be detected and analyzed by fluorescence detection.

Flicker and Green improved the trapping methods of carbon-centered radicals from the gas phase smoke by employing glass beads as trapping media solid support (Flicker and Green 1998). 3-amino-2, 2,5,5, -tetramethyl-1-pyrrolidinyloxy (3AP) was coated onto 3 mm diameter solid glass beads by dissolving 3AP into a small amount of acetone, which was added to the beads in a round bottom flask and dried via slow rotary evaporation at room temperature. After the beads are dried, they are transferred to a standard 15 cm distillation column to work as the solid support as shown in Figure 2.1. Radicals in gas phase smoke are trapped by 3AP on the coated beads when the smoke is passing through the column. After sampling, the radicals containing 3AP adducts are washed off the beads by a borate buffer, and then derivatized by naphthalenedicarboxaldehyde (NDA) for later analysis as shown in Scheme 2.4.



Scheme 2.4. Trapping of carbon-centered radical ($\cdot R$) by 3AP, followed by solution-phase derivatization with NDA to produce the fluorescent radical-adduct.

It has also been noted that Flicker and Green's work was the first case of gas phase radicals being trapped via the spin trap on the solid supported surface of glass beads (Flicker and Green 1998, 2001). This method greatly minimized the occurrence of potential secondary radicals, which is common in aqueous trapping methods.

In addition, with the separation of high performance liquid chromatography (HPLC), it is possible to individually identify and quantify radicals in tobacco smoke by their retention times and fluorescence intensities respectively. Flicker and Green found that different tobacco types produced a unique radical suite of 4-10 distinct peaks, each of which indicates a different radical. Based on the fluorescence intensity, 52-194 nmol of carbon-centered radicals was quantified from different types of tobacco including Marlboro cigarette, Djarum clove cigarette and Swisher Sweet cigar (Flicker and Green 2001).

While the separation and quantification of the fluorescence tagging methods by HPLC greatly enhanced the understanding of the numbers and quantities of radicals in cigarette smoke, the specific structures of the trapped radicals are still

unidentified. To detect and analyze specific structure of trapped radical in tobacco smoke, a combined liquid chromatography/mass spectrometry method was employed.

2.1.4 Nitroxide Spin Trapped Radicals Analysis by Mass

Spectrometry

During the last ten years, many applications of mass spectrometry in trapped radical identification and quantification have been found. Because of the complex nature of tobacco smoke, it is very difficult to identify trapped radicals from the smoke mixture by simple MS alone. The liquid chromatography tandem mass spectrometry allows both separation and identification for a smoke sample, providing better results for the structure identification. Electrospray ionization mass spectrometry (ESI-MS) is sensitive to the fragmentation of 3AP-R adducts, which allows structural identification of the nitroxide trapped smoke radicals. Many other instrumental methods including Precursor Ion Monitoring (PIM), Selected Ion Monitoring (SIM) were also conducted for smoke sample screening. In Wooten's work, precursor ion monitoring (PIM) was utilized for screening 3AP-R samples for the major fragments at m/z 98 to identify less abundant radical adducts (Bartalis et al. 2009). High-resolution mass spectrometry was also used to identify the exact mass of the trapped radicals from cigarette smoke.

Departing from the long accepted steady state mechanism, two types of radicals, acyl and alkylaminocarbonyl radicals, were first time identified from cigarette by Bartalis et al. using HPLC-MS/MS, a high-resolution mass spectrometer,

in analysis of 3-AP and the 3-cyano-proxyl free radical, suggesting a new mechanism for radical generation in tobacco smoke.

2.2 Trapping and Analysis Methods in This Study

In this study, we adopted a solvent-free radical trapping method to trap carbon-centered radicals, based on previous work (Flicker and Green 1998, 2001). We modified the bead trapping method by directly coating the trapping agent, 3-amino-2, 2, 5, 5-tetramethyl-proxyl (3AP), onto the inner wall of a distillation column to reduce the effect of total particulate matter (TPM) trapped by the beads. Smoke from a burning cigarette, or the gas mixture in the model system, flowed through the coated distillation column; 3AP reacted with the carbon-centered radicals to form stable 3AP adducts, which were then either identified by LC-MS or, for quantification, derivatized with naphthalene-2, 3-dicarboxaldehyde (NDA).

3AP-R adducts were identified and quantified after trapping by high-performance liquid chromatography with fluorescence detection (HPLC-FLD) analysis, electrospray mass spectrometry (ESI-MS) tandem mass spectrometry (MS/MS), and liquid chromatography tandem mass spectrometry (LC-MS). The analysis flow diagram is shown in Figure 2.1 below.

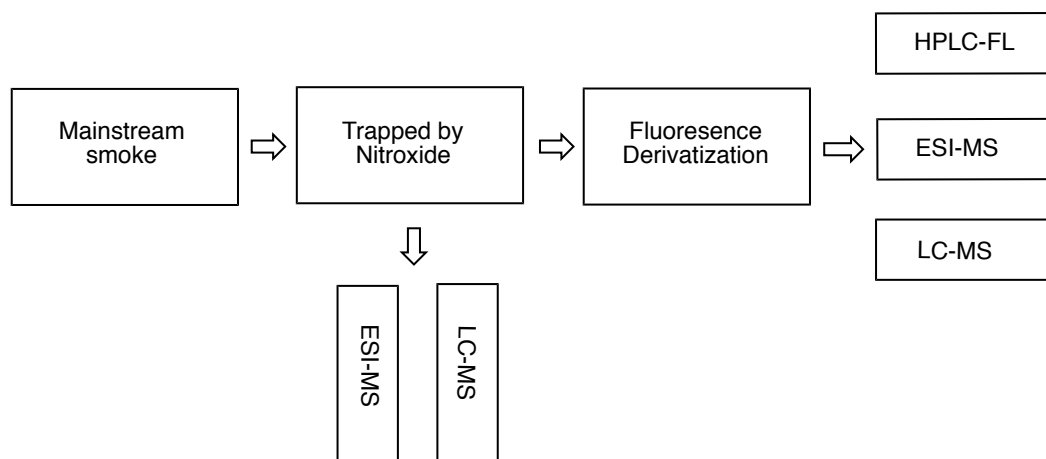


Figure 2.1. Analysis flow diagram for the radicals in mainstream smoke.

The detection of free radicals in gas phase cigarette smoke by mass spectrometry and high performance liquid chromatogram will be discussed in the chapter 3 and 4.

The concentration sensitivity of 3AP as the trapping agent will be investigated by computational simulation in Chapter 5.

2.3 References

- Baum SL, Anderson IGM, Baker RR, Murphy DM, Rowlands CC. 2003. Electron spin resonance and spin trap investigation of free radicals in cigarette smoke: development of a quantification procedure. *Anal Chim Acta* 481(1): 1-13.
- Bluhm AL, Weinstein J, Sousa JA. 1971. Free radicals in tobacco smoke. *Nature* 229(5285): 500.
- Flicker TM, Green SA. 1998. Detection and separation of gas-phase carbon-centered radicals from cigarette smoke and diesel exhaust. *Analytical Chemistry* 70(9): 2008-2012.
- Flicker TM, Green SA. 2001. Comparison of gas-phase free-radical populations in tobacco smoke and model systems by HPLC. *Environ Health Perspect* 109(8): 765-771.
- Green SA, Simpson DJ, Zhou G, Ho PS, Blough NV. 1990. Intramolecular Quenching of Excited Singlet-States by Stable Nitroxyl Radicals. *Journal of the American Chemical Society* 112(20): 7337-7346.
- Jia M, Tang Y, Lam YF, Green SA, Blough NV. 2009. Prefluorescent Nitroxide Probe for the Highly Sensitive Determination of Peroxyl and Other Radical Oxidants. *Analytical Chemistry* 81(19): 8033-8040.
- Johnson CG, Caron S, Blough NV. 1996. Combined liquid chromatography/mass spectrometry of the radical adducts of a fluorescamine-derivatized nitroxide. *Analytical chemistry* 68(5): 867-872.

Kieber DJ, Blough NV. 1990. Determination of Carbon-Centered Radicals in Aqueous-Solution by Liquid-Chromatography with Fluorescence Detection. *Analytical Chemistry* 62(21): 2275-2283.

Lyons MJ, Gibson JF, Ingram DJ. 1958. Free-radicals produced in cigarette smoke. *Nature* 181(4614): 1003-1004.

Maskos Z, Khachatryan L, Dellinger B. 2008. Formation of the persistent primary radicals from the pyrolysis of tobacco. *Energ Fuel* 22(2): 1027-1033.

Pryor WA, Hales BJ, Premovic PI, Church DF. 1983a. The radicals in cigarette tar: their nature and suggested physiological implications. *Science* 220(4595): 425-427.

Pryor WA, Prier DG, Church DF. 1983b. Electron-Spin Resonance Study of Mainstream and Sidestream Cigarette-Smoke - Nature of the Free-Radicals in Gas-Phase Smoke and in Cigarette Tar. *Environ Health Persp* 47(Jan): 345-355.

Pryor WA, Tamura M, Church DF. 1983c. Spin Trapping Study of the Radicals Produced in Nox Olefin Reactions - a Model for Cigarette-Smoke. *Abstr Pap Am Chem S* 186(Aug): 221-ORGN.

Chapter 3: Structural Identifications of Gas Phase Tobacco Smoke Radicals by Mass Spectrometry¹

¹ Part of this chapter will be submitted to a peer-reviewed journal.

3.1 Introduction

As discussed in Chapter 2, the unambiguous detection of radicals in cigarette smoke is one of the advantages of the LC-MS method over the spin trapping methods. In this work, liquid chromatography tandem electrospray ionization mass spectrometry was employed to analyze the structures for the radicals trapped from acetone photolysis standard, NO/air/CH₃CHO model system, and gas phase cigarette smoke. Direct infusion and LC-MS extracted ion chromatogram (EIC) of the CH₃CO-3AP were applied to derivatized NDA-3AP-R and underivatized 3AP-R adducts respectively.

3.1.1 Principles of Electrospray Ionization Mass Spectrometry

Electrospray ionization mass spectrometry (ESI-MS) is a soft ionization technique, which provides molar mass information on a molecular ion $[M+1]^+$. Collision induced dissociation (CID) occurs during the ionization and travelling processes, revealing fragmentation structure information. It is an ideal mass spectrometry technique to couple with liquid separation methods such as high performance liquid chromatography (HPLC) and capillary electrophoresis (CE). Because of the complex nature of tobacco smoke sample, LC-MS is a good choice for separation and structural identification. A schematic of the electrospray ionization process is shown in Figure 3.1.

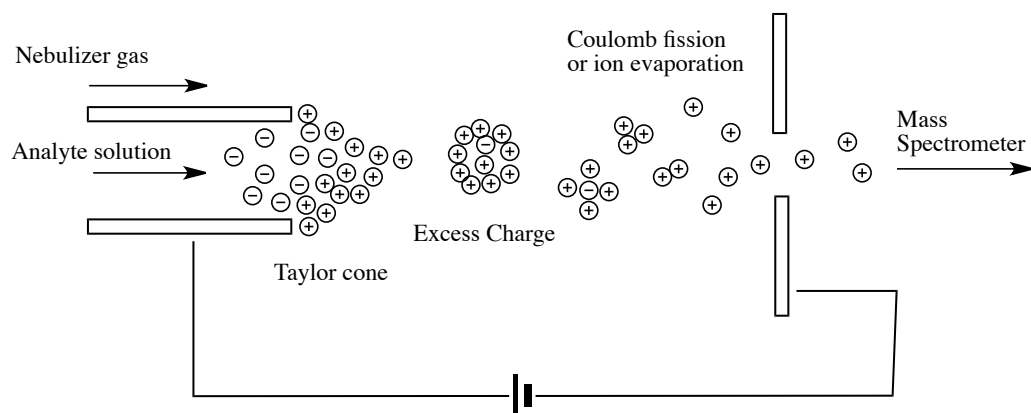


Figure 3.1. Schematic representation of the electrospray ionization process adapted from Cech and Enke 2001.

To accomplish this analysis, a very slow flow of diluted analyte or HPLC separated solution is pumped through a capillary tube by direct infusion, where a positive or negative voltage is applied at 2-5 kV. This voltage results in a charge separation at the surface of the introduced solution, and causes the liquid to protrude from the capillary tip to form a “Taylor cone”. When the coulombic repulsion of the surface charge is equal to the surface tension of the solution, the cone reaches the Rayleigh limit, and positively or negatively charged droplets detach from its tip and travel down a pressure gradient towards the analyzer of the mass spectrometer. As far as the generation of molecular ions is concerned, there are several proposed mechanisms, including the coulomb fission mechanism and ion evaporation mechanism. The coulomb fission or charge residue mechanism refers to a process in which large charged droplets undergo successive breakup into smaller and smaller droplets because of the increased charge density due to solvent evaporation (Gu et al. 2007). The ion evaporation mechanism suggests that when the coulombic repulsion resulting from solvent evaporation eventually overcomes the liquid’s surface tension,

charged ions are expelled from the droplet surfaces (Cech and Enke 2001). Both mechanisms result in single ions with one or more charges, which can be detected by a range of mass analyzers based on their m/z ratio.

Collision-induced Dissociation

Collision-induced dissociation (CID), sometimes referred to as collision-activated dissociation (CAD), is ion dissociation that happens when part of the translational energy of the ion is converted to internal energy during collision with neutral species such as a carrier gas or instrument interfaces. The dissociation can be controlled by the voltage applied to the capillary tip, and provides different degrees of fragmentation, which reveal the partial or complete structural information for targeted compounds.

Multiply Charged Ions

In ESI-MS, the ionization process can provide molecules in multiply charged states in the form of $[M+nH]^{n+}$. In addition, when sodium or other metal salts are present in the solution, a metal adduct ion, such as $[M+Na]^+$ can also be observed.

3.1.2 Principles of Liquid Chromatography Mass Spectrometry

Liquid chromatography-mass spectrometry (LC-MS) is a combination of high performance liquid chromatography (HPLC) and mass spectrometry (MS). As a powerful technique widely used in pharmaceutical, environmental, biochemical and biotechnological areas, LC-MS has the capabilities of both separation and mass analysis for unknown analytes in a mixture. As shown in Figure 3.2, LC-MS is composed of a sample injector system (a fixed-volume loop or autosampler), the

HPLC system for analyte separation, a mass spectrometer, and a LC-MS interface connecting the two instruments.

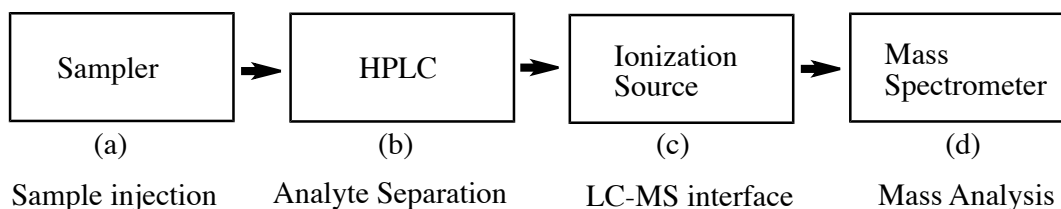


Figure 3.2. The LC-MS components: (a) Sampler, usually a fixed-volume loop injector or autosampler for multiple samples, introducing analytes into a high-pressure system; (b) HPLC, separating analytes, usually based on their polarities; (c) ionization source, the interface between LC and MS; (d) Mass spectrometer, conducting mass analysis for analytes eluted at different retention times.

The interface connecting liquid chromatogram and mass spectrometry is one of the challenging aspects of LC-MS. First, the flow rate of the HPLC mobile phase has to be optimized to meet ion source requirements in the MS. In HPLC, the common flow rate is 0.5 to 1.0 mL/min, while the ESI interfaces are optimized for flow-rates between 50 and 200 μ L/min for ionization in the MS. The nano-ESI interfaces, however, are usually applied at sub- μ L/min flow rates (Niessen 1999).

Second, the mobile phase for HPLC should be volatile and easily ionized in the mass spectrometer. Non-volatile materials such as buffer salts, which improve the HPLC separation efficiency, may be a cause for concern in the mass spectrometric analysis. Although a small amount of salt can aid the ionization, extra nonvolatile salts may contaminate the ion source and suppress the signal in the mass spectrometry. In addition, nonvolatile buffers such as phosphate and borate buffers can block the capillary in the probe. To avoid this issue, volatile buffers such as triethylamine (TEA), ammonium acetate, acetic acid, and formic acid are added to the mobile phase to maintain the pH. Otherwise, an additional salt removal procedure is required before introducing the separated analytes into the mass spectrometer.

Electrospray ionization (ESI) and atmospheric pressure chemical ionization (APCI) are two common ion sources that can be used as the interface between the HPLC and mass spectrometer. The principle of ESI is described in 3.1.1. In APCI, the effluents from HPLC are heated and vaporized in dry nitrogen, and then ionized via chemical ionization mechanisms to produce charged analyte ions (Bruins et al. 1987).

LC-MS is an extremely valuable technique for molecular mass determination of nitroxide-adducts, especially because LC facilitates analysis by providing separation ability to a complex matrix such as tobacco smoke. Based on the nature of this technique, many parameters can be varied to optimize this signal. For example, flow rate, mobile phase composition, buffer concentration, pH, and fragmentation voltage are adjustable for better performance.

3.1.3 The Application of Liquid Chromatography Mass

Spectrometry in Identification of Radicals

As one of the most powerful techniques for structural analysis, mass spectrometry is a great tool for determination of the molecular mass of nitroxide-adducts from a complex matrix such as tobacco smoke. The soft-ionization of electrospray provides information on the molecular mass, and the collision-induced dissociation further elucidates the structure. In addition, LC-MS provides information on both polarities and masses for the smoke sample. Especially significant is the selected ion monitoring (SIM) in LC-MS, as it can select and monitor the mass range of the targeted 3AP adducts and compare the retention times between smoke and the standard sample for better structural identification.

Liquid chromatography mass spectrometry was chosen over gas chromatography mass spectrometry (GC-MS) because the R-3AP samples were already in liquid phase after being washed off from the 3AP coated beads. In addition, 3AP-R adducts decompose at high temperature in GC-MS (Johnson et al. 1996). Considering the structure of the R-3AP precursor, which contains an amine group, a positive mode was chosen. As soft ionization techniques, electrospray (ESI) and matrix-assisted laser desorption/ionization (MALDI) both provide molecular ion mass information. For MALDI, the matrix is placed on the plate or mixed with the sample before spotting analytes onto the metal plate. The energy absorbed by the matrix causes the ionization of the analytes. Typically, the charged ions are analyzed by the time-of-flight (TOF) mass analyzer known as MALDI-TOF analysis. However, ESI

surpasses MALDI in chromatographic compatibility, which allows separation before the sample is introduced into the mass spectrometry. To separate the complex components in the tobacco smoke sample, a good separation method such as a C18 column is required. The tandem mating of LC and MS greatly improves the results and provides information on the compositions and structures.

The mass range of the targeted ions is from 50 to about 1000 amu. Several different mass analyzers can be used to analyze these ions. Triple quadrupole MS is one of the most common MS/MS techniques. Combined with soft ionization techniques such as ESI and APCI, it gives structural information for the intact molecule. Compared to single quadrupole, triple quadrupole can provide more information about the sample. Both precursor-ion spectrum and product-ion spectrum can be obtained with the triple quadrupole instrument by scanning and holding different quadrupoles alternatively. In Wooten's work (Bartalis et al. 2009), precursor ion monitoring (PIM) was utilized for screening 3AP-R samples for the major fragments at m/z 98 to identify less abundant radical adducts. In our work, selected ion monitoring (SIM) was applied to $\text{CH}_3\text{C}(\text{O})\text{-3AP}$ at m/z of 201 to compare the retention times in all the samples from fresh Marlboro cigarette smoke, gas phase model, and aqueous acetone photolysis.

The identical m/z values of many organic compounds present in the smoke plume make it impossible to differentiate those with the same nominal mass by low-resolution mass spectrometry. High-resolution mass spectrometry is suggested to resolve this problem by providing the exact mass measurement.

In this study, mass spectrometric analysis was conducted with a Thermo

Finnigan LCQTM Advantage LC-MS with ion trap mass spectrometer, which can perform single stage LC/MS and two-stage LC/MS/MS experiment. The LC-MS is composed of an ESI interface, LC pump, syringe pump, quadruple ion trap, and photodiode array (PDA) detector. The sensitivity test is conducted by injecting 5 μ L of 10 ng of Reserpine, resulting in a signal noise ratio of 10:1 at m/z 609 with positive ion mode. Based on the results in our experiment, the mass resolution at m/z 376 is 2500 and at m/z 157 is 830.

3.2 Experimental and Methods Development

3.2.1 Sample Preparation

Chemicals: 3-amino-2, 2, 5, 5-tetramethyl-proxyl (3AP), naphthalene-2, 3-dicarboxaldehyde (NDA), sodium cyanide, cyclopentylamine (CPA), and HPLC grade methanol were purchased from ACROS. All chemicals were of the highest purity available and were used without further purification. Marlboro brand cigarettes were purchased from a local vendor and 3R4F Kentucky Reference cigarettes were purchased from University of Kentucky, Lexington (Davies and Vaught 1990). These cigarettes were 84 mm long, weighing 1.06 g and with filter length of 27 mm. A detailed description of these cigarettes has been reported (RCP 2011). Solutions of NDA in acetonitrile (10.0 mM) and sodium cyanide solutions (10.0 mM) were prepared every two weeks and stored at -5 °C. Water used for all solutions was from a Millipore Milli-Q system.

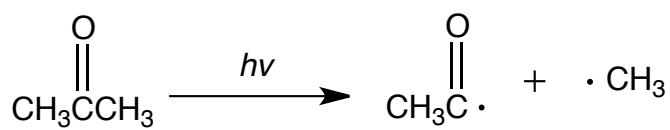
Acetone Photolysis Standard Preparation

Standard adducts of acetyl radical were made photochemically by the

following procedure: 3AP (0.5 mM) and acetone (50 mM in water) were irradiated in a 1-cm quartz cell with a 150-W xenon lamp for 30 min. The solution was deoxygenated for 5 min with an N₂ flow before and during the irradiation by bubbling with N₂ (99.99%, Praxair Distribution Inc.).

Scheme 3.1 shows that when acetone is photolysized under ultraviolet light, the bond between C=O and CH₃ breaks, resulting in an acetyl radical and a methyl radical.

Both radicals from acetone photolysis are trapped by 3AP later as standards. 3AP-R standard solution in 50/50 methanol/H₂O were directly injected into the mass spectrometry and detected by ESI-MS.



Scheme 3.1. Acetyl radical and methyl radical are generated by acetone photolysis

Smoke Sample Preparation

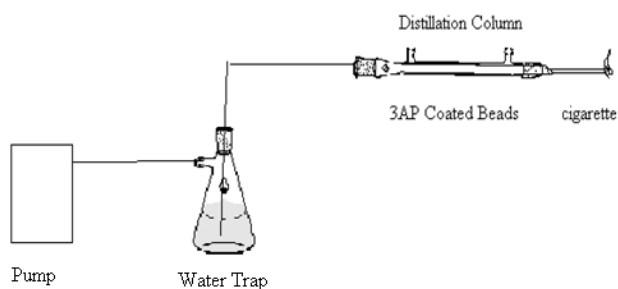


Figure 3.3. Apparatus used to trap carbon-centered radicals from the burning cigarette.

0.02 g 3AP in small amount of acetone was coated to the inner wall of the column and dried by rotary evaporation at room temperature. A pump with flow rate 0.6 L/min was used to draw smoke across the column. To avoid smoke entering the pump directly, a water trap was applied to absorb the most organic compounds after the trapping process as shown in Figure 3.3. Five Marlboro cigarettes were smoked sequentially for one sample. It took about 2 minutes to finish one cigarette under the working pump flow rate. Nothing else besides the manufacturer's cigarette filter was used before it reached the 3AP-coated column.

Comparison experiments employed the FTC smoking methods, which consists of a 35 mL puff volume drawn over a 2 second duration once per minute. The total volume of column and tubing is about 146 mL, while each puff is 35 mL. Neglecting diffusion, it takes 250 s for one puff of smoke to be completely removed from the trapping column. Five Marlboro or 3R4F Kentucky Reference cigarettes were smoked sequentially for each analysis.

NO/CH₃CHO/O₂ Model Sample Preparation

A similar procedure was followed for a NO/CH₃CHO/O₂ model. A solution of 0.02 g 3AP in a small amount of acetone was coated on the inner wall of the 140-mL sampling column and dried by rotary evaporation at room temperature. A model system employed to assess the gas-phase reaction of NO₂ and CH₃CHO is shown in Figure 3.5. Air was flowed across 3 mL of liquid phase acetaldehyde at room temperature to carry gas phase CH₃CHO to a Y-junction, where it encountered 1000 ppm NO (certified 1003.1 ppm, Praxair Distribution Inc.) in N₂. As NO met the air, it was oxidized to NO₂ by oxygen, producing a distinctive brown color. A distillation

column, which was coated with 3AP on the inner wall, acted as the reaction vessel and the trapping surface. When the gas mixture reached the column, radicals were trapped by 3AP (Figure 3.5) and analyzed later by HPLC and LCMS. The airflow came from the building supply. Trace NO_2 from the NO tank was removed by bubbling NO through a 50% solution of sodium hydroxide (Not shown in Figure 3.4).

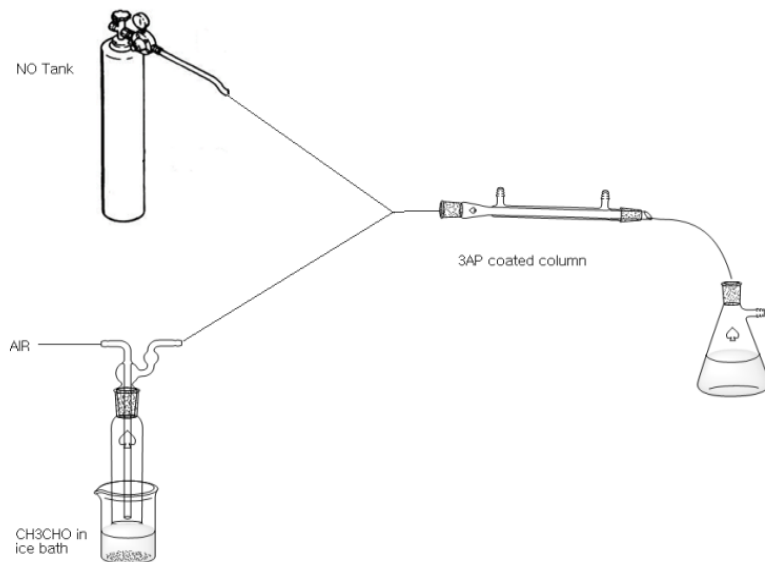


Figure 3.4. Diagram of gas mixture model reaction apparatus.

NDA Derivatization and Purification

After sampling, the 3AP adducts were washed from the sampling column with 10 mL methanol. Next the solution was filtered with a Hyper Sep C18 column (Thermo Electron Corporation[®]), giving a light yellow solution, while the dark colored R-3AP adducts remained on the column. 10 mL of methanol was used to flush the sample from the column, giving a dark yellow solution. For derivatization, 500 μL of filtered sample solution, 200 μL of sodium cyanide solution, and 200 μL of

NDA solution were added sequentially to a foil-wrapped glass vial and allowed to react for 30 min.

After derivatization, the 3AP adduct solution was filtered with a 0.2- μ m syringe filter (HPLC syringe filter, Alltech[®]), and yellow material (R-3AP-NDA) precipitated onto the filter. This yellow precipitate was washed off with 1 mL of 80% methanol in water. The filtered solution and reconcentrated precipitate were diluted by 50 times in 50/50 MeOH/H₂O to be injected into electrospray mass spectrometry (ESI-MS) and liquid chromatography mass spectrometry (LC-MS).

3.2.2 Instrumentation

Mass spectrometric analyses were conducted with a Thermo Finnigan LCQTM Advantage LC-MS. The mobile phase was 50/50 methanol/H₂O with 0.2% acetic acid. The Thermo BioBasic-18125 \times 4mm 5 μ m particle-packed HPLC column was used for LC separation. The LC-MS operating parameters are listed in Table 3.1. Selected ion monitoring (SIM) was employed to detect 3AP-C (O) CH₃ (m/z 200.15).

Table 3.1. Thermo Finnigan LCQTM Advantage LC-MS conditions.

| | |
|------------------------|--------------|
| flow rate | 0.200 mL/min |
| capillary voltage | 3.95 kV |
| cone voltage | 35 V |
| sheath gas flow | 29.00 L/min |
| auxiliary gas flow | 49.47 L/min |
| capillary temperature | 252.30 °C |
| ND collision potential | 20 V |

3.3 Results

To better compare the mass spectrometry patterns among different samples, we investigated several standard samples including 3AP solution and acetone photolysis standard for both underivatized and derivatized samples.

3.3.1 3AP Standard Analysis

As shown in Figure 3.5, the full mass spectrum of the 3AP solution in 50/50 MeOH/H₂O provides the molecular formula of the oxidized 3AP or so-called oxoammonium cation, C₈H₁₇N₂O⁺ (Jia et al. 2009), with m/z of 157.13 as shown in Scheme 3.2. This oxidization reaction may occur during the collision-induced dissociation.

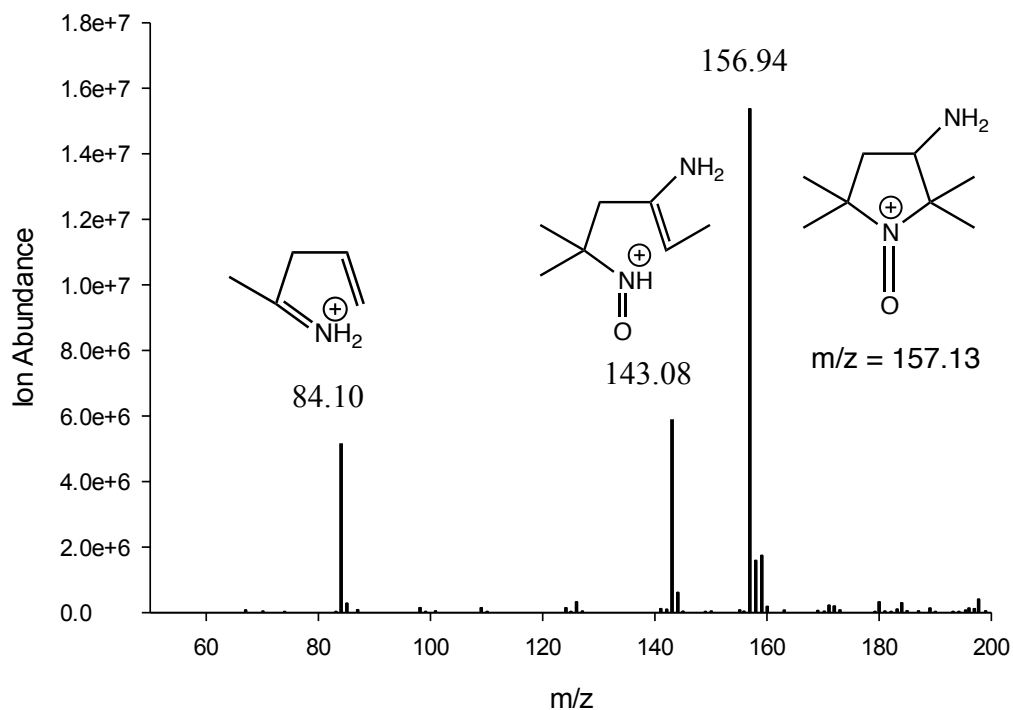
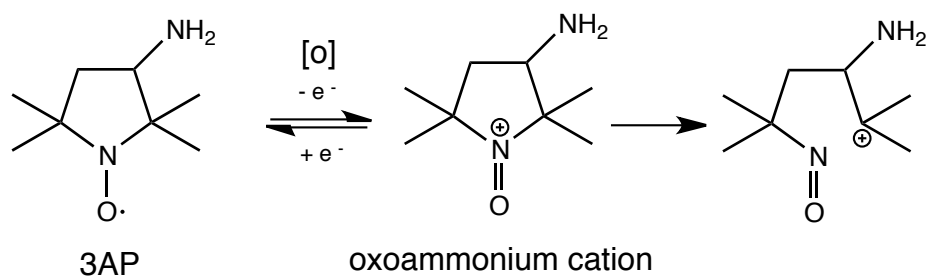


Figure 3.5. The full mass spectrum for 3AP solution in 50/50 MeOH/H₂O with m/z range of 50-200 acquired in profile mode.



Scheme 3.2. 3AP oxidization reactions and adducts.

Further CID revealed a species with molecular formula C₅H₁₀N⁺ at m/z 84.08. The peak at m/z of 84 is common fragmentation of 3AP (Bartalis et al. 2009), which could have resulted from ring opening and rearrangement. The isotopic ratio of 85.08/84.08 of the suggested structure is 5.8%, which is close to 4.6% in Figure 3.5.

3.3.2 Acetone Photolysis Standard Analysis

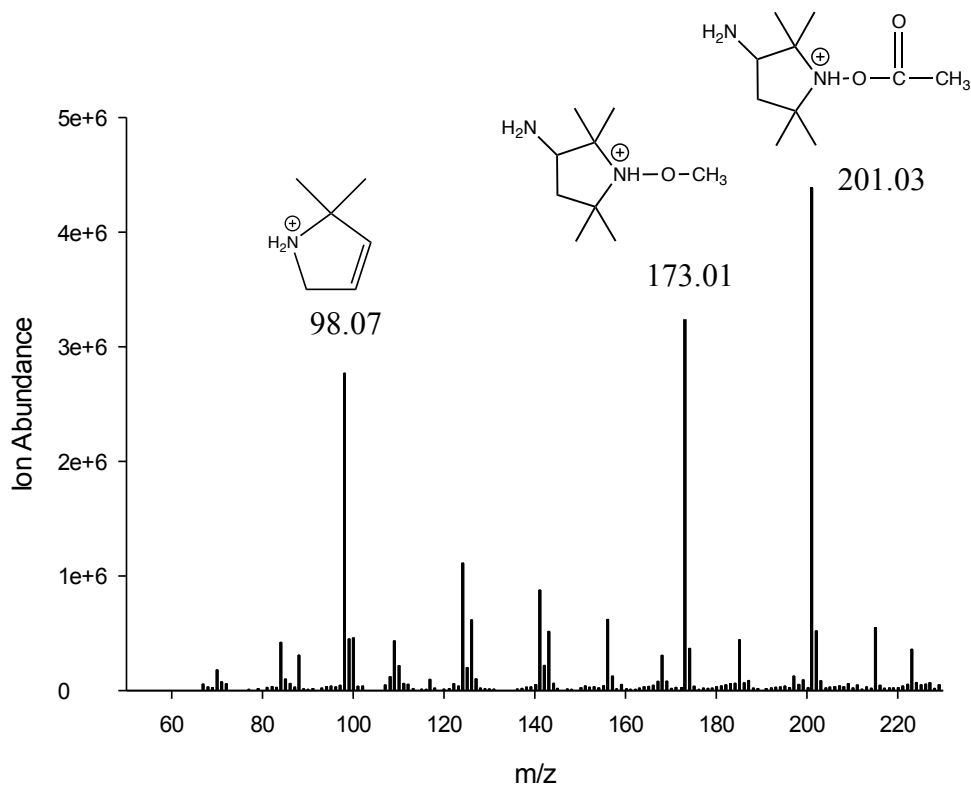


Figure 3.6. Full mass spectrum for the acetone photolysis standard sample with m/z range of 50-500 acquired in profile mode.

The full mass spectrum for the acetone photolysis sample is shown in Figure 3.6. The resulting acetyl and methyl radicals from acetone photolysis were trapped by 3AP and detected by ESI-MS. Figure 3.6 shows the presence of the $[M+1]^+$ peak of $\text{CH}_3\text{C}(\text{O})\text{-3AP}$ at m/z of 201.03 and $\text{CH}_3\text{-3AP}$ at m/z of 173.01. Collision-induced dissociation (CID) revealed a fragmentation peak at m/z of 98.07, which corresponds to a major fragment of 3AP's structure with molecular formula $\text{C}_6\text{H}_{12}\text{N}^+$ (Bartalis et al. 2009).

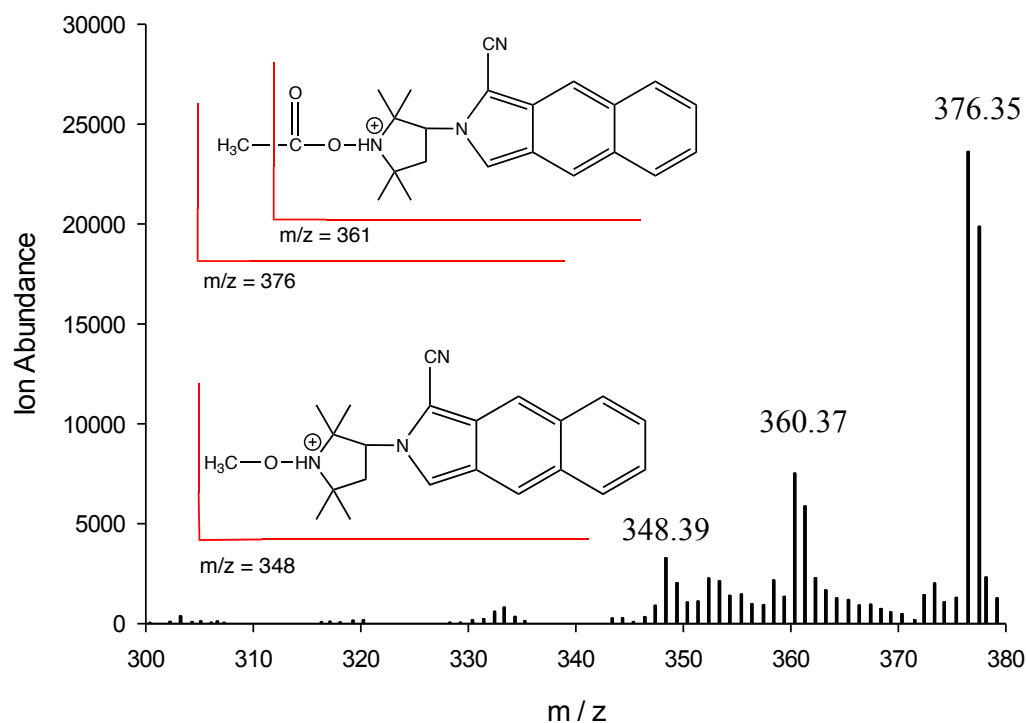


Figure 3.7. ESI-MS spectrum of R-3AP-NDA adduct of the acetone photolysis sample with m/z range of 300-380.

The acetone photolysis sample trapped by 3AP was derivatized by naphthalene-2, 3-dicarboxaldehyde (NDA) and was analyzed by ESI-MS as an additional means to confirm the structures. Both molecular ions of CH_3 -3AP-NDA (m/z 376) and CH_3CO -3AP-NDA (m/z 348) were detected as shown in Figure 3.7. In addition, a loss of methyl group (-15) from the CH_3CO -3AP-NDA (m/z 376) due to CID was also observed in Figure 3.7.

3.3.3 Smoke Samples

Two different cigarettes, a commercial Marlboro cigarette and the research 3R4F reference cigarette, were sampled under two different smoking conditions, including continuous pump drawn method and FTC standard syringe drawn method.

After sampling, the 3AP adducts were washed from the sampling column with 10 mL methanol and filtered with a Hyper Sep C18 column. Each sample was derivatized as described in the experimental section. Before injecting into LC-MS, all the samples were desalted and diluted with 50/50 MeOH/H₂O.

The acetyl radical was detected unambiguously in all of the cigarette smoke samples by electrospray ionization mass spectrometry (ESI-MS) and tandem mass spectrometry (MS/MS) for both the 3AP-trapped smoke sample and its NDA derivative are shown in the figures below.

3AP-R from the Marlboro Pump Drawn Sample

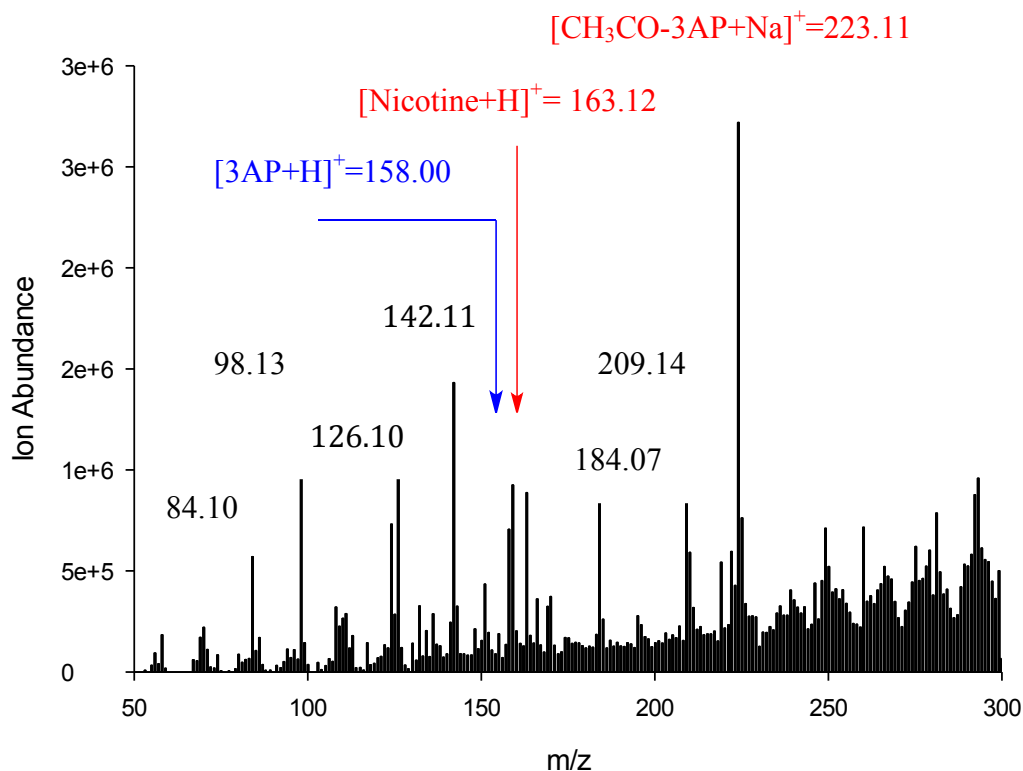


Figure 3.8. ESI-MS full spectrum of smoke sample from Marlboro continuous drawn method with m/z range of 50-300.

Full scan provides a full mass spectrum of the Marlboro continuously drawn smoke sample. The mass analyzer is scanned from m/z of 50 to 2000 and the spectrum in Figure 3.8 was expanded from m/z 50 to 300 to show the targeted peaks.

The most abundant peak, m/z 223, corresponds to CH_3CO -3AP with sodium adduct. In addition, excess unreacted 3AP appears at m/z 158 as the molecular ion. Expected fragmentation of 3AP at m/z 98 and 84 also appears in the spectrum. As one of the major components in cigarette smoke, peak of nicotine is also observed at m/z 163. Many other peaks suggest the presence of other less abundant radicals trapped

by 3AP. Other components of cigarette smoke that were rinsed off the column with the 3AP adducts also contribute to the background peaks.

To better compare the pattern, 5 μM Nicotine in 50/50 MeOH/H₂O was directly infused into ESI-MS as a standard, and the molecular ion and couple CID fragmentation peaks were observed in Figure 3.9. The molecular ion $[\text{M}+\text{H}]^+$ is at 162.93, which corresponds to nicotine ($[\text{M}+\text{H}]^+$ of 162.12) with a hydrogen ion.

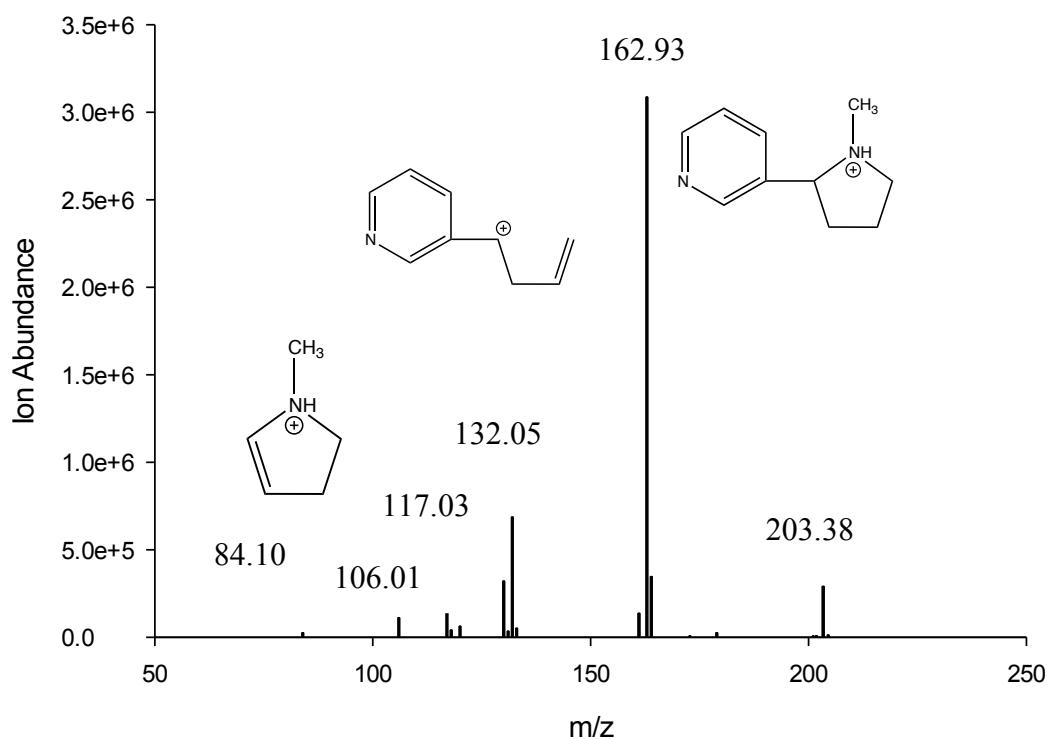


Figure 3.9. ESI-MS analysis of nicotine with m/z range of 50-210 acquired in profile mode, showing the molecular ion at m/z 162.93. CID also occurred in this mass spectrum, resulting in a loss of $\text{NH}_2\text{-CH}_3$ at m/z 31.

3AP-R from Marlboro Pump Drawn Sample

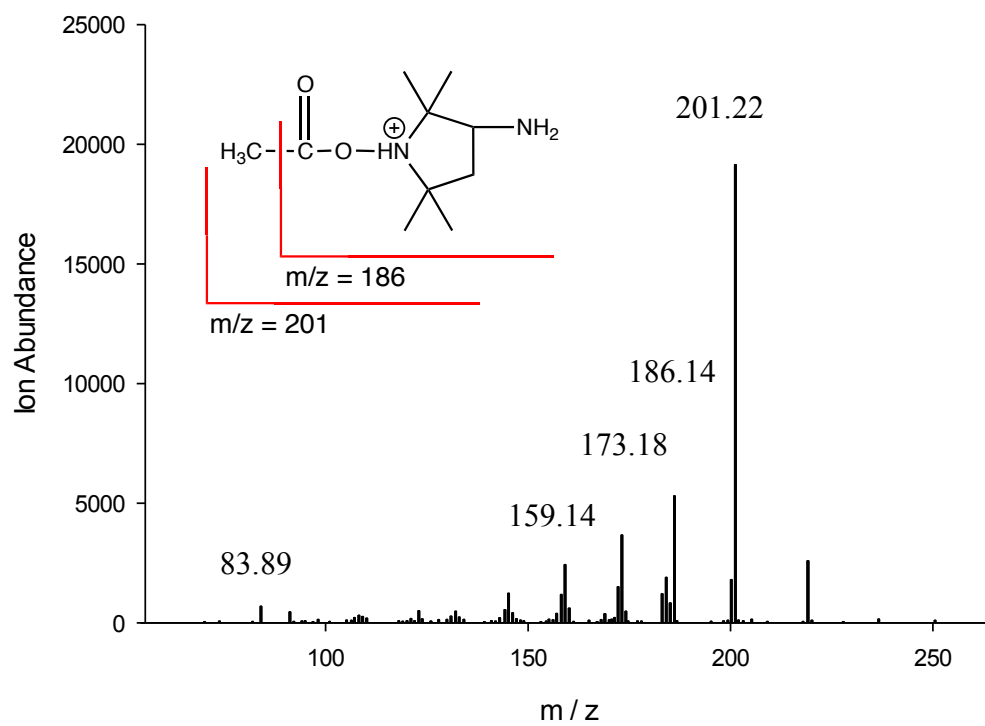


Figure 3.10. ESI-MS/MS spectrum of R-3AP adduct of the Marlboro continuously drawn smoke sample with m/z range of 50-270.

As shown in Figure 3.10, MS/MS was applied to the targeted peak at m/z of 201, which corresponds to CH_3CO -3AP. MS/MS of the peak at m/z of 201 shows a methyl group loss (-15) from the molecular ion.

NDA-3AP-R from Marlboro FTC Drawn Sample

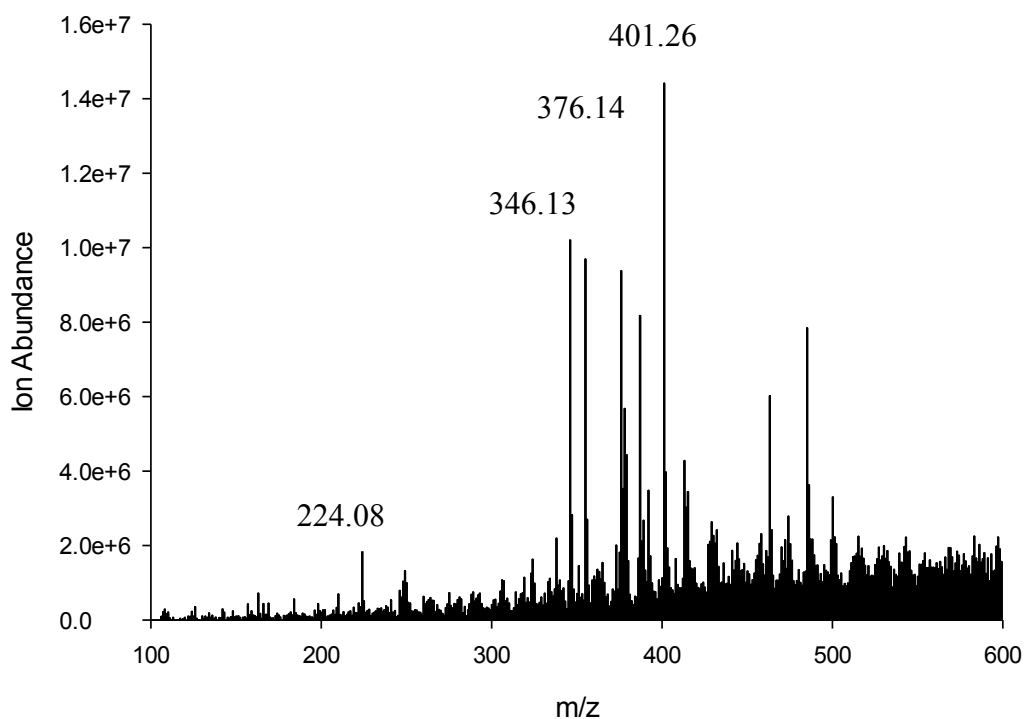


Figure 3.11. ESI-MS full spectrum of R-3AP-NDA adduct of the Marlboro FTC drawn smoke sample with m/z range of 100-600.

Figure 3.11 shows that multiple peaks are present in the ESI-MS full spectrum of the derivatized Marlboro continuously drawn smoke sample. Further structural identification of the most abundant peak at m/z of 376 were investigated by MS/MS as shown in Figure 3.12.

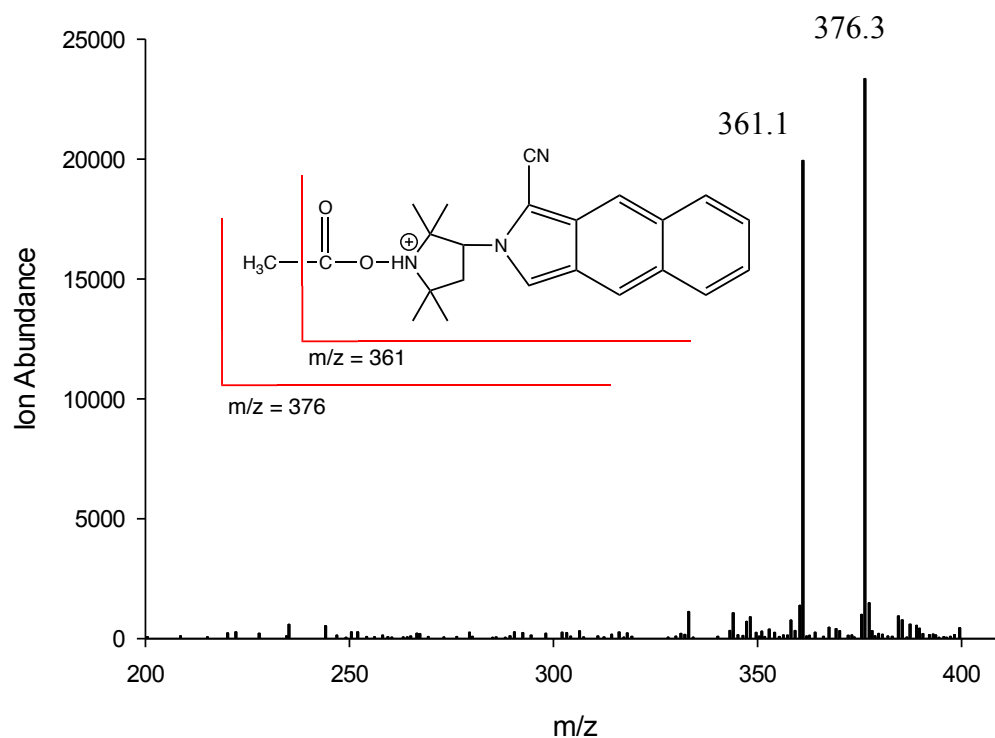


Figure 3.12. ESI-MS/MS spectrum of R-3AP-NDA adduct of the Marlboro continuously drawn smoke sample with m/z range of 200-400. MS/MS of 376 at 20.00 shows a methyl group loss (-15).

ESI-MS spectrum of the smoke sample shows the presence of the $[M+1]^+$ peak of $\text{CH}_3\text{C}(\text{O})$ -3AP-NDA at m/z of 376.39 in Figure 3.12. Collision-induced dissociation (CID) of this peak in the tandem mass spectrometer revealed a loss of the methyl group (-15). Based on the MS and MS/MS, this peak is assigned to CH_3CO -3AP-NDA.

3AP-R from 3R4F FTC Drawn Sample

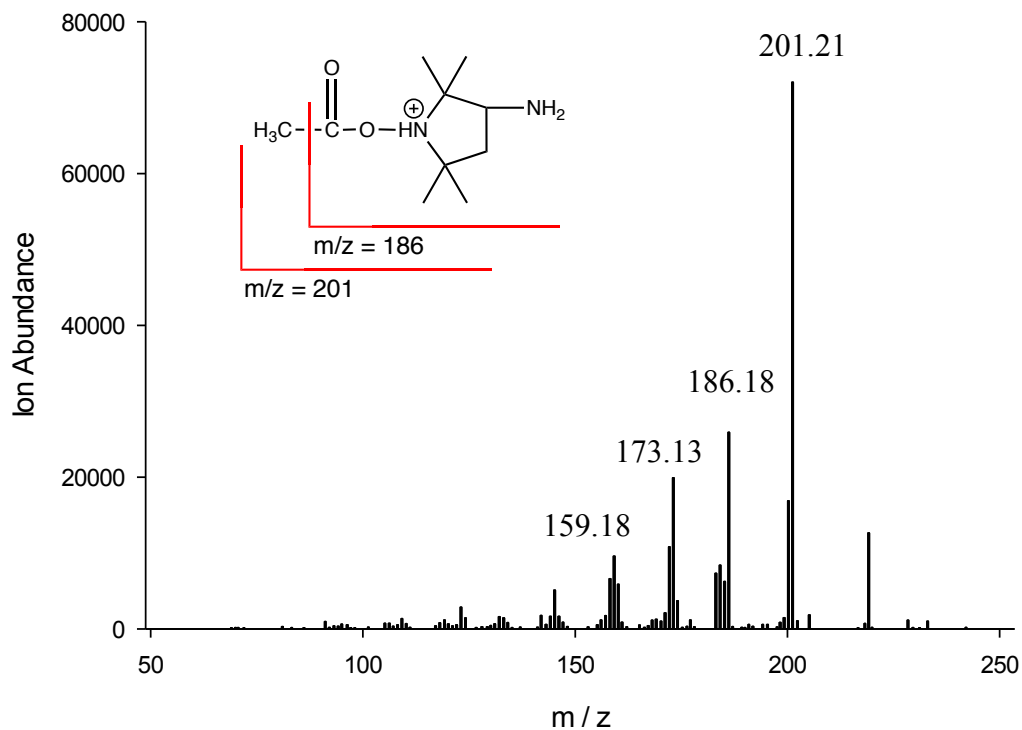


Figure 3.13. ESI-MS/MS spectrum of R-3AP adducts of the 3R4F reference cigarette smoke sample under FTC smoking conditions with m/z range of 50-250.

The ESI-MS/MS spectrum of R-3AP adducts of the 3R4F reference cigarette smoke sample under FTC smoking conditions is shown in Figure 3.13. MS/MS of the peak of m/z 201 shows a methyl group loss (-15) from the molecular ion.

NDA-3AP-R from 3R4F FTC Drawn Sample

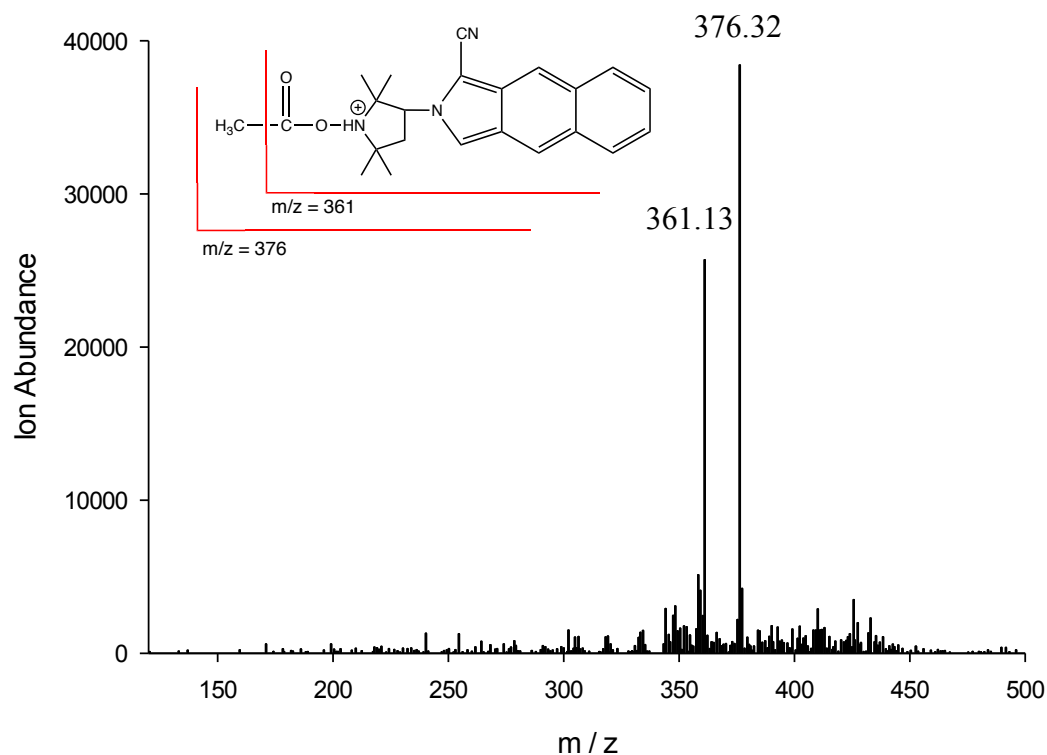


Figure 3.14. ESI-MS/MS spectrum of R-3AP-NDA adducts of the 3R4F reference cigarette smoke sample under FTC smoking conditions with m/z range of 100-500.

The ESI-MS/MS spectrum of R-3AP-NDA adducts of the 3R4F reference cigarette smoke sample under FTC smoking conditions is shown in Figure 3.14. MS/MS of the peak at m/z 376 shows a methyl group loss (-15) from the molecular ion.

3.3.4 NO/air/CH₃CHO Model

A model system was employed to assess the gas-phase reaction of NO₂ and CH₃CHO. After the sampling, 3AP adducts from the model system was derivatized by the same procedure before injecting into the LC-MS.

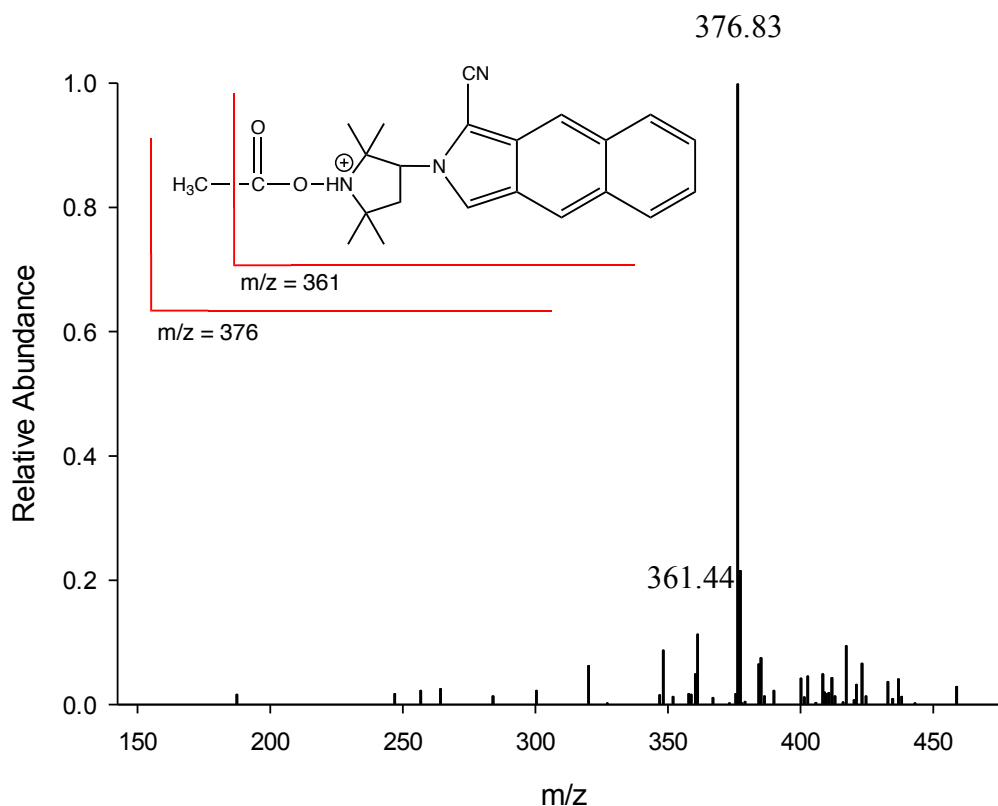


Figure 3.15. ESI-MS/MS spectrum of R-3AP-NDA adducts of NO/air/ CH₃CHO model with *m/z* range of 150-500.

As shown in Figure 3.15, the ESI-MS/MS spectrum shows that CID at 376 reveals a methyl group loss (-15) from the molecular ion, which shows the same fragmentation pattern as these from cigarette smoke samples.

3.3.5 LC-MS Spectrum

3-dimensional LC-MS

3-dimensional LC-MS can provide a full picture and elucidate the presence of 3AP-trapped radicals at different retention times.

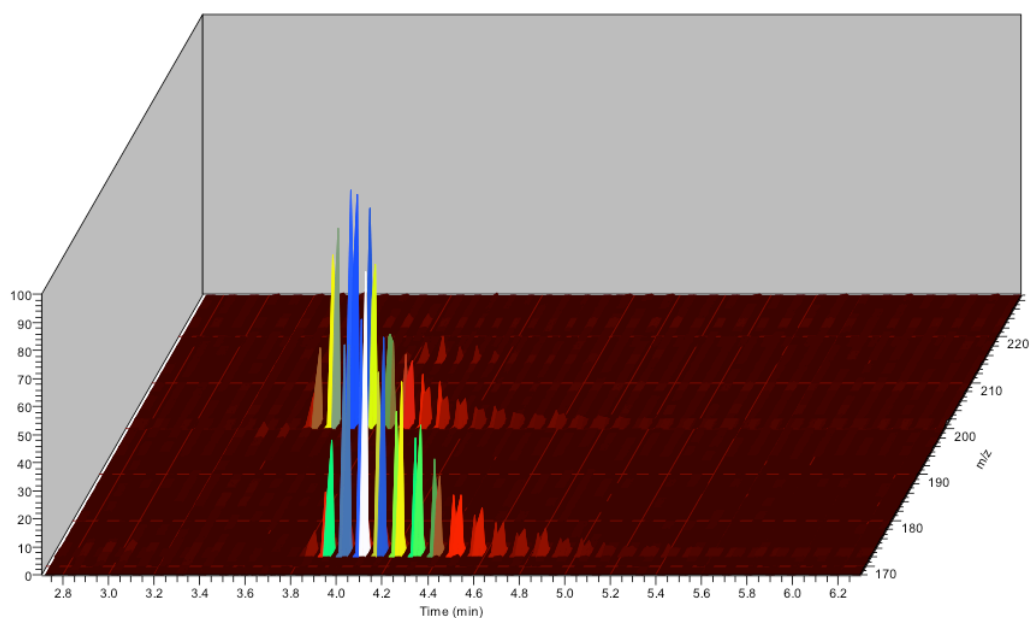


Figure 3.16. 3D LC-MS for acetone irradiation standard.

In Figure 3.16, the 3D LC-MS of the acetone irradiation sample shows two clearly defined chromatographic peaks with distinct masses, which corresponds to $\text{CH}_3\text{C}(\text{O})\text{-3AP}$ with m/z of 201 eluted at 3.70 min and $\text{CH}_3\text{-3AP}$ with m/z of 173 eluted at 4.10 min.

Because the 3D LC-MS spectrum can show both polarity and molecular mass at the same time, it is a great tool for radical analysis in complex matrices such as cigarette smoke.

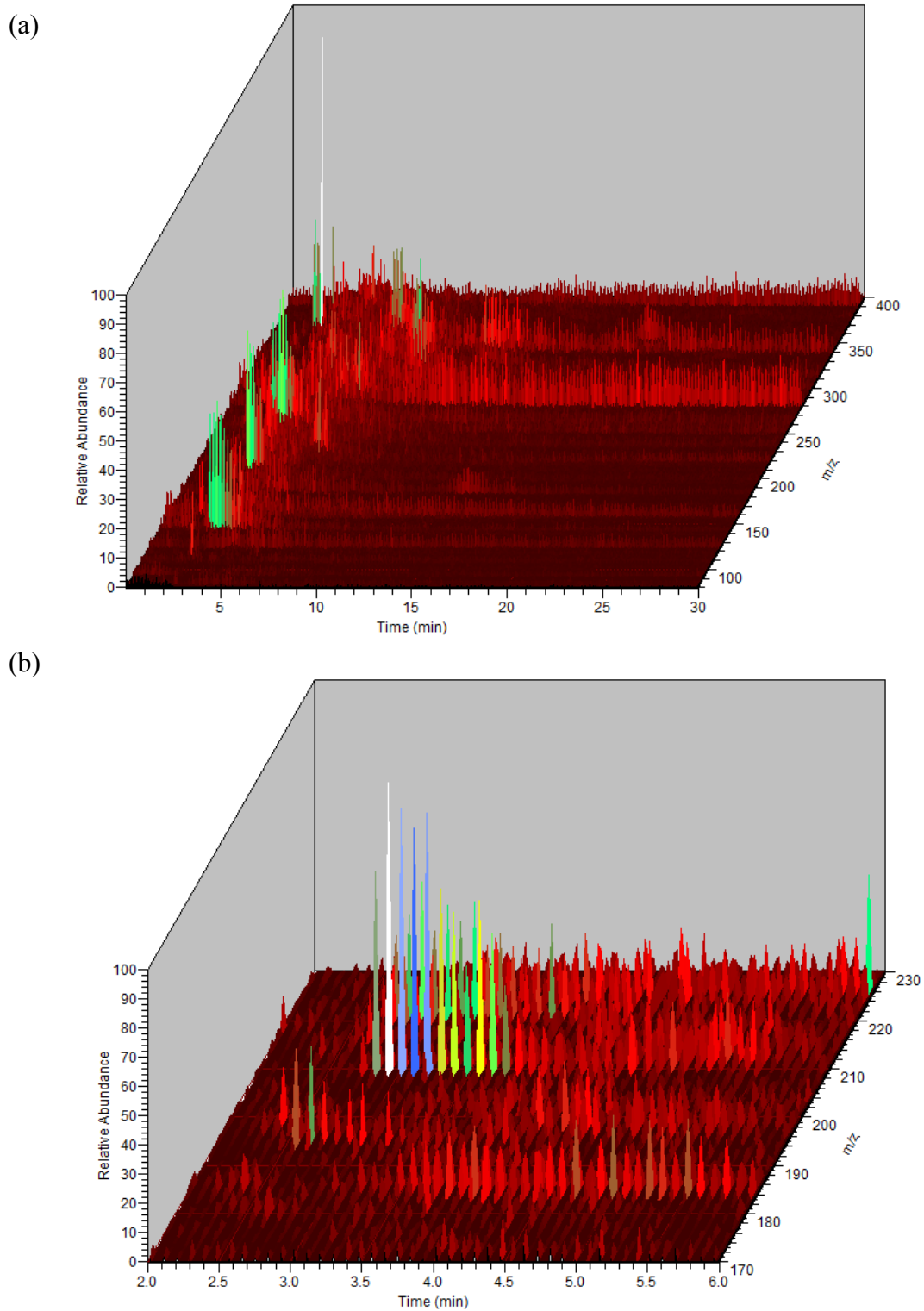


Figure 3.17. (a) 3D LC-MS for smoke sample for m/z range [80-400] from 0 to 30 min. **(b)** 3D LC-MS for smoke sample for m/z range [170-230] from 2.0 to 6.0 min.

The LC-MS spectrum of the full smoke sample shows that there are multiple chromatographic peaks, with a significant amount of overlapping, and large mass ranges (m/z 80~400) with quite different polarities.

Multiple radicals trapped by 3AP in the cigarette smoke sample makes the 3D LC-MS for smoke sample spectrum with mass range from m/z of 80 to 400 very crowded and difficult to interpret, as shown in Figure 3.17 (a). To clearly show the result, a narrower mass range from m/z 170 to 230 is shown in Figure 3.17 (b), which shows that $\text{CH}_3\text{C}(\text{O})\text{-3AP}$ with m/z of 201 is eluted at around 3.8 min, a similar retention time as that of the acetone photolysis standard sample. Many other species, with or without 3AP, are also present in the background.

Extracted Ion Chromatogram (EIC) of the $\text{CH}_3\text{CO-3AP}$

Because of the complex nature of the cigarette smoke sample, it is very helpful to show specific mass ranges of targeted analytes to compare the retention time among various samples in the LC-MS spectrum. An extracted ion chromatogram (EIC), also called reconstructed ion chromatogram (RIC), can extract a restricted mass range of interesting analytes from the entire data set and provide clean chromatograms of targeted compounds.

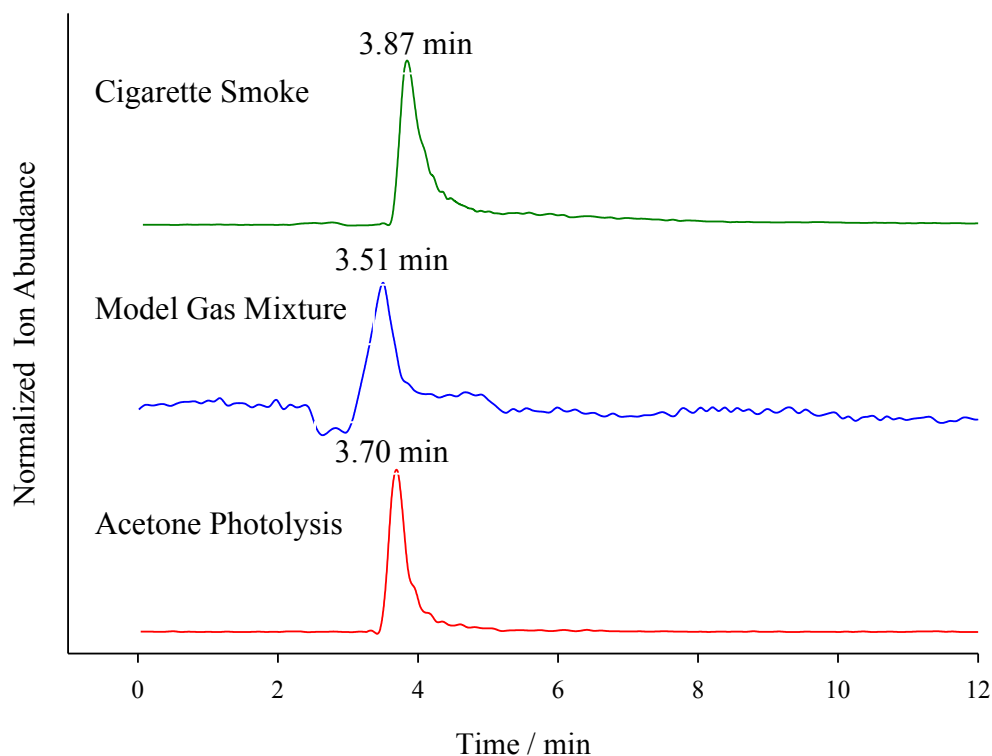


Figure 3.18. Representative extracted ion chromatogram (EIC) from LC-MS. The m/z range was 200.60-201.60 for 3AP-CH₃CO adducts from fresh Marlboro cigarette smoke, gas phase model, and aqueous acetone photolysis sample.

Figure 3.18 shows the extracted ion chromatogram (EIC) of 200.60-201.60 for 3AP adducts by the representative LC-MS chromatograms. This mass range corresponds to the $[M+1]^+$ peak for 3AP-C(O)CH₃, which eluted at 3.87 min, 3.51 min, and 3.70 min from the fresh Marlboro cigarette smoke, gas phase model, and aqueous acetone photolysis samples respectively. All clearly show the expected peak, confirming the presence of acetyl radical. The small differences in retention time could be due to the peak broadening in the chromatogram or the low mass resolution of 3350 at m/z 201.

3.4 Discussion

3AP adducts from acetone photolysis standards, cigarette smoke and the models with or without fluorescence derivatization were analyzed by electrospray mass spectrometry in this chapter. Fragmentation patterns from different samples are summarized in Table 3.2 for comparison.

Table 3.2. Fragmentation patterns from different samples in ESI-MS spectrum.

| Samples | Fragmentation Patterns (m/z) | |
|---------------------------------|--------------------------------|------------------------|
| | 3AP-R | R-3AP-NDA |
| 3AP | 156.94, 143.08, 84.10 | / |
| Acetone Photolysis | 201.03, 173.01, 98.07 | 376.30, 360.37, 348.39 |
| Marlboro Pump Drawn | 201.21, 186.14, 173.18, 159.14 | 376.10, 361.13 |
| 3R4F FTC | 201.21, 186.18, 173.13, 159.18 | 376.32, 361.13 |
| NO/air/CH ₃ CO Model | / | 376.83, 361.44 |

Table 3.2 shows that the same fragmentation patterns occur in both the 3AP-R and the R-3AP-NDA samples from acetone photolysis, continuously drawn commercial cigarette, 3R4F reference cigarette under FTC conditions, and the NO/air/CH₃CO model. For 3AP-R samples, the molecular ions of CH₃C(O)-3AP were observed in all of the samples because of the soft ionization of the electrospray ion source. When the 3AP-R adducts were derivatized by NDA, the same molecular peak and fragmentation patterns were observed from the smoke sample, model system and standard radicals resulting from acetone photolysis. The molecular ions of CH₃C(O)-3AP-NDA were also observed in all of the samples. In addition, both 3AP-R and R-3AP-NDA showed a loss of 15 amu, which corresponds to the methyl group of the acetyl moiety.

From the mass spectrum of pure 3AP standard in 50/50 MeOH/H₂O solution, we can see that this compound underwent oxidation during the MS interface, resulting in the oxidization products shown in Figure 3.5.

Both R-3AP and R-3AP-NDA from the smoke samples were analyzed by the mass spectrometry. Although it is possible to analyze 3AP adducts without further derivatization with NDA, several advantages are gained by employing the fluorescent tag for the mass spectrometry analysis. First, the addition of fluorescent tag to the 3AP adducts can optimize ionization in the mass spectrometry and increase the signal from 10^6 to 10^7 as shown in Figure 3.8 and Figure 3.11, respectively. Second, the derivatization by NDA can bring the molecular weights of small molecules of R-3AP adducts into a large mass range where less interference is present. At the same time, the mass resolution is also improved with the increasing molecular weights. Third, R-3AP-NDA also shows very characteristic fragment peaks (a loss of methyl group), which provides additional evidence for radical identification.

Extracted ion chromatogram (EIC) of 200.60-201.60 for CH₃CO-3AP adducts in LC-MS chromatograms show similar retention times for all of the samples from fresh Marlboro cigarette smoke, gas phase model, and aqueous acetone photolysis.

The three dimensional LC-MS can demonstrate the presence of the 3AP-trapped radicals with different mass-charge ratios at different retention times, providing a big picture view of the radicals in cigarette smoke.

3.5 Conclusion

Several mass spectrometry approaches were explored for identifying the acetyl radical in the smoke samples. CID fragmentations of the molecular ions of 3AP-R adducts and NDA-3AP-R adducts from acetone photolysis standard, cigarette smoke samples from continuously drawn and FTC conditions, and NO/air/CH₃CHO were compared.

The presence of CH₃C(O)• in the smoke and gas phase model has been confirmed by a variety of analytical techniques, specifically MS/MS of NDA-3AP-C(O)CH₃ and LC-MS of 3AP-C(O)CH₃. In the following Chapter the quantitative analysis of CH₃(O)-3AP by HPLC with fluorescence detection will be discussed.

3.6 References

- Bartalis J, Zhao YL, Flora JW, Paine JB, Wooten JB. 2009. Carbon-centered radicals in cigarette smoke: acyl and alkylaminocarbonyl radicals. *Anal Chem* 81(2): 631-641. BristolUniversity. <http://www.bris.ac.uk/nerclsmsf/techniques/hplcms.html>.
- Bruins AP, Covey TR, Henion JD. 1987. Ion Spray Interface for Combined Liquid Chromatography/Atmospheric Pressure Ionization Mass-Spectrometry. *Analytical Chemistry* 59(22): 2642-2646.
- Cech NB, Enke CG. 2001. Practical implications of some recent studies in electrospray ionization fundamentals. *Mass Spectrom Rev* 20(6): 362-387.
- Davies MH, Vaught A. 1990. The Reference Cigarette. Kentucky Tobacco Research and Development Center; University of Kentucky: Lexington, KY.
- Gu W, Heil PE, Choi H, Kimb K. 2007. Comprehensive model for fine Coulomb fission of liquid droplets charged to Rayleigh limit. *Appl Phys Lett* 91(6).
- Jia M, Tang Y, Lam YF, Green SA, Blough NV. 2009. Prefluorescent Nitroxide Probe for the Highly Sensitive Determination of Peroxyl and Other Radical Oxidants. *Analytical Chemistry* 81(19): 8033-8040.
- Johnson CG, Caron S, Blough NV. 1996. Combined liquid chromatography/mass spectrometry of the radical adducts of a fluorescamine-derivatized nitroxide. *Analytical chemistry* 68(5): 867-872.
- Niessen WM. 1999. State-of-the-art in liquid chromatography-mass spectrometry. *Journal of chromatography A* 856(1-2): 179-197.
- RCP. 2011. Reference Cigarette Program, College of Agriculture, University of Kentucky Homepage. Available: <http://www.ca.uky.edu/refcig/>.

Chapter 4: Comparisons and Quantitative analysis of acetyl radical in smoke, standard, and model samples by HPLC-FL²

² Part of this chapter will be submitted to a peer-reviewed journal.

4.1 Introduction

Many respiratory health risks, including lung cancer, are induced by cigarette smoke (Jones et al. 2006; Kindt and Muller 2004). Free radicals in cigarette smoke are implicated in lipid peroxidation, protein oxidation and damage to lungs and other tissues (Ozguner et al. 2005; Pryor 1986). Free radicals in tobacco smoke have been studied since 1958 (Lyons et al. 1958), but the mechanisms of their formation have remained elusive because of the chemical and physical complexity of smoke (Borgerding and Klus 2005; Polzin et al. 2007; Stabbert et al. 2003a; Stabbert et al. 2003b) and its dynamic instability (Huang et al. 2005; Maskos et al. 2008). Surprisingly, inconsistent with their highly reactive nature, free radicals are detected well beyond the burning site, even as long as 10 minutes post combustion. (Cueto and Pryor 1994; Flicker and Green 1998, 2001; Pryor et al. 1993). To explain this paradox, Pryor et al. (Pryor et al. 1993) proposed that radicals are continuously formed and destroyed in the gas phase by a steady state mechanism based on the addition of NO_2 to alkyl dienes. However, recent studies have raised questions about this steady state mechanism because of the lack of evidence for NO_2 -containing radicals and the discovery of apparently unrelated radicals, such as alkylaminobocarbonyl and acyl radicals in mainstream smoke (Bartalis et al. 2007; Bartalis et al. 2009). In addition, several studies have indicated that the Cambridge filter, which separates gas phase smoke from total particulate matter (TPM), substantially influences the generation of radicals in smoke (Wooten 2011).

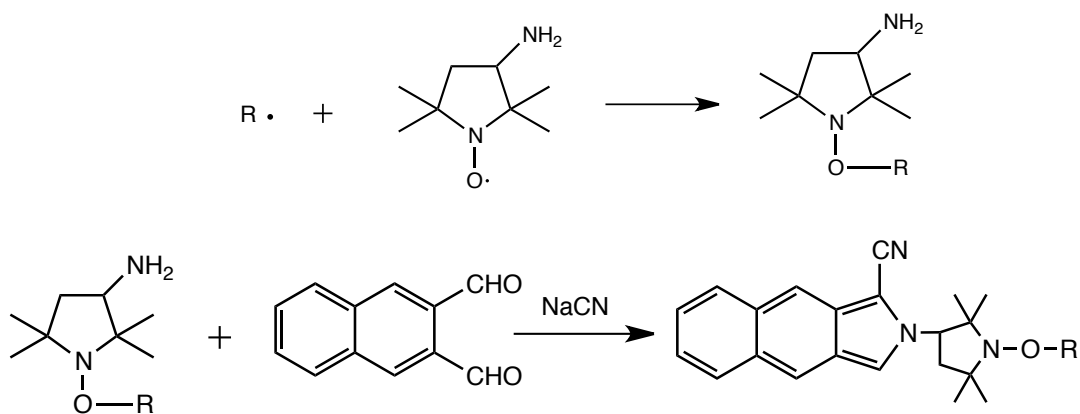
Mainstream smoke, sometimes called whole smoke, is the aerosol gas mixture generated during a puff from the burning site drawn through the cigarette rod, and

inhaled by the smoker. Instead of reaching the rod, sidestream smoke is primarily formed between puffs during the smoldering process at lower temperatures. Cigarette smoke contains a myriad of organic compounds in dynamic, non-equilibrium conditions and distributed between gas and particulate phases. When whole smoke passes through a glass fiber filter, the fraction collected on the filter is defined as the particulate phase, known as total particle matter (TMP), while the fraction passing through is defined as the gas phase (Baker 1999). In this work, we mainly focus on the generation of acetyl radical in mainstream smoke and compare whole smoke to gas phase smoke.

All cigarette smoke sampling experiments were conducted under both Federal Trade Commission (FTC) conditions and a pump-drawn continuous flow method, with or without a filter. Two different types of cigarettes, Marlboro and 3R4F Kentucky Reference cigarettes were sampled by each smoking method. A simplified gas mixture consisting of nitric oxide, air and acetaldehyde was employed as a model to mimic the gas phase reaction in cigarette smoke.

Based on previous work (Flicker and Green 1998, 2001), we adopted a solvent-free radical trapping method to trap carbon-centered radicals. We modified the bead trapping method by directly coating the trapping agent, 3-amino-2, 2, 5, 5-tetramethyl-proxyl (3AP), onto the inner wall of a distillation column to reduce the effect of total particulate matter (TPM) trapped by beads. Smoke from a burning cigarette, or the gas mixture in the model system, flows through the coated distillation column; 3AP reacts with the carbon-centered radicals to form stable 3AP adducts, which are then either identified by LC-MS or, for quantification, derivatized with

naphthalene-2, 3-dicarboxaldehyde (NDA) as shown in Scheme 4.1 below. The derivatized adduct was then detected by HPLC/FLD or ESI-MS.



Scheme 4.1. Trapping of carbon-centered radical ($\cdot R$) by 3AP, followed by solution-phase derivatization with NDA to produce the fluorescent radical-adduct.

As shown in Scheme 4.1, the alkoxyamine adducts resulting from 3AP rapidly reacting with carbon-centered radicals are very stable because of the robustness of the di-tert-alkyl structure. To produce highly fluorescent products for better analysis, the resulting 3AP adducts were derivatized with NDA for quantitative analysis. The parent 3AP-NDA, however, doesn't exhibit fluorescence owing to the efficient intermolecular quenching of the excited singlet by 3AP. When 3AP traps carbon-centered radicals, it forms diamagnetic products and eliminates the intermolecular quenching pathway, producing intensive fluorescence signals that can be detected and analyzed by HPLC-FL.

4.2 Experimental Methods

Chemicals: 3-amino-2, 2, 5, 5-tetramethyl-proxyl (3AP), naphthalene-2, 3-dicarboxaldehyde (NDA), sodium cyanide, cyclopentylamine (CPA), and HPLC

grade methanol were purchased from ACROS. All chemicals were of the highest purity available and were used without further purification. Marlboro brand cigarettes were purchased from a local vendor and 3R4F Kentucky Reference cigarettes were purchased from University of Kentucky, Lexington (Davies and Vaught 1990). These cigarettes were 84 mm long, weighing 1.06 g with filter length of 27 mm. A detailed description of this cigarette has been reported. Solutions of NDA in acetonitrile (10.0 mM) and sodium cyanide solutions (10.0 mM) were prepared every two weeks and stored at -5 °C. Water used for all solutions was from a Millipore Milli-Q system.

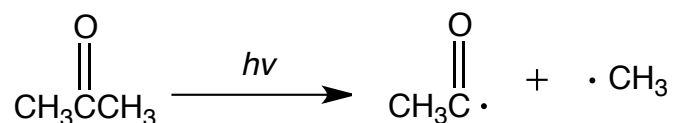
Instrumentation: The HPLC was a Shimadzu Prominence LC-20AD with DGU-20A₅ vacuum degasser, and Shimadzu SPD-20AU UV/Vis detector, and RF-10A_{XL} (FLD) fluorescence detector. Thermo BioBasic-18125×4mm 5μ particle-packed HPLC column was used and the injection volume was 20 μL. The FLD was operated at 420/480 nm excitation/emission wavelengths for all separations. Separation of R-3AP-NDA adducts were carried out isocratically at 25°C, with a flow rate of 0.500 mL/min. The mobile phase composition was 30%/70% H₂O/methanol.

Acetone Photolysis Standard Preparation

Standard adducts of acetyl radical were made photochemically by the following procedure: 3AP (0.5 mM) and acetone (50 mM in water) were irradiated in a 1-cm quartz cell with a 150-W xenon lamp for 30 min. The solution was deoxygenated for 5 min before and during the irradiation by bubbling with N₂ (99.99%, Praxair Distribution Inc.).

Scheme 4.2 shows that when acetone is photolysized under ultraviolet light, the bond between C=O and CH₃ breaks, resulting in an acetyl radical and a methyl radical.

Both radicals from acetone photolysis are trapped by 3AP later as standards. 3AP-R standard solution in 50/50 methanol/H₂O were directly injected into the mass spectrometer and detected by ESI-MS.



Scheme 4.2. Acetyl radical and methyl radical are generated by acetone photolysis

Smoke Sample Preparation

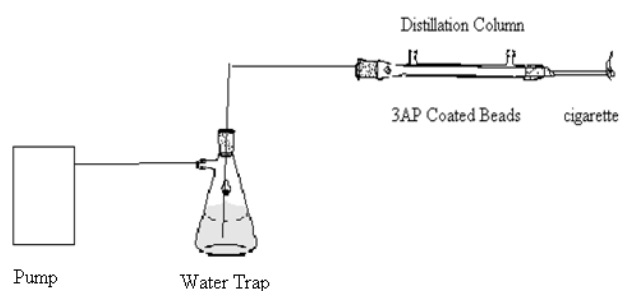


Figure 4.1. Apparatus used to trap carbon-centered radicals from the burning cigarette.

0.02 g 3AP in small amount of acetone was coated to the inner wall of the column and dried by rotary evaporation at room temperature. A pump with flow rate 0.6 L/min was used to draw smoke across the column. To avoid smoke entering the pump directly, a water trap was applied to absorb most organic compounds after the trapping process as shown in Figure 4.1. Five Marlboro cigarettes were smoked sequentially for one sample. It took about 2 minutes to finish one cigarette under the working pump flow rate. Nothing else beside the manufacturer's cigarette filter was used before it reached the 3AP-coated column.

Comparison experiments employed the FTC smoking methods, which consists of a 35 mL puff volume drawn over 2 second duration once per minute. The total volume of column and tubing is about 146 mL, while each puff is 35 mL. Neglecting diffusion, it takes 250 s for one puff of smoke to be completely removed from the trapping column. Five Marlboro or 3R4F Kentucky Reference cigarettes were smoked sequentially for each analysis.

NO/CH₃CHO/O₂ Model Sample Preparation

A similar procedure was followed for a NO/CH₃CHO/O₂ model. As above, a solution of 0.02 g 3AP in acetone was coated on the inner wall of the 140-mL sampling column and dried by rotary evaporation at room temperature. A schematic of the model system employed to assess the gas-phase reaction of NO₂ and CH₃CHO is shown in Figure 4.2. Air was flowed across 3 mL of liquid phase acetaldehyde at room temperature to carry gas phase CH₃CHO to a Y- junction where it met 1000 ppm NO (certified 1003.1 ppm, Praxair Distribution Inc.) in N₂. As NO met the air, it was oxidized to NO₂ by oxygen, producing a distinctive brown color. A distillation

column, which was coated with 3AP on the inner wall, acted as the reaction vessel and the trapping surface. When the gas mixture reached the column, radicals were trapped by 3AP (Figure 4.2) and analyzed later by HPLC and LCMS. The airflow was from the building supply. Trace NO_2 from the NO tank was removed by bubbling NO through a 50% solution of sodium hydroxide. (Not shown in Figure 4.2.)

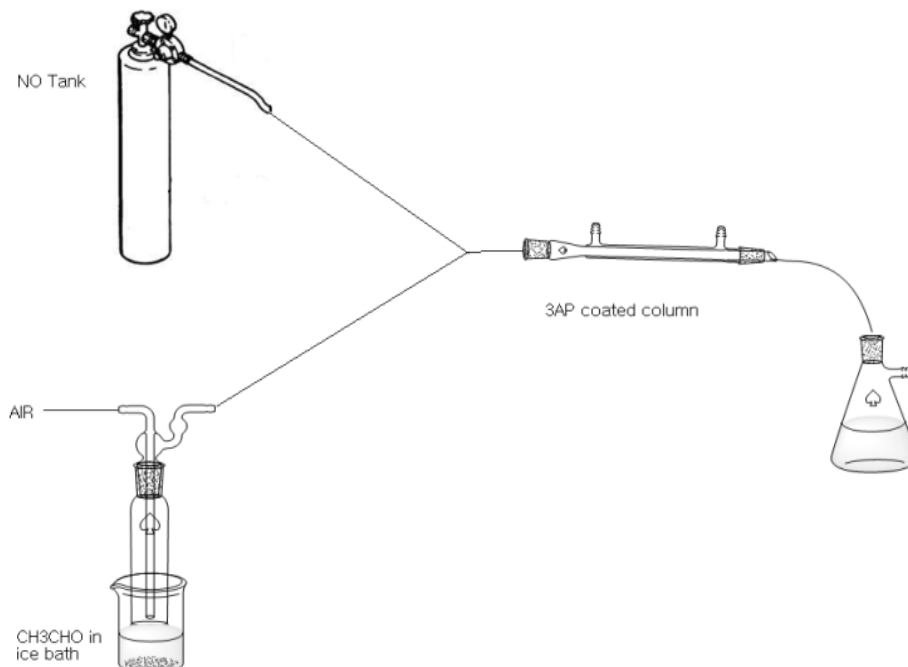


Figure 4.2. Diagram of gas mixture model reaction apparatus.

NDA Derivatization and Purification

After sampling, the 3AP adducts were washed from the sampling column with 10 mL methanol. Next the solution was filtered with a Hyper Sep C18 column (Thermo Electron Corporation[®]), giving a light yellow solution, while the dark colored R-3AP adducts remained on the column. 10 mL of methanol was used to flush the sample from the column, giving a dark yellow solution. For derivatization, 500 μL of filtered sample solution, 200 μL of sodium cyanide solution, and 200 μL of

NDA solution were added sequentially to a foil-wrapped glass vial and allowed to react for 30 min.

After derivatization, the 3AP adduct solution was filtered with a 0.2- μ m syringe filter (HPLC syringe filter, Alltech[®]), and yellow material (R-3AP-NDA) precipitated on the filter. This yellow precipitate was washed off with 1 mL of 80% methanol in water.

4.3 Results

The chromatograms illustrate in the following sections are representatives of HPLC/FLD chromatograms of radicals trapped from fresh cigarette smokes, model gas mixture, and aqueous acetone photolysis sample. All samples included the radical trap (3AP) and were derivatized with NDA.

4.3.1 Marlboro Cigarette Smoke Sample with the Continuously

Drawn Method

A representative chromatogram resulting from continuous drawn smoke sample from five Marlboro cigarettes is shown in Figure 4.3. Each fluorescent peak in the chromatogram corresponds to a different trapped carbon-centered radical, oxidized 3AP, or amine-containing compounds from the smoke sample.

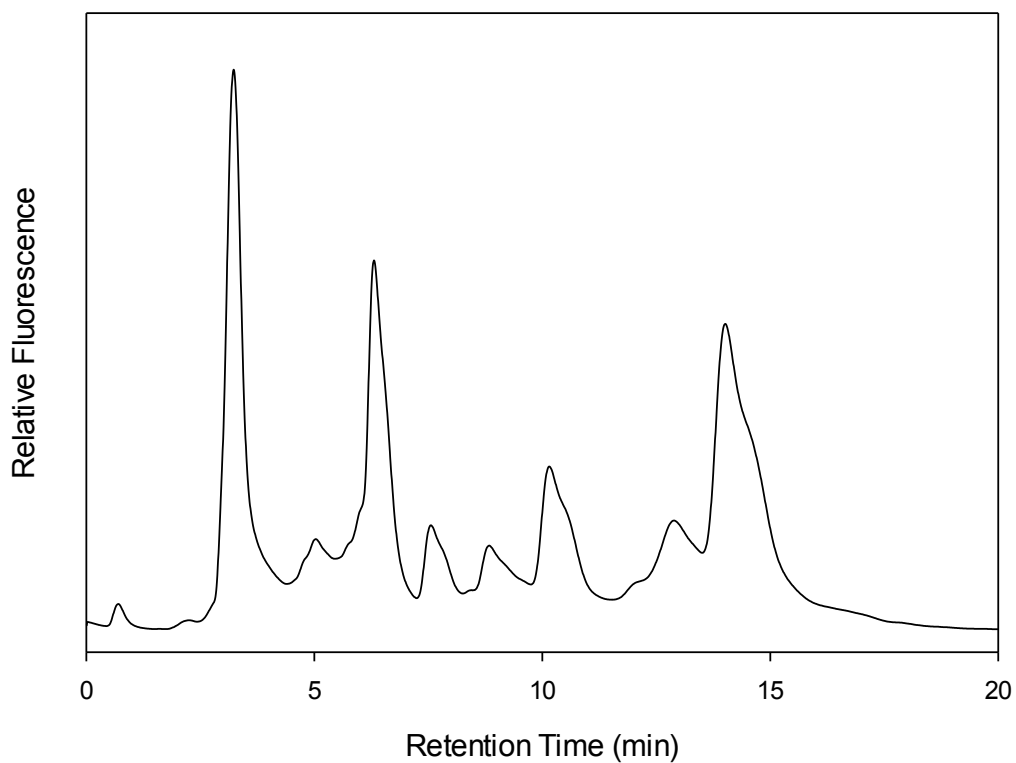


Figure 4.3. Representative fluorescence chromatogram of the carbon-centered radical suite collected from Marlboro cigarette smoke sample with the continuous drawn method.

As shown in Figure 4.3, Major peaks are observed at 3.19, 6.28, 7.48, 10.08, 12.78, and 14.00 min. Numerous overlapping peaks and shoulders are also observed.

4.3.2 Marlboro Cigarette Smoke Sample with the FTC Puff-based

Method

A representative chromatogram resulting from FTC puff-based method smoke sample from five Marlboro cigarettes is shown in Figure 4.4. Each fluorescent peak in the chromatogram corresponds to a different trapped carbon-centered radical, oxidized 3AP, or amine-containing compounds from the smoke sample.

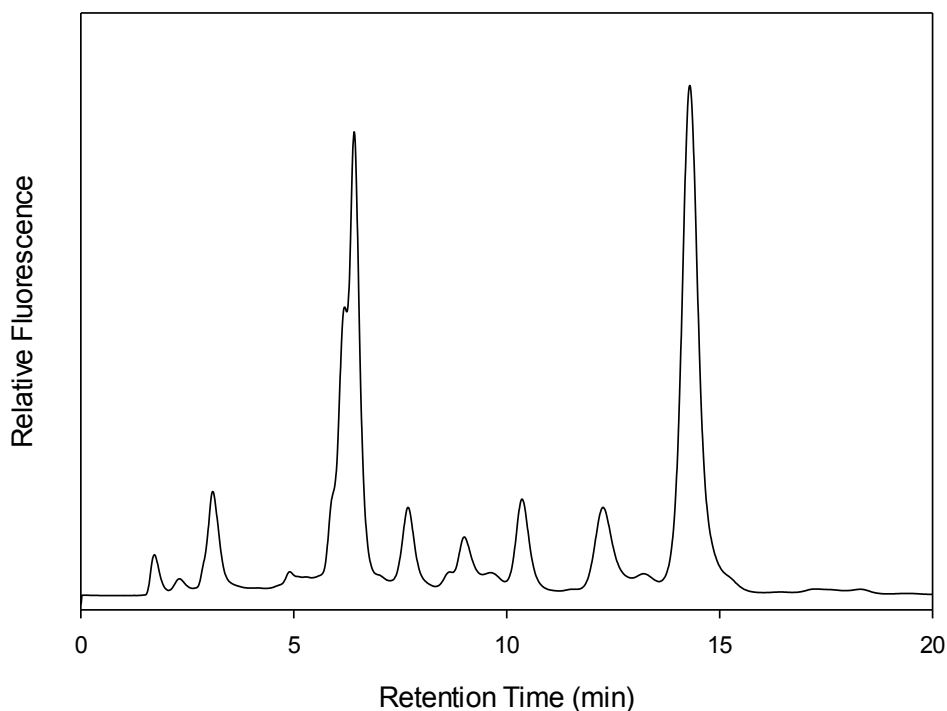


Figure 4.4. Representative fluorescence chromatogram of the carbon-centered radical suite collected from Marlboro cigarette smoke sample with FTC puff-based method.

As shown in Figure 4.4, major peaks are observed at 3.10, 6.40, 7.69, 10.35, and 14.28 min. The peaks were generally better resolved than those in Figure 4.3, but still lots of small and shoulder peaks are also observed.

4.3.3 Marlboro Cigarette Smoke Sample with the FTC Puff-based Method with GF/F

A representative chromatogram resulting from FTC puff-based method smoke sample with GF/F from five Marlboro cigarettes is shown in Figure 4.5. Each fluorescent peak in the chromatogram corresponds to a different trapped carbon-centered radical, oxidized 3AP, or amine-containing compounds from the smoke sample.

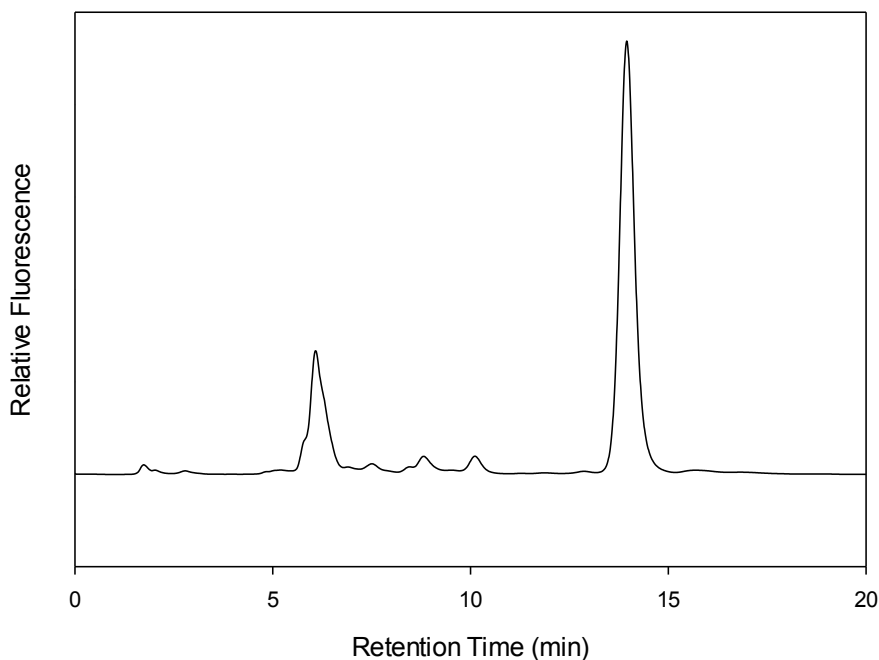


Figure 4.5. Representative fluorescence chromatogram of the carbon-centered radical suite collected from Marlboro cigarette smoke sample with FTC puff-based method with GF/F.

As shown in Figure 4.5, two major peaks are observed at 6.09 and 13.97 min. The peaks were well separated with only a few tiny peaks around 8.8 and 10.0 min.

4.3.4 3R4F Cigarette Smoke Sample with Continuously Drawn

Method

A representative chromatogram resulting from continuously drawn smoke from five 3R4F cigarettes is shown in Figure 4.6. Each fluorescent peak in the chromatogram corresponds to a different trapped carbon-centered radical, oxidized 3AP, or amine-containing compounds from the smoke sample.

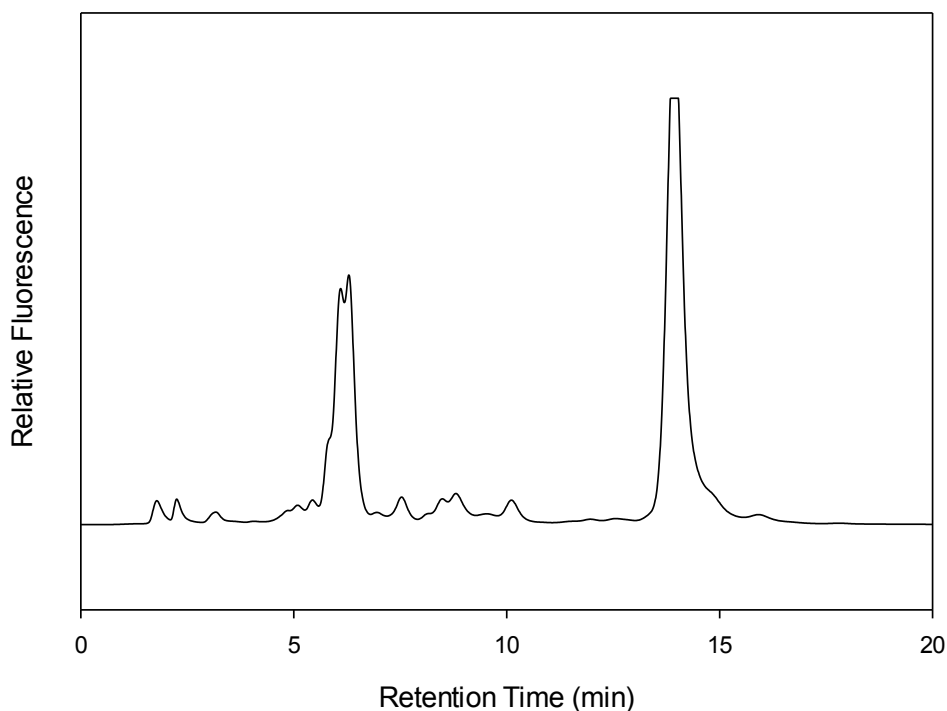


Figure 4.6. Representative fluorescence chromatogram of the carbon-centered radical suite collected from 3R4F cigarette smoke sample with continuously drawn method.

As shown in Figure 4.6, major peaks are observed at 6.15, 6.34 and 13.94 min. Double peaks were observed around 6.2 min and lots of small and shoulder peaks are also observed.

4.3.5 3R4F Cigarette Smoke Sample with FTC Puff-based Method

A representative chromatogram resulting from FTC puff-based method smoke sample from five 3R4F cigarettes is shown in Figure 4.7. Each fluorescent peak in the chromatogram corresponds to a different trapped carbon-centered radical, oxidized 3AP, or amine-containing compounds from the smoke sample.

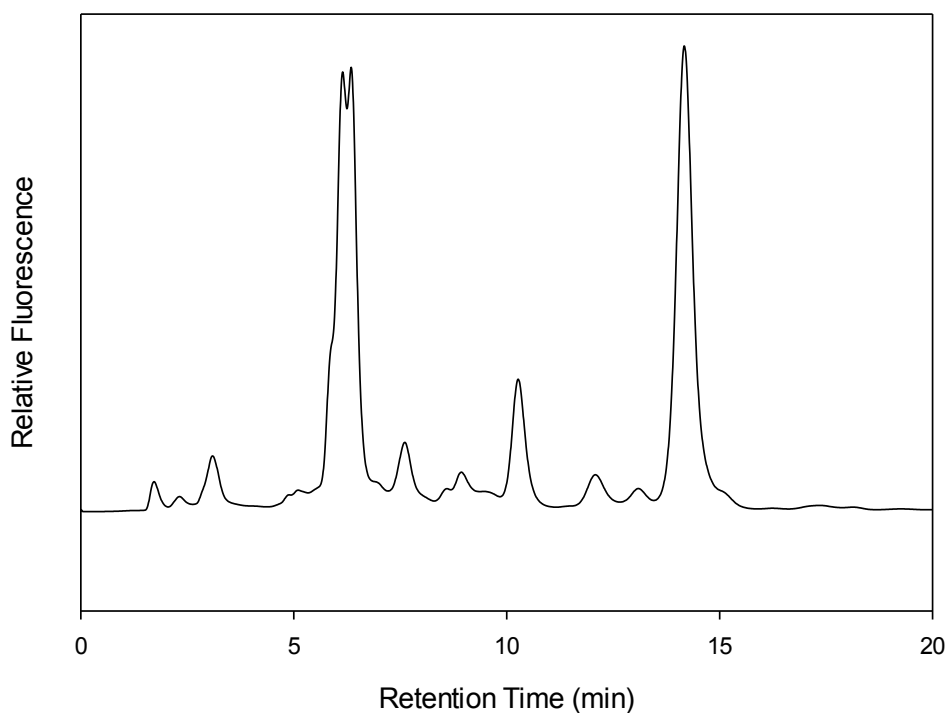


Figure 4.7. Representative fluorescence chromatogram of the carbon-centered radical suite collected from 3R4F cigarette smoke sample with FTC puff-based method.

As shown in Figure 4.7, major peaks are observed at 6.12, 6.34, 7.62, 10.28 and 14.16 min. Double peaks were observed around 6.2 min again and lots of small and shoulder peaks are also observed. The peaks in Figure 4.6 are very similar to those of 3R4F cigarette smoke sample with continuously drawn method sample in

Figure 4.7; main difference between these two samples is relative intensities in each peak.

4.3.6 3R4F Cigarette Smoke Sample with FTC Puff-based Method with GF/F

A representative chromatogram resulting from FTC puff-based method smoke sample with GF/F from five 3R4F cigarettes is shown in Figure 4.8. Each fluorescent peak in the chromatogram corresponds to a different trapped carbon-centered radical, oxidized 3AP, or amine-containing compounds from the smoke sample.

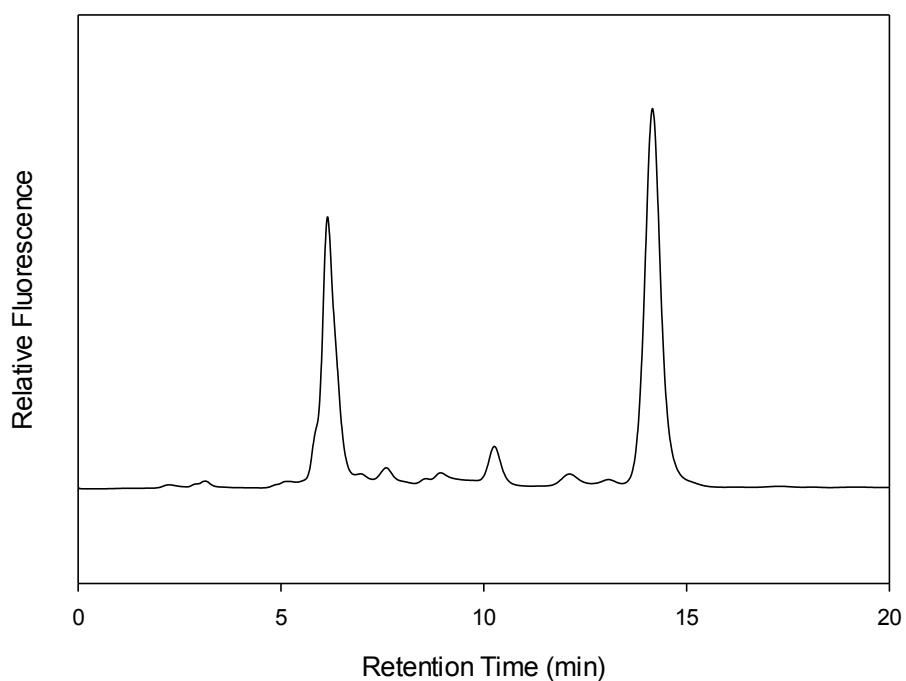


Figure 4.8. Representative fluorescence chromatogram of the carbon-centered radical suite collected from 3R4F cigarette smoke sample with FTC puff-based method with GF/F.

As shown in Figure 4.8, major peaks are observed at 6.15, 10.25 and 14.13 min. A few of small peaks are also observed.

4.3.7 Model Mixture

A representative chromatogram resulting from gas phase model mixture of NO, air and acetaldehyde is shown in Figure 4.9. Each fluorescent peak in the chromatogram corresponds to a different trapped carbon-centered radical, oxidized 3AP.

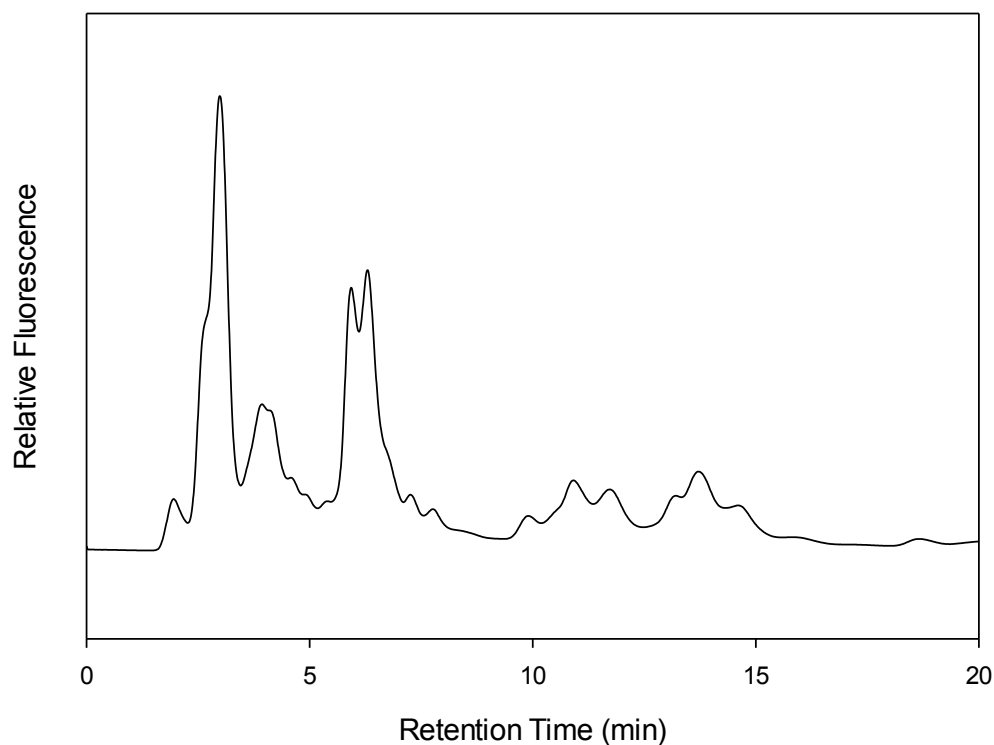


Figure 4.9. Representative fluorescence chromatogram of the carbon-centered radical suite collected from model mixture.

As shown in Figure 4.9, major peaks are observed at 2.96, 3.96, 5.94, 6.32, 10.94 and 13.72 min.

4.3.8 Acetone Photolysis Sample

A representative chromatogram resulting from FTC puff-based method smoke sample with GF/F from five 3R4F cigarettes is shown in Figure 4.10. Each fluorescent peak in the chromatogram corresponds to a different trapped carbon-centered radical, oxidized 3AP.

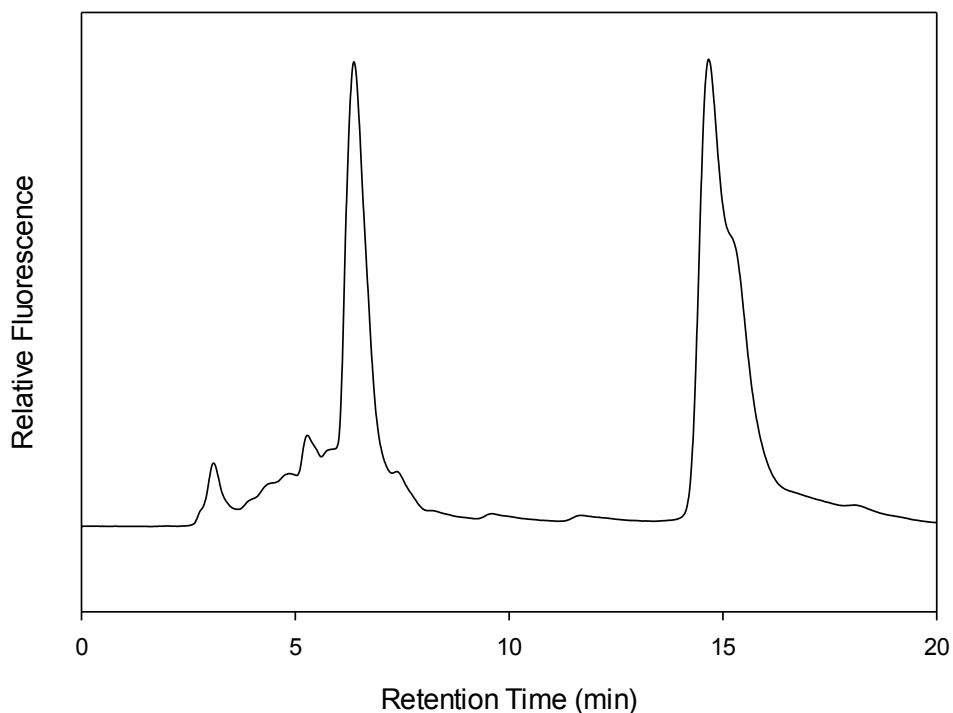


Figure 4.10. Representative fluorescence chromatogram of the carbon-centered radical suite collected from acetone photolysis standards. Each peak represents a different trapped radical.

As shown in Figure 4.10, major peaks are observed at 3.07, 5.25, 6.37 and 14.64 min.

4.3.9 Fluorescence Calibration Curve

For quantitative analysis, NDA-derivatized cyclopentylamine (CPA-NDA), eluting at 7.1 min, was employed as an external standard. CPA-NDA has a similar structure to the R-3AP-NDA compounds and is assumed to give the same fluorescence response. Five standards were run by HPLC, yielding a linear calibration curve with a correlation coefficient of 0.972 as shown in Figure 4.11.

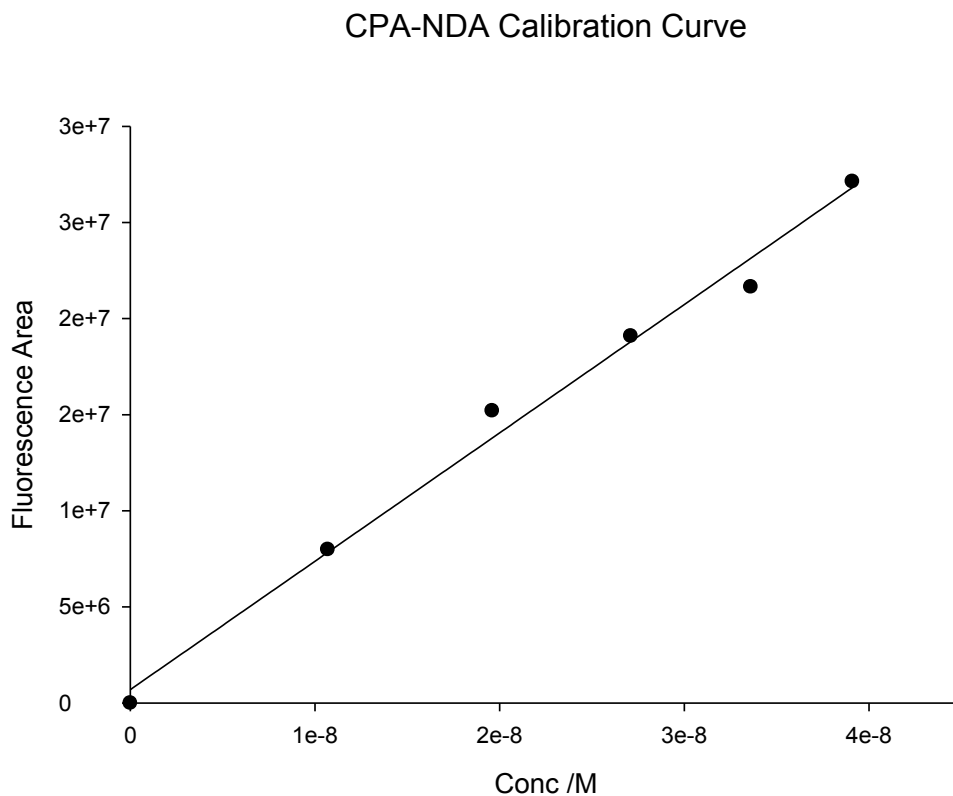


Figure 4.11. CPA-NDA calibration curve. The equation is $y=7 \times 10^{14}x$ and R-squared value is 0.972.

4.4 Discussion

Retention times of major peaks of the radical suites collected from Marlboro Continuous Draw, Marlboro FTC, Marlboro FTC GF/F, 3R4F Continuous Draw, 3R4F FTC, 3R4F FTC GF/F, gas phase model and acetone photolysis standard samples are compared in Table 4.1. Each fluorescent peak in the normalized chromatograms corresponds to a different trapped carbon-centered radical.

Table 4.1. Retention time of peaks from acetone photolysis standard, gas phase model and smoke samples.

| Figure No. | Sample | Retention time of Peaks (min) |
|------------|-----------------------------|---|
| 4.3 | Marlboro Continuous Draw | 3.19, 6.28 , 7.48, 10.08, 12.78, 14.00 |
| 4.4 | Marlboro FTC | 3.10, 6.40 , 7.69, 10.35, 14.28 |
| 4.5 | Marlboro FTC GF/F | 6.09 , 13.97 |
| 4.6 | 3R4F Continuous Draw | 6.15, 6.34 , 13.94 |
| 4.7 | 3R4F FTC | 6.12, 6.34 , 7.62, 10.28, 14.16 |
| 4.8 | 3R4F FTC GF/F | 6.15 , 10.25, 14.13 |
| 4.9 | Gas Phase Model | 2.96, 3.96, 5.94, 6.32 , 10.94, 13.72 |
| 4.10 | Acetone Photolysis Standard | 3.07, 5.25, 6.37 , 14.64 |

As shown in Table 4.1, the peak at around 6.3 min was observed from all the samples and is identified as $\text{CH}_3\text{CO-3AP-NDA}$, which was also verified by mass spectrometry in Chapter 3. Compared to other smoke samples, the retention times for both peaks from Marlboro FTC GF/F sample in Figure 4.5 were a little earlier, which may due to poor column equilibrium in that experiment.

Representative chromatograms of the fluorescent radical adduct resulting from smoke samples from Marlboro and 3R4F cigarettes under different smoking conditions, with or without a particle filter, and the model mixture are compared to acetyl and methyl adducts generated by photolysis of aqueous acetone are shown in Figure 4.12.

Smoking Methods, Brands, Model and Standard Comparisons

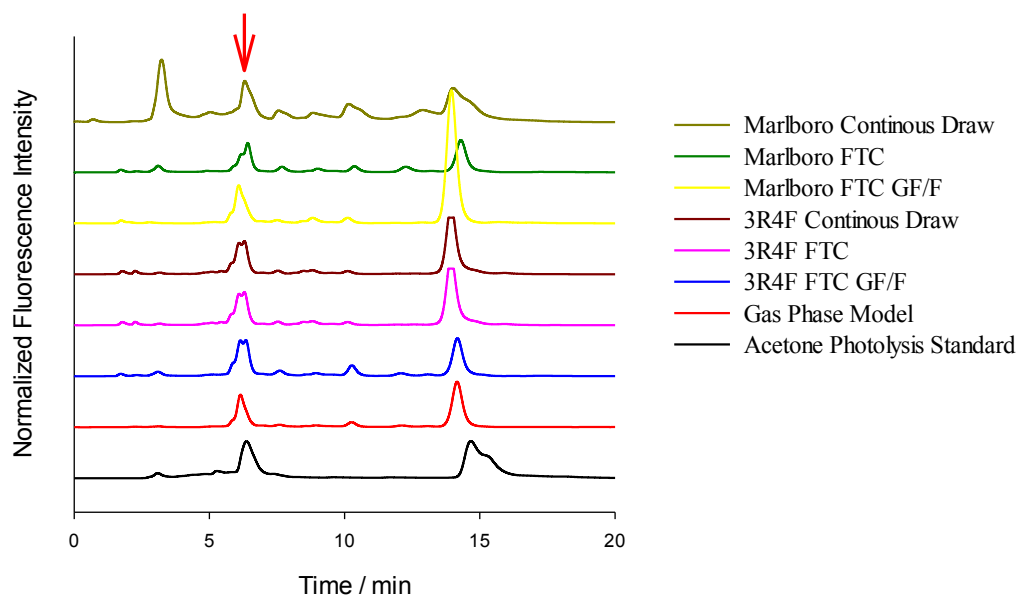
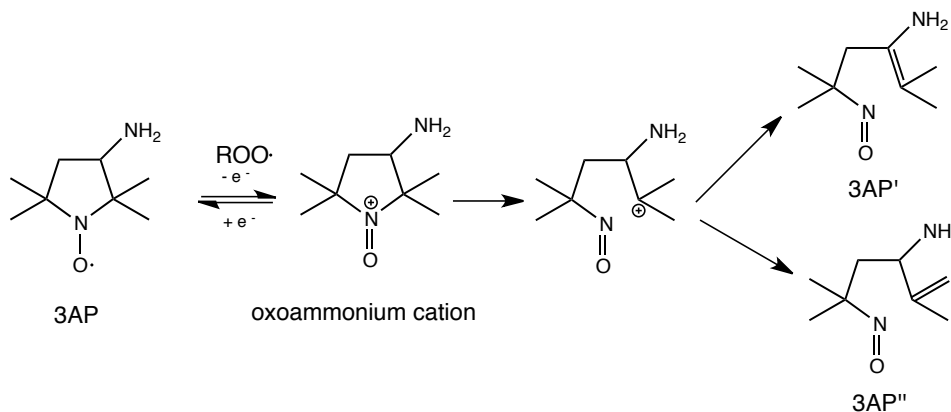


Figure 4.12. Representative HPLC/FLD chromatograms of radicals trapped from fresh cigarette smokes, model gas mixture, and aqueous acetone photolysis sample. All samples included the radical trap (3AP) and were derivatized with NDA. NDA-3AP-C(O)CH₃ elutes at around 6.3 min, as indicated by the red arrow. Conditions: Thermo BioBasic-18 125×4 mm 5μ particle-packed HPLC column; isocratic elution at 0.500 mL/min with 70/30 methanol/H₂O; fluorescence detection at 420 nm (Ex)/480 nm (Em).

As shown in Figure 4.3-4.8, the chromatograms from cigarette smoke indicate the presence of at least 7 major and several minor radicals. The red arrow indicates the peak where the HPLC chromatograms overlap at around 6.3 min, corresponding to the acetyl radical. The model gas mixture also shows several peaks in addition to the peak corresponding to acetyl radical eluting at 6.3 min. Acetyl radicals from the photodecomposition of acetone in aqueous solution provide standards eluting at 6.4 min respectively. A blank control containing only NDA derivatized 3AP showed

negligible fluorescence background (not shown in Figure 4.12). The double peaks around 14 min corresponds to oxidized 3AP adducts shown as 3AP' and 3AP'' in Scheme 4.3 below (Jia et al. 2009), each of which can be derivatized with NDA.



Scheme 4.3. 3AP oxidation reactions and adducts.

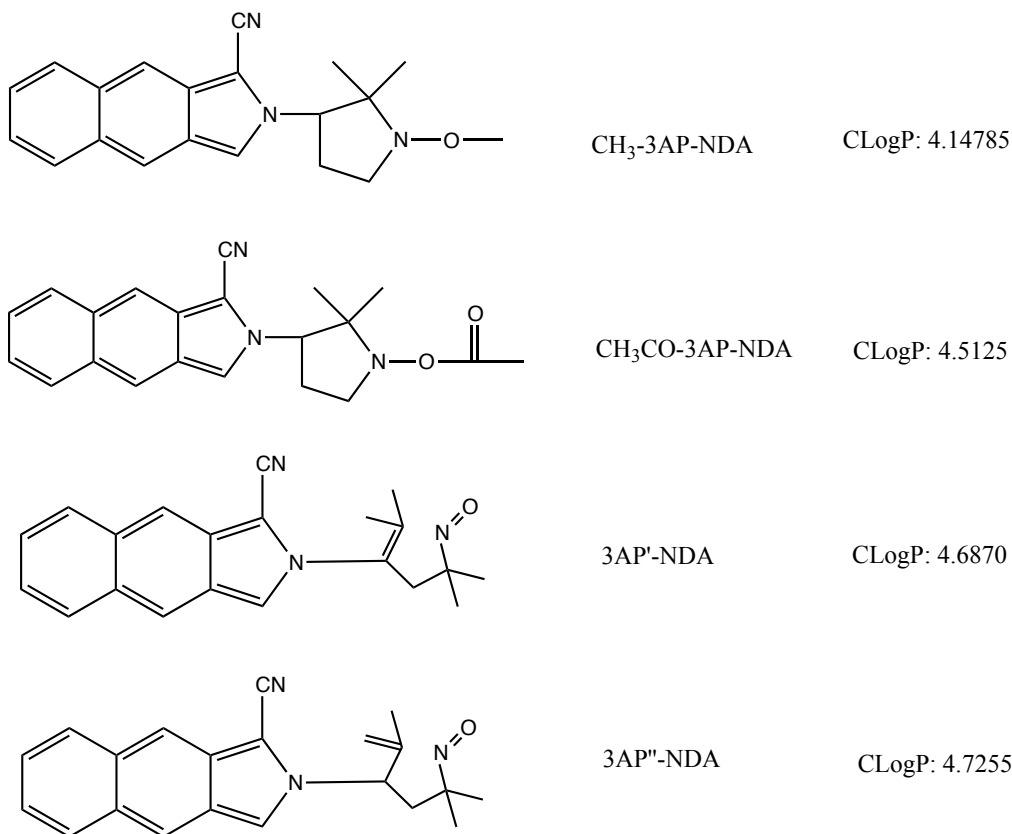
3AP can be oxidized by peroxides and produce oxoammonium cation, which rapidly undergoes ring cleavage and forms two types of products by losing a proton as shown in Scheme 4.3. To clarify their elution behavior, the partition coefficients of CH₃-3AP-NDA, CH₃CO-3AP-NDA and NDA derivatization of the 3AP oxidized products 3AP' and 3AP'' were investigated by ChemDraw as shown in Scheme 4.4.

The partition coefficient is a ratio of concentrations of un-ionized compound between hydrophilic and hydrophobic solutions, normally water and octanol. This coefficient shows how hydrophilic or hydrophobic a chemical substance is. The logarithm of the ratio is called log P as shown in Equation 4.1 below.

$$\log P_{oct/wat} = \log \left(\frac{[solute]_{oct}}{[solute]_{water}} \right)$$

Equation 4.1. Definition of the partition coefficient of a substance in octanol and water.

As shown in the Equation 4.1, the less polar the solute is, the bigger partition coefficient is.



Scheme 4.4. The partition coefficient for CH₃-3AP-NDA, CH₃CO-3AP-NDA and the 3AP oxidized products 3AP'-NDA and 3AP''-NDA.

We can see from the Scheme 4.4 that, the polarity order is CH₃-3AP-NDA > CH₃CO-3AP-NDA > 3AP'-NDA ~ 3AP''-NDA. Since C18 column was employed in the HPLC analysis, the most polar specie eluted from the column first while the least polar ones last. Hence, CH₃-3AP-NDA eluted from the column first while the oxidized 3AP-NDA eluted last. Because the polarities of 3AP'-NDA and 3AP''-NDA are very close, they eluted at 14 min as double peaks, as shown in Figure 4.3, 4.6, 4.10.

Since cigarette design varies from brand to brand (Thompson and Mizaikoff 2006) and human smoking behaviors are very personal and inconsistent, two types of cigarettes, Marlboro and 3R4F Kentucky Reference cigarettes, were investigated under two different smoking conditions to provide a general picture of radicals generation in tobacco smoke. The integration and comparison of fluorescence peaks gives a variable CH_3CO radical concentration among different cigarette samples and smoking conditions.

Table 4.2. Comparison of acetyl radical concentrations in different cigarettes types, smoking conditions and particle filter set up.

| Acetyl Radical Conc (nmol/cig) | Samples | Smoking Conditions | Reference |
|--------------------------------|--|----------------------------------|------------------------|
| 10 ± 2 | Marlboro | Continuous Draw | This study |
| 56 ± 27 | Marlboro | FTC | This study |
| 67 ± 12 | Marlboro | FTC GF/F | This study |
| 22 ± 5 | 3R4F | Continuous Draw | This study |
| 67 ± 17 | 3R4F | FTC | This study |
| 148 ± 5 | 3R4F | FTC GF/F | This study |
| 12 ± 8 | Single-component and blended cigarette samples | Radical yield in gas phase smoke | (Bartalis et al. 2009) |
| 143 ± 68 | Single-component and blended cigarette samples | Radical yield in whole smoke | (Bartalis et al. 2009) |

Table 4.2 shows that the highest concentration at 153 nmol/cig was from the 3R4F Kentucky Reference cigarette with a GF/F particle filter under FTC smoking condition, while the lowest at 8 nmol/cig was from the Marlboro continuously drawn sample without a particle filter.

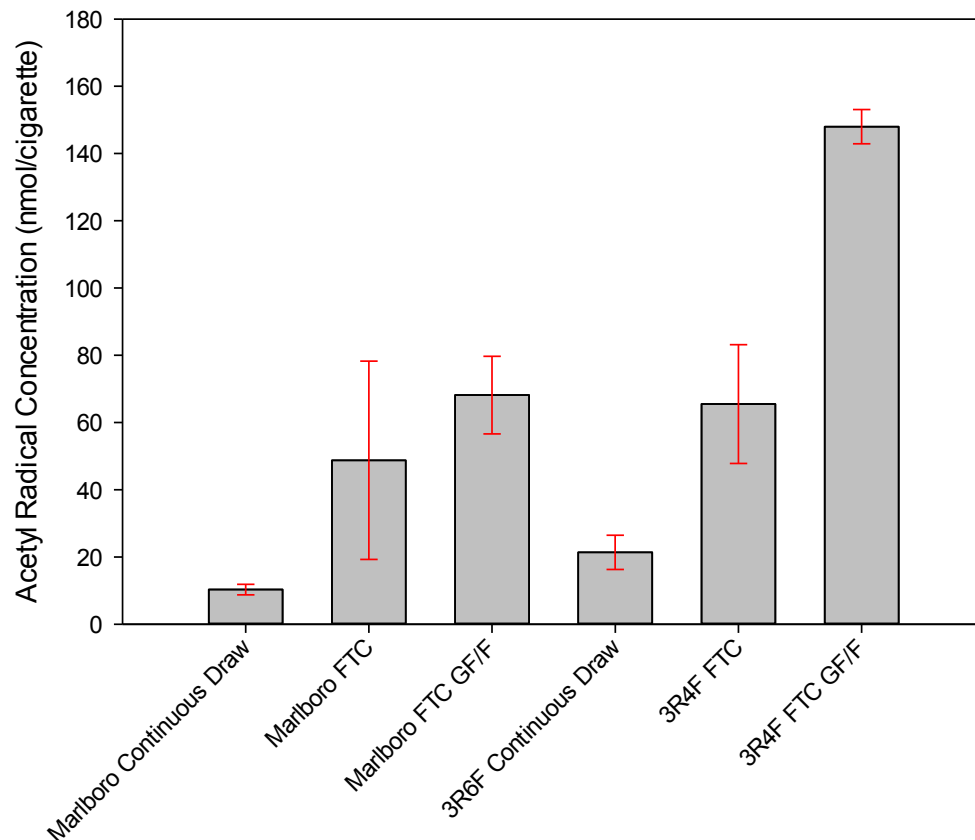


Figure 4.13. Acetyl radical concentrations compared for different cigarettes types, smoking conditions and particle filter set up. Error bars on the column diagram represent standard deviations of three parallel samples.

As shown in Figure 4.13, the bar graph compares the acetyl radical concentrations detected from both types of cigarettes sampled under different smoking conditions, with or without a GF/F particle filter.

Several immediate conclusions can be drawn from this quantitative analysis results. First, 10-150 nmol/cigarette of acetyl radicals were detected from both types of cigarettes sampled under all conditions investigated, including continuous draw methods and FTC standard conditions, with or without a GF/F particle filter. Second,

in comparing smoking conditions, more acetyl radicals were generated by the FTC puff-resolved method than by the continuous draw method. Third, a rather unexpected result is that, under the same FTC smoking conditions, both Marlboro and 3R4F cigarettes produced more acetyl radical in the presence of a GF/F particle filter.

Several computational models to investigate the generation of acetyl radical in smoke and the sensitivity of the trapping agent will be discussed in Chapter 5.

4.5 Conclusion

Acetyl radicals were trapped using 3AP from gas phase tobacco smoke of both commercial and research cigarettes under several different smoking conditions. A range of 10-150 nmol acetyl radical/cigarette were detected and identified by HPLC and mass spectroscopy. More radicals were detected from the puff smoking method compared to continuous flow sampling. Approximately twice as many acetyl radicals were trapped when a filter was placed before the trapping zone.

4.6 References

- Baker R. 1999. Tobacco: production, chemistry, and technology. Blackwell Science: 398-439.
- Bartalis J, Chan WG, Wooten JB. 2007. A new look at radicals in cigarette smoke. *Anal Chem* 79(13): 5103-5106.
- Bartalis J, Zhao YL, Flora JW, Paine JB, Wooten JB. 2009. Carbon-centered radicals in cigarette smoke: acyl and alkylaminocarbonyl radicals. *Anal Chem* 81(2): 631-641.
- Borgerding M, Klus H. 2005. Analysis of complex mixtures - Cigarette smoke. *Experimental and Toxicologic Pathology* 57: 43-73.
- Cueto R, Pryor WA. 1994. Cigarette-Smoke Chemistry - Conversion of Nitric-Oxide to Nitrogen-Dioxide and Reactions of Nitrogen-Oxides with Other Smoke Components as Studied by Fourier-Transform Infrared-Spectroscopy. *Vib Spectrosc* 7(1): 97-111.
- Davies MH, Vaught A. 1990. The Reference Cigarette. Kentucky Tobacco Research and Development Center; University of Kentucky: Lexington, KY.
- Flicker TM, Green SA. 1998. Detection and separation of gas-phase carbon-centered radicals from cigarette smoke and diesel exhaust. *Analytical Chemistry* 70(9): 2008-2012.
- Flicker TM, Green SA. 2001. Comparison of gas-phase free-radical populations in tobacco smoke and model systems by HPLC. *Environ Health Perspect* 109(8): 765-771.

- Green SA, Simpson DJ, Zhou G, Ho PS, Blough NV. 1990. Intramolecular Quenching of Excited Singlet-States by Stable Nitroxyl Radicals. *Journal of the American Chemical Society* 112(20): 7337-7346.
- Huang MF, Lin WL, Ma YC. 2005. A study of reactive oxygen species in mainstream of cigarette. *Indoor Air* 15(2): 135-140.
- Jia M, Tang Y, Lam YF, Green SA, Blough NV. 2009. Prefluorescent Nitroxide Probe for the Highly Sensitive Determination of Peroxyl and Other Radical Oxidants. *Analytical Chemistry* 81(19): 8033-8040.
- Johnson CG, Caron S, Blough NV. 1996. Combined liquid chromatography/mass spectrometry of the radical adducts of a fluorescamine-derivatized nitroxide. *Analytical chemistry* 68(5): 867-872.
- Jones AR, Beckstead JW, Lockey RF, Mohapatra SS. 2006. Cigarette smoke-induced gene expression analysis in normal human bronchial epithelial cells. *J Allergy Clin Immun* 117(2): S26-S26.
- Kieber DJ, Blough NV. 1990. Determination of Carbon-Centered Radicals in Aqueous-Solution by Liquid-Chromatography with Fluorescence Detection. *Analytical Chemistry* 62(21): 2275-2283.
- Kieber DJ, Johnson CG, Blough NV. 1992. Mass spectrometric identification of the radical adducts of a fluorescamine-derivatized nitroxide. *Free Radic Res Commun* 16(1): 35-39.
- Kindt R, Muller T. 2004. Toxic effects of cigarette smoke fractions and constituents in vitro by analysis of cell death and stress protein expression. *N-S Arch Pharmacol* 369: R119-R119.

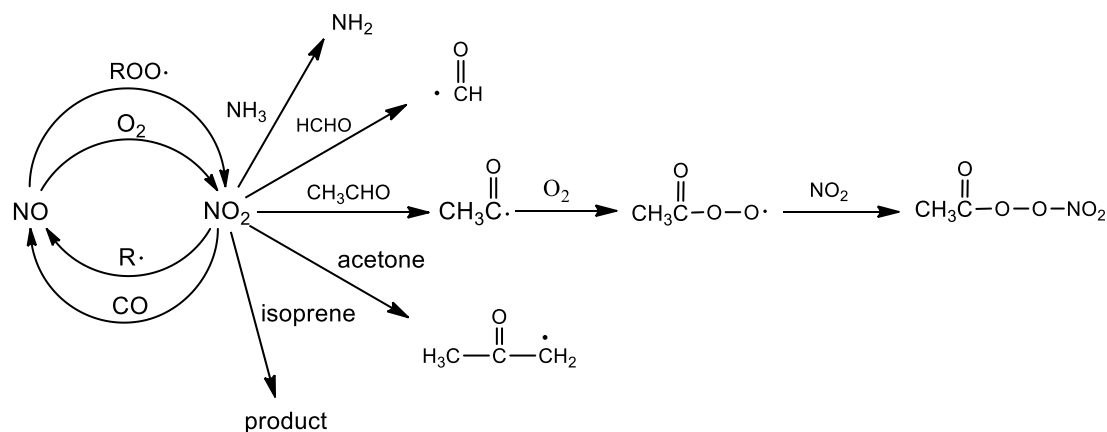
- Lyons MJ, Gibson JF, Ingram DJ. 1958. Free-radicals produced in cigarette smoke. *Nature* 181(4614): 1003-1004.
- Maskos Z, Khachatryan L, Dellinger B. 2008. Formation of the persistent primary radicals from the pyrolysis of tobacco. *Energ Fuel* 22(2): 1027-1033.
- Ozguner F, Koyu A, Cesur G. 2005. Active smoking causes oxidative stress and decreases blood melatonin levels. *Toxicol Ind Health* 21(1-2): 21-26.
- Polzin GM, Kosa-Maines RE, Ashley DL, Watson CH. 2007. Analysis of volatile organic compounds in mainstream cigarette smoke. *Environmental Science & Technology* 41(4): 1297-1302.
- Pryor WA. 1986. Cancer and free radicals. *Basic Life Sci* 39: 45-59.
- Pryor WA, Stone K, Stone K, Cross CE, Machlin L, Packer L. 1993. Oxidants in Cigarette-Smoke - Radicals, Hydrogen-Peroxide, Peroxynitrate, and Peroxynitrite. *Ann Ny Acad Sci* 686: 12-28.
- Stabbert R, Schafer KH, Biefel C, Rustemeier K. 2003a. Analysis of aromatic amines in cigarette smoke. *Rapid Commun Mass Sp* 17(18): 2125-2132.
- Stabbert R, Voncken P, Rustemeier K, Haussmann HJ, Roemer E, Schaffernicht H, et al. 2003b. Toxicological evaluation of an electrically heated cigarette. Part 2: Chemical composition of mainstream smoke. *J Appl Toxicol* 23(5): 329-339.
- Thompson BT, Mizaikoff B. 2006. Real-time Fourier transform-infrared analysis of carbon monoxide and nitric oxide in sidestream cigarette smoke. *Applied Spectroscopy* 60(3): 272-278.
- Wooten JB. 2011. Gas-phase Radicals in Cigarette Smoke: A Re-evaluation of the Steady-State Model and the Cambridge Filter Pad. *Organic Chemistry*.

Chapter 5: Models and Computational Simulations on Acetyl Radical Generation in Cigarette smoke³

³ Part of this chapter will be submitted to a peer-reviewed journal.

5.1 Introduction

Cigarette smoke is a complex mixture and dynamic system. Many factors are interactive and interrelated. As shown in Scheme 5.1, nitrogen dioxide can react with a range of volatile organic species present in smoke including acetaldehyde, isoprene, acetone, ammonia, and formaldehyde to produce radicals.



Scheme 5.1. Possible sources and sinks for NO₂ in cigarette smoke and other possible radicals generated by NO_x chemistry.

Pryor and coworkers (Pryor et al. 1983a) first suggested that the production of carbon-centered radicals in smoke is closely related to NO_x reactions, and that NO from cigarette smoke can be oxidized to NO₂ during and after the burning process. This early work proposed that NO₂ could react with species such as alkenes and dienes to produce carbon-centered radicals (Pryor et al. 1983b). The proposed reactions are shown in Table 5.1 below.

Table 5.1. Mechanisms proposed by Pryor and coworkers for radical generation in gas phase smoke. (Cueto and Pryor 1994)

| No. | Reaction |
|-----|---|
| 1 | $2NO + O_2 \rightarrow 2NO_2$ |
| 2 | $NO_2 + \text{isoprene} \longrightarrow \text{isoprenyl radical} + HNO_2$ <p style="text-align: center;">(R•)</p> |
| 3 | $R \cdot + O_2 \rightarrow RO_2 \cdot$ |
| 4 | $RO_2 \cdot + NO \rightarrow RO \cdot + NO_2$ |
| 5 | $RO_2 \cdot + NO_2 \rightarrow RO_2 - NO_2$ |
| 6 | $RO \cdot + NO_2 \rightarrow RO - NO_2$ |
| 7 | $RO \cdot + NO \rightarrow RO - NO$ |
| 8 | $R \cdot + NO_2 \rightarrow R - NO_2$ |
| 9 | $R \cdot + NO \rightarrow R - NO$ |

The dynamic nature of radical cycling in smoke makes it impossible to define a fixed concentration of radical species. The number trapped depends on the age of the smoke at the trapping point and the rates of competing scavenging reactions up to that point (Flicker and Green 2001). In addition, different trapping methods could have various effects on the amount of radical trapped. For example, Flicker and Green's application of glass beads (Bartalis et al. 2009; Flicker and Green 1998, 2001) can increase the surface area for trapping surface area but also accumulate tar and aerosols from the plumes, which affects the radical generation. Furthermore, the deposited tar and aerosols can result in more interference in HPLC, MS and LC-MS measurements.

Based on the abundant compounds in cigarette smoke shown in Table 5.2, several efforts have been made to mimic the generation of radicals in gas mixtures consisting of NO, air, and other species, such as isoprene (Pryor et al. 1983a), and with methanol as an OH scavenger (Flicker and Green 2001). However, no direct evidence has been shown for this reaction and the expected NO₂ addition products have not been found. Both Flicker and Green (Flicker and Green 2001) and Bartalis et al. (Bartalis et al. 2009) tried similar gas mixtures employing NO and isoprene, but obtained contrasting results. Flicker and Green showed that this model system produced several radicals, two of which matched peaks in tobacco smoke chromatograms; however, Bartalis and Wooten detected no radical production from the same reagent mix.

Table 5.2. Several abundant compounds and their concentrations in gas phase cigarette smoke.

| Compound | Concentration | |
|--------------|---------------|------------------|
| | µg/cig | ppm ^a |
| Nitric oxide | 300 | 700 |
| Isoprene | 400 | 410 |
| Methanol | 180 | 390 |
| Acetaldehyde | 900 | 1430 |
| Formaldehyde | 30 | 70 |

^aBased on 350 mL of smoke per cigarette, 298K, 1 atm. (Cueto and Pryor 1994)

In this study, model systems comprised of NO/air/acetaldehyde and NO/air/acetaldehyde/isoprene were investigated to study the acetyl radical generation in cigarette smoke. In addition to the experimental investigations, computational simulation by Matlab and the Master Chemical Mechanism (Jenkin et al. 1997; Saunders et al. 2003) were employed to study the reaction kinetics of the proposed mechanisms. The time profiles for the disappearance of NO and the appearance of

NO₂ and acetyl radical generation in cigarette smoke and in the model systems were simulated by a Matlab program (Brook 2005; ERI 2010). The Master Chemical Mechanism (Jenkin et al. 1997; Saunders et al. 2003) was also used to investigate a series of reactions with different initial concentrations.

5.2 Experiment and Method

Chemicals: 3-amino-2, 2, 5, 5-tetramethyl-proxyl (3AP), naphthalene-2, 3-dicarboxaldehyde (NDA), sodium cyanide, and HPLC grade methanol were purchased from ACROS. All chemicals were of the highest purity available and were used without further purification.

A solution of 0.02 g 3AP in a small amount of acetone was coated on the inner wall of the 140-mL sampling column and dried by rotary evaporation at room temperature. A model system employed to assess the gas-phase reaction of NO₂ and CH₃CHO is shown in Figure 5.1. Air was flowed across 3 mL of liquid phase acetaldehyde at room temperature to carry gas phase CH₃CHO to a Y-junction where it met 1000 ppm NO in N₂ (certified 1003.1 ppm, Praxair Distribution Inc.). As NO met the air, it was oxidized to NO₂ by oxygen, producing a distinctive brown color. A distillation column, which was coated with 3AP on the inner wall, acted as the reaction vessel and the trapping surface. When the gas mixture reached the column, radicals were trapped by 3AP (Figure 5.1) and analyzed later by HPLC and LCMS. The airflow was from the building supply. Trace NO₂ from the NO tank was removed by bubbling NO through a 50% solution of sodium hydroxide. (Not shown in Figure 5.1.) Additional 3 mL of acetaldehyde was added to the gas phase mixtures to study the promoting effect of isoprene for acetyl radical generation.

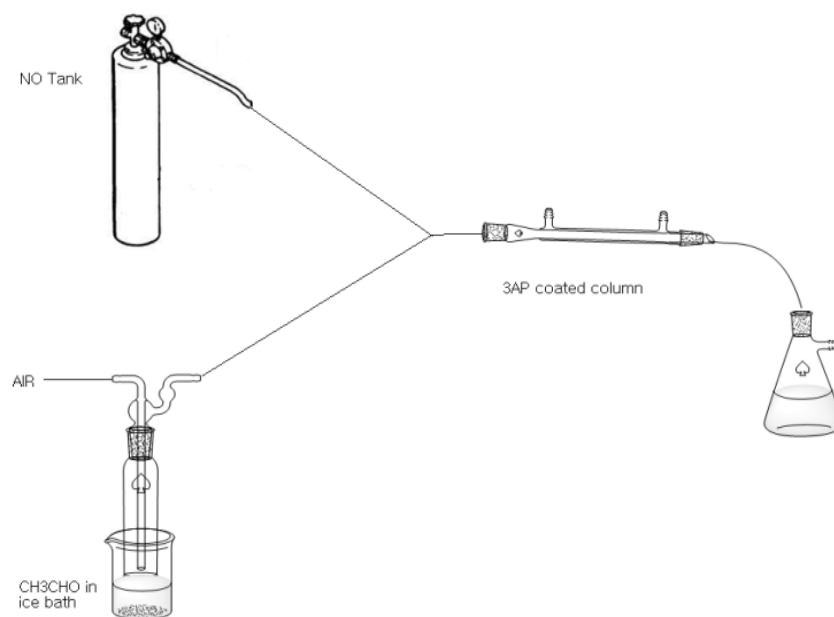


Figure 5.1. Diagram of gas mixture model reaction apparatus.

After sampling, 3AP adducts were washed from the sampling column with 10 mL methanol. Next the solution was filtered with a Hyper Sep C18 column (Thermo Electron Corporation[®]), giving a light yellow solution, while the dark colored R-3AP adducts remained on the column. 10 mL methanol was used to flush the sample from the column, giving a dark yellow solution. For derivatization, 500 μ L of water, 500 μ L of filtered sample solution, 200 μ L of sodium cyanide solution, and 200 μ L of NDA solution were added sequentially to a foil-wrapped glass vial and allowed to react for 30 min.

After derivatization, the 3AP adduct solution was filtered with a 0.2- μ m syringe filter (HPLC syringe filter, Alltech[®]), and yellow material (R-3AP-NDA) precipitated onto the filter. This yellow precipitate was washed off with 1 mL 80% methanol in water. The filtered solution and reconcentrated precipitate were combined to inject into HPLC.

Instrumentation: The HPLC was a Shimadzu Prominence LC-20AD with DGU-20A₅ vacuum degasser, and Shimadzu SPD-20AU UV/Vis detector, and RF-10A_{XL} fluorescence detector (FLD). Thermo BioBasic-18125×4mm 5μ particle-packed HPLC column was used and the injection volume was 20 μL. The FLD was operated at 420/480 nm excitation/emission wavelengths for all separations. Separation of R-3AP-NDA adducts were carried out isocratically at 25 °C, with a flow rate of 0.500 mL/min. The mobile phase composition was 30%/70% H₂O/methanol.

A stock solution of 10 mM CPA was used to make a calibration curve to estimate concentrations of trapped radicals. CPA was derivatized by NDA as above, sequentially diluted and used as an external standard for quantitative analysis.

Mass spectrometric analyses were conducted with a Thermo Finnigan LCQTM Advantage LC/MS. The mobile phase was 50%/50% methanol/H₂O with 0.2% acetic acid. The Thermo BioBasic-18125×4mm 5μm particle-packed HPLC column was used for LC separation. The flow rate was 0.200 mL/min. Ionization conditions were capillary voltage 3.95 kV, cone voltage 35 V, sheath gas flow 29.00 L/min, auxiliary gas flow 49.47 L/min, capillary temperature at 252.30 °C, ND collision potential 20 V. Selected ion monitoring (SIM) was employed to detect 3AP-C (O) CH₃ (*m/z* 200.15).

Computations

Publically available Matlab routines (Brook 2005; ERI 2010) were employed to run simplified kinetic calculations of the generation of acetyl radicals from model gas mixture and cigarette smoke. For additional information on computational modeling, see code samples for Figure 5.3 and 5.4 in Appendix.

The more complex chain reactions simulations employed the Master Chemical Mechanisms (MCM). The Master Chemical Mechanism is a large near-explicit chemical mechanism developed by Jenkin et al. at Leeds University to describe the complete gas-phase chemical reactions of primary emitted volatile organic compounds (VOCs) in the atmosphere. The current version of the MCM (MCMv3.1) contains 143 primary emitted VOCs with a resultant mechanism containing 17,000 reactions and 6700 primary, secondary and radical species (Jenkin et al. 1997; Saunders et al. 2003).

MCM provides extractable versions of the full or subsets of the reactions based on marked species. In this study, reactions, reaction rates and initial concentrations were directly input based on our model. MCM was demonstrated as a powerful tool in our radical chemical reactions modeling.

5.2 Result

Mass spectrum, LC-MS and HPLC fluorescence spectrum results of the NO/air/CH₃CHO model were shown in previous Chapter 3 and Chapter 4 respectively.

Comparison of the representative chromatograms resulting from NO/air/CH₃CHO model and NO/air/CH₃CHO/isoprene model is shown in Figure 5.2. From Figure 5.2, we can see that the intensity of acetyl radical around 6.3 min increased when isoprene was added to the NO/air/CH₃CHO model.

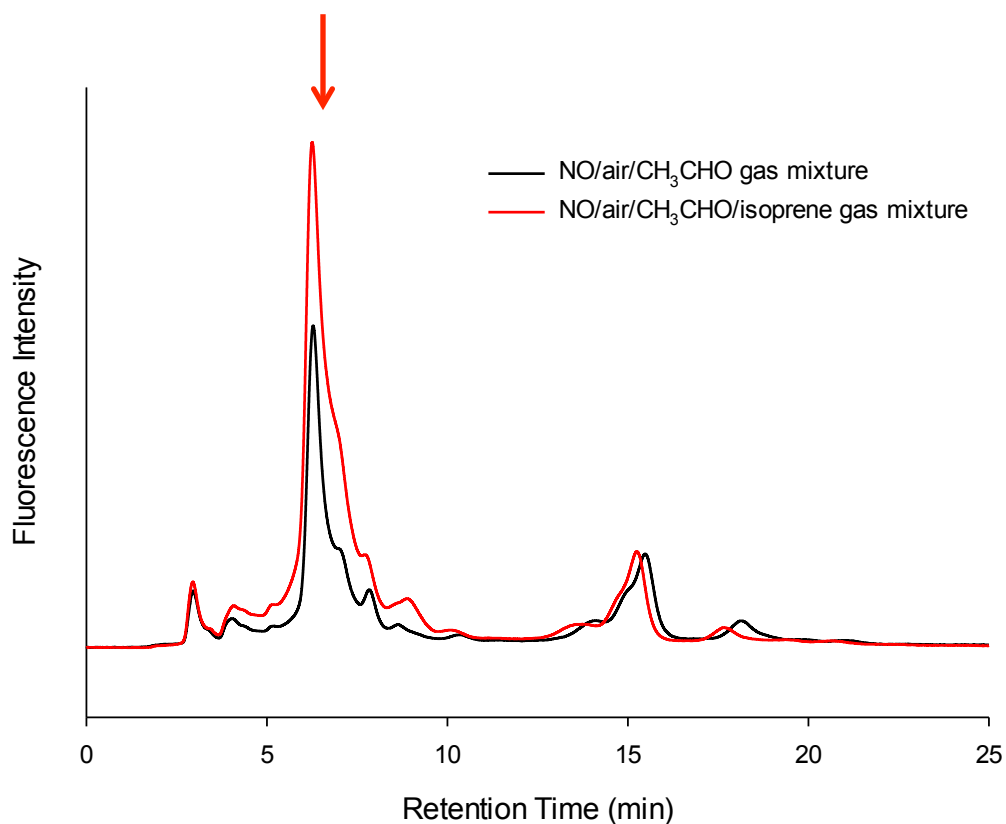


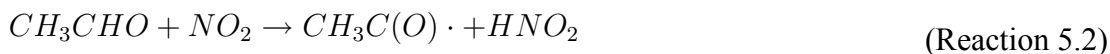
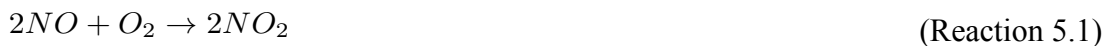
Figure 5.2. Comparison of the representative chromatograms resulting from NO/air/CH₃CHO model and NO/air/CH₃CHO/isoprene model. Conditions: Thermo BioBasic-18 125×4 mm 5μ particle-packed HPLC column; isocratic elution at 0.500 mL/min with 50/50 methanol/H₂O; fluorescence detection at 420 nm (Ex)/480 nm (Em).

Both NO/air/CH₃CHO and NO/air/CH₃CHO/isoprene models produce similar chromatograms as shown in Figure 5.2. As identified in previous chapters, the peak eluted at around 6.3 min is acetyl radical and the broad peak with shoulder at 15 min is oxidized 3AP adducts. Quantitatively, while the oxidized 3AP adducts show similar intensity in two models, the addition of isoprene in second model remarkably produces more acetyl radical as indicated by the red arrow. It shows that isoprene can be an additional source of acetyl radical in cigarette smoke. Further computational simulation is investigated below.

5.3 Discussion

5.3.1. Simplified NO-NO₂-CH₃CHO Mechanism Investigation by Matlab

To better understand how acetyl radicals are generated, we used a computational simulation to investigate a series of reactions in gas phase. Our specific goal was to identify the key precursors and reaction pathways that produce this primary radical. We first consider mechanisms based on NO and acetaldehyde, both of which are major components of smoke.



As in previous studies, the reactive species is taken to be NO₂, which is slowly produced by oxidation of NO in the plume (Reaction 5.1). In a second step, NO₂ abstracts hydrogen from acetaldehyde to give the acetyl radical (Reaction 5.2). As one of the major components in tobacco smoke (900±250 µg/cig) (Borgerding and

Klus 2005), acetaldehyde is a likely precursor of the dominant acetyl radical observed.

The presence of NO is well documented in tobacco smoke (Baren et al. 2004; Borgerding and Klus 2005) with the accepted values typically 300 to 600 ppm or 1.7 ± 0.2 $\mu\text{g}/\text{cig}$ (Baren et al. 2004; Pryor et al. 1993). However, the concentration of NO₂ continues to be disputed (Shorter et al. 2006; Wooten 2011).

Cueto and Pryor (1994) reported that nitric oxide disappeared as nitrogen dioxide appeared in tobacco smoke and in mixtures of nitric oxide, methanol, and isoprene in air (Cueto and Pryor 1994). In contrast, Shorter and colleagues, using a very sensitive technique called quantum cascade tunable infrared laser differential absorption spectroscopy (TILDAS), detected very little NO₂ in mainstream cigarette smoke (Shorter et al. 2006).

Several important differences in the experiments can reconcile this discrepancy. Cueto and Pryor sampled undiluted smoke over a period of 800 s. In Shorter's experiment, the mainstream smoke was diluted by a factor of 4.2 before being drawn into the gas cell to remove particles, which interfere with TILDAS measurements. The concentration was further decreased because the pressure in the sample cell was extremely low, about 0.059 atm. This dilution greatly reduced the initial NO concentration, which dramatically slows NO-NO₂ conversion. Under these conditions very little NO₂ would be expected within the 0.16 s sampling period, and little was detected. An additional potential discrepancy is the practice of "conditioning" cigarettes over a supersaturated ammonium nitrate solution in a desiccator to maintain constant humidity (Cueto and Pryor 1994); presumably this

practice could increase the nitrogen content of the tobacco.

To simplify the problem, we started our simulation of reactions 5.1 and 5.2 by employing two sets of initial concentrations of acetaldehyde and nitrogen dioxide: (i) our experimental gas mixture, and (ii) literature data for 3R4F reference cigarette. For the model gas system, the initial concentration of acetaldehyde was obtained by assuming that it is saturated in the gas phase at 20°C according to its vapor pressure of 98.65 kPa and NO was defined by the tank standard as 1000 ppm. The simulation was run for 8000 s to fully reproduce the rise and decrease of NO₂.

Reaction 1 occurs with a third-order rate constant of 2.00×10^{-38} cm⁶/molecules²·s at 298K (Atkinson et al. 2004). Reactive NO₂, produced from relatively unreactive NO in smoke, can abstract H from CH₃CHO to produce CH₃C(O)· with a second-order rate constant of 3.36×10^{-23} cm³/molecules·s at 298K (Jaffe and Wan 1974). A Matlab-based kinetic analysis using concentrations employed in our gas mixture reaction gives a plot of concentrations vs. time (shown in Figure 5.3.). The acetyl radical is generated and allowed to accumulate, neglecting scavenging reactions (e.g. CH₃C(O)· reacting with 3AP, NO₂ or O₂). Although neglecting scavenging is obviously unrealistic, this gives a first approximation of the feasibility of this mechanism.

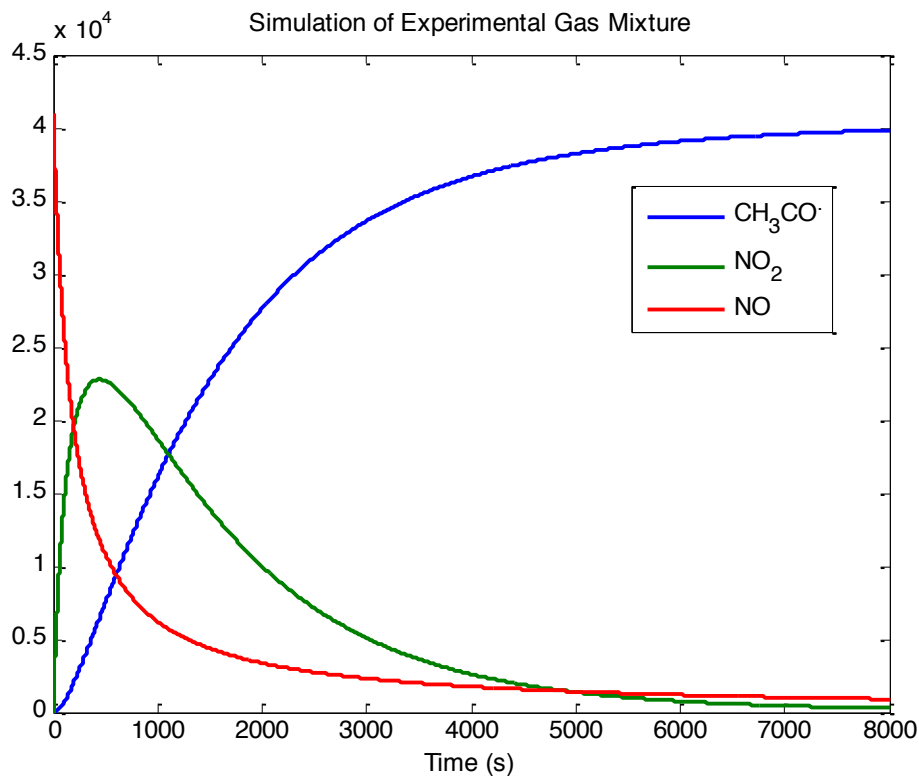


Figure 5.3. Matlab computational simulation of generation of $\text{CH}_3\text{C}(\text{O})\cdot$ from our experimental gas mixture. $[\text{NO}]_0 = 2.47 \times 10^{16}$ molecules/ cm^3 ; $[\text{CH}_3\text{CHO}]_0 = 2.44 \times 10^{19}$ molecules/ cm^3 ; $[\text{O}_2]_0 = 5.65 \times 10^{18}$ molecules/ cm^3 . Please see a sample of coding in the Appendix.

Figure 5.3 shows that NO_2 concentration increases in the first few minutes, reaching its maximum at about 300 s, and afterwards decreases because of the combined effects of depletion by acetaldehyde and the consumption of NO in the gas mixture. The NO/ NO_2 concentration simulation shows a similar profile to the appearance and disappearance of NO/ NO_2 measured by FT-IR in previous experiments (Cueto and Pryor 1994). Acetyl radical concentration increases in the beginning and reaches a plateau several minutes later after all reactants are consumed.

Based on this computational simulation, it is not a surprise that puff-resolved FTC generates more acetyl radical than the continuous method, for the puff-resolved FTC methods allow longer residence time (at least 60 s) than its counterpart (~ 10 s) for NO_2 to evolve in the smoke as it passes through the trapping column.

For a real-world cigarette smoke scenario, we take 3R4F Kentucky Reference cigarette under FTC standard smoking conditions as an example. Literature values for 2R4F (which were replaced by the 3R4F series) were chosen for the initial concentrations of NO and acetaldehyde because the concentration data for 3R4F are not available. We expect the acetaldehyde concentration of 584 $\mu\text{g}/\text{cig}$ (mainstream smoke) to be similar (Lin and Yu 2011). Based on an average of 8 puffs for each cigarette, there is 73 μg of acetaldehyde in each 35 mL puff, neglecting the loss from smoldering process. Hence, 2.85×10^{16} molecules/ cm^3 of acetaldehyde was used as the initial concentration for the smoke simulation (which is 850 times less than the model gas example). A similar calculation provided the initial nitrogen oxide concentration for the smoke simulation. The concentration of NO in mainstream smoke for a 2R4F cigarette is from 300 ppm to 600 ppm, which is 7.38×10^{15} to 1.61×10^{16} molecules/ cm^3 (Baren et al. 2004; Cueto and Pryor 1994); a value of 1.35×10^{16} molecules/ cm^3 was selected, similar to the value for the model gas mixture.

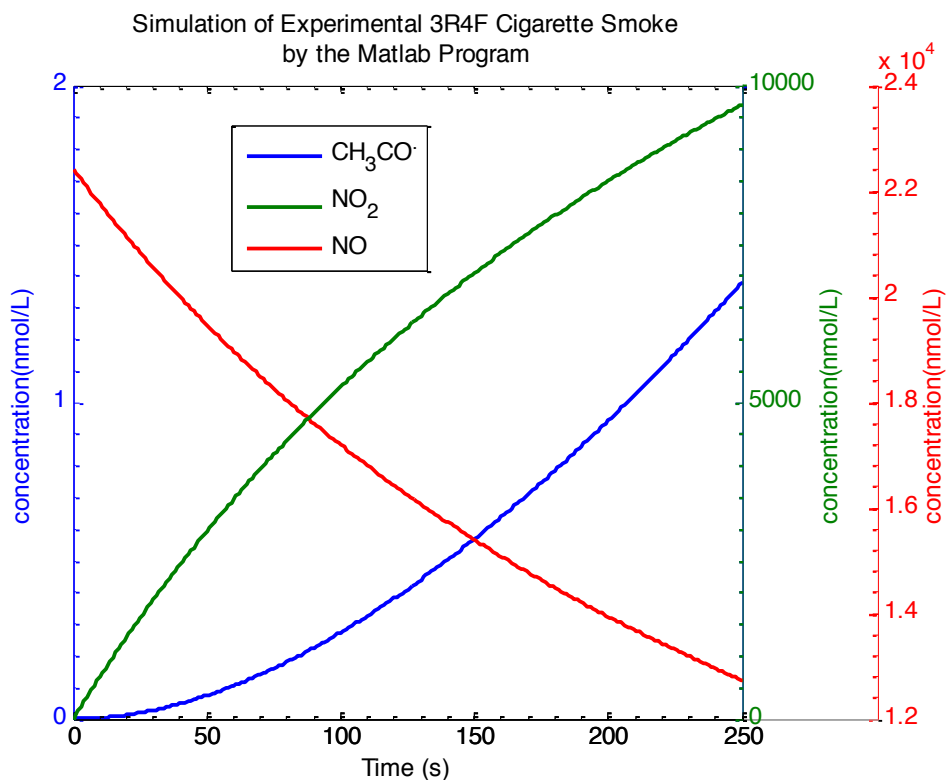


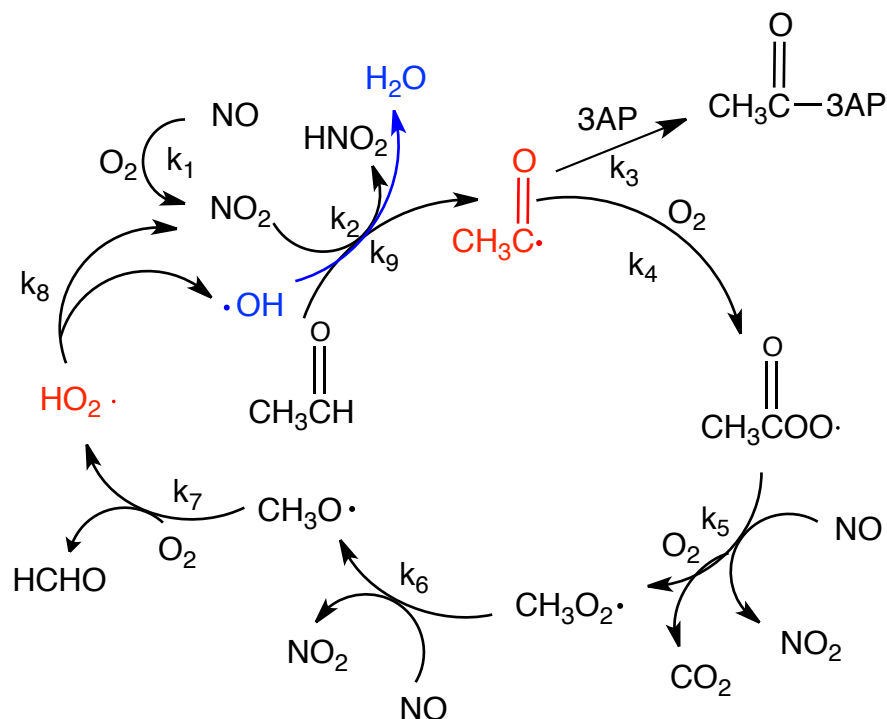
Figure 5.4. Matlab-based kinetic calculation of the production of $\text{CH}_3\text{C}(\text{O})\cdot$ from the 3R4F Kentucky Reference cigarette smoke based on literature reported initial concentrations of CH_3CHO and NO in the smoke. $k_1 = 2.0 \times 10^{-38} \text{ cm}^6/\text{molecule}^2 \cdot \text{s}$ at 298K. $k_2 = 3.36 \times 10^{-23} \text{ cm}^3/\text{molecules} \cdot \text{s}$ at 298K; $[\text{NO}]_0 = 1.35 \times 10^{16} \text{ molecules}/\text{cm}^3$; $[\text{CH}_3\text{CHO}]_0 = 2.85 \times 10^{16} \text{ molecules}/\text{cm}^3$; $[\text{O}_2]_0 = 5.65 \times 10^{18} \text{ molecules}/\text{cm}^3$. Please see a sample of coding in the Appendix.

The total volume of column and tubing is about 146 mL, while each puff is 35 mL. If we neglect diffusion, it takes 250 s for one puff of smoke to be completely removed from the trapping column. As shown in Figure 5.4, the maximum accumulated concentration of $\text{CH}_3\text{CO}\cdot$ at 250 seconds, which is the longest residence time of FTC puff-resolved smoke in the column, is 1.3 nmol/L, or about 0.36 nmol in total for the 280 mL of smoke sampled for each cigarette. This is far less than the number trapped experimentally, 50-84 nmol/cigarette, from the 3R4F Kentucky Reference cigarette under FTC conditions (Table 4.2). Thus, while acetyl radical generation by reactions of CH_3CHO and NO_2 is kinetically feasible, at plausible initial concentrations of these major components in tobacco smoke, these gas phase reactions cannot account for the amount of acetyl radical detected.

5.3.2. Atmospheric Chain Reactions Model Investigation by Master of Chemical Mechanisms

To determine whether subsequent reactions can increase the yield of acetyl radical, we investigated the series of chain reactions shown in Scheme 5.2, simulated by the MCM program. In the presence of oxygen, acetyl radical can be rapidly oxidized into acetyl peroxide radical (Table 5.4, Reaction 5.4), which can again convert NO into NO_2 at a much faster rate compared to NO- NO_2 conversion by oxygen (Table 5.4, Reactions 5.5 and 5.6). The resulting $\text{RO}\cdot$ can produce $\text{HO}_2\cdot$ (Table 5.4, Reaction 5.7), which can again convert NO into NO_2 and generate an OH radical (Table 5.4, Reaction 5.8), which is well known for its rapid hydrogen

abstraction ability (Table 5.4, Reaction 5.9). The reaction rate of OH with acetaldehyde is 10^{12} times larger than that for hydrogen abstraction by NO_2 ; but in a simple mix starting with only acetaldehyde and NO, its concentration is at least 10^{12} times smaller. As shown in Scheme 5.2, the generation of OH radical could accelerate acetyl radical production and initiate another faster acetyl radical generation cycle.

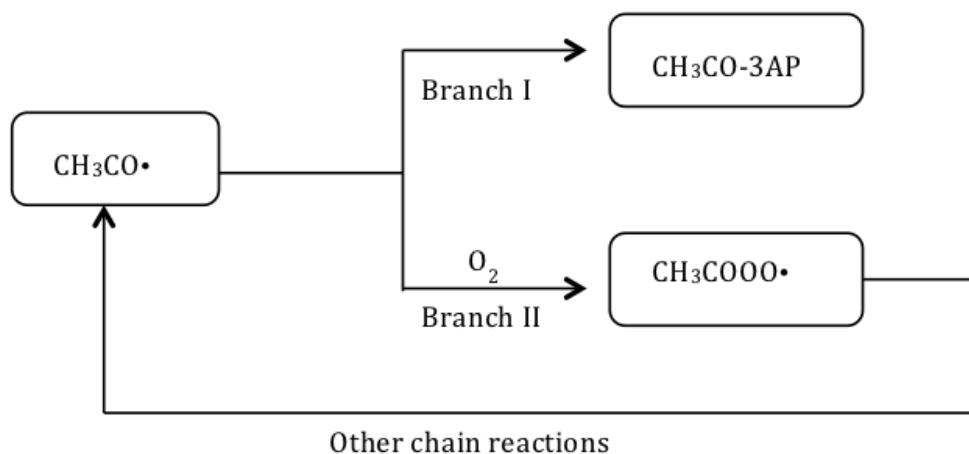


Scheme 5.2. Acetaldehyde-based chain reactions of acetyl radical generation in tobacco smoke.

These chain reactions and their capacity to produce acetyl radical were investigated by the Master Chemical Mechanism (MCM) program from Leeds University (Saunders et al. 1997, 2003). This program is designed to simulate atmospheric reactions given selected initial species and, importantly, includes reactions of peroxide species resulting from addition of oxygen to primary radicals.

In modeling these chain reaction mechanisms we must explicitly include the 3AP radical trap. Because the O_2 scavenging reaction is very fast ($k_4=5.00\times 10^{-12}\text{cm}^3/\text{molecule s}$) and O_2 is present in high concentrations ($5.56\times 10^{18}\text{ molecules/cm}^3$), the steady state concentration of acetyl radical is extremely small. However, radical trapping schemes, with 3AP or nitron spin traps, do not measure steady state radical concentrations; rather they act as competitive scavengers for the radicals, removing a fraction of them from the chain process. The process is depicted as a simplified flowchart in Scheme 5.3, which shows the two possible fates for acetyl radicals. Through Branch I, acetyl radicals are trapped by 3AP and removed from the reaction cycle; through Branch II, the radicals react with oxygen to produce acetyl peroxide, which can ultimately regenerate acetyl radical through a series of chain reactions. As shown in Scheme 5.3, 3AP cannot trap all the acetyl radicals from model or smoke sample in the presence of oxygen and other radicals. Hence, the amount of acetyl trapped by 3AP depends on the relative ratio of $k_{3AP}[3AP]/k_{O_2}[O_2]$. To simulate experimental results, we must specify a trapping rate, e.g. $k_{3AP}[3AP]$, which is not well defined because 3AP is adsorbed to the surface. Flicker and Green (Flicker and Green 2001) studied the dependence of the amount of radicals trapped from the gas phase smoke on the 3AP coating surface area, taken as proportional to the 3AP concentration, based on a 100% coating coverage and appropriate orientation for reaction. They expected that the amount of radical trapped would increase with increasing 3AP concentration until all of the radicals were trapped by a sufficiently high 3AP concentration, and then level off at a maximum value. They found that the amount of radicals trapped increased with the increasing surface area of 3AP coating

from 80 cm² to 150 cm² by employing smaller beads. Unfortunately, they didn't obtain the maximum value for trapping radicals since it was impossible to out-compete oxygen by increasing 3AP surface area.



Scheme 5.3. The flowchart of acetyl radical cycling and sinks in gas phase.

The initial concentrations for investigated compounds by the MCM modeling are shown in Table 5.3 below. The initial concentration for 3AP was varied from 5.56×10^{10} to 5.56×10^{20} molecules/cm³ to study the trapping efficiency. The reactions and rate constants for this simulation are shown in Table 5.4. The simulation then gives the concentration of CH₃O-3AP trapped in the first 25 seconds. We ran the simulation on these chain reactions for only the first 25 seconds because with certain initial concentrations the simulation became unstable at a longer time because of the limitation of the program at small time steps.

Table 5.3. Compounds and initial concentrations for MCM simulation on 3AP sensitivity by NO/air/CH₃CHO model.

| Compounds | Initial Concentration (molecules/cm ³) |
|------------------------|---|
| NO | 1.35×10^{16} |
| CH ₃ CHO | 2.85×10^{16} |
| O ₂ | 5.56×10^{18} |
| 3AP | $5.56 \times 10^{(10-20)}$ ^a |
| CH ₃ CO | 0 |
| NO ₂ | 0 |
| CH ₃ COOO | 0 |
| CH ₃ COO | 0 |
| CH ₃ O | 0 |
| CO | 0 |
| HCHO | 0 |
| HO ₂ | 0 |
| OH | 0 |
| H ₂ O | 0 |
| CH ₃ CO-3AP | 0 |

^a Initial concentration for 3AP is varied from 5.56×10^{10} to 5.56×10^{20} molecules/cm³ to study the sensitivity.

Table 5.4. Reactions from mcm_subset for MCM simulation on 3AP sensitivity by NO/air/CH₃CHO model.

| No. | Reaction | Rate Constant ^{a,b} |
|-----|--|------------------------------|
| 5.1 | $2NO + O_2 \rightarrow 2NO_2$ | $k_1 = 2.0 \times 10^{-38}$ |
| 5.2 | $CH_3CHO + NO_2 \rightarrow CH_3C(O) \cdot + HNO_2$ | $k_2 = 3.36 \times 10^{-23}$ |
| 5.3 | $CH_3C(O) \cdot + 3AP \rightarrow CH_3C(O) - 3AP$ | $k_3 = 5.00 \times 10^{-12}$ |
| 5.4 | $CH_3C(O) \cdot + O_2 \rightarrow CH_3C(O)O_2 \cdot$ | $k_4 = 5.00 \times 10^{-12}$ |
| 5.5 | $CH_3C(O)O_2 \cdot + NO + O_2 \rightarrow CH_3O_2 \cdot + NO_2 + CO_2$ | $k_5 = 2.4 \times 10^{-11}$ |
| 5.6 | $CH_3O_2 \cdot + NO \rightarrow CH_3O \cdot + NO_2$ | $k_6 = 8.9 \times 10^{-12}$ |
| 5.7 | $CH_3O \cdot + O_2 \rightarrow HCHO + HO_2 \cdot$ | $k_7 = 1.65 \times 10^{-15}$ |
| 5.8 | $HO_2 \cdot + NO \rightarrow NO_2 + OH \cdot$ | $k_8 = 8.91 \times 10^{-12}$ |
| 5.9 | $CH_3CHO + OH \cdot \rightarrow CH_3C(O) \cdot + H_2O$ | $k_9 = 1.50 \times 10^{-11}$ |

^a. Units for second order reaction: cm³/molecule s;

Third order third reaction: cm⁶/molecule² s

^b. Reaction rates citations: (Atkinson et al. 2004; Atkinson et al. 1997; Atkinson 2001; Jaffe and Wan 1974; Orlando et al. 2003; Pandis 1998; Paulson et al. 1992)

Figure 5.5-5.7 shows MCM-based kinetic calculation of the production of CH₃C(O)· trapped by 3AP from the 3R4F Kentucky Reference cigarette smoke at 25 s when $k_{3AP}[3AP]/k_{O_2}[O_2]$ equals to 10⁻⁸, 10⁻⁴ and 100 respectively. Additional figures for different $k_{3AP}[3AP]/k_{O_2}[O_2]$ ratios are shown in the Appendix 1-16.

As we can see from Figure 5.5, NO, CH₃CHO, O₂, and 3AP are consumed while CH₃CO, NO₂, CH₃COOO, CH₃O, HCHO, HO₂, OH, H₂O and CH₃CO-3AP are produced during the chain reactions. When $k_{3AP}[3AP]/k_{O_2}[O_2]$ increases from 10⁻⁸ in Figure 5.5 to 10⁻⁴ in Figure 5.6, more CH₃CHO-3AP is generated. However, when $k_{3AP}[3AP]/k_{O_2}[O_2]$ increases from 10⁻⁴ in Figure 5.6 to 100 in Figure 5.7, the

concentration of CH_3CHO -3AP drops. At the same time, it must be pointed out that some graphs may visibly exaggerate the concentration change by how the scales are displayed. For example, it appears that the concentration of O_2 significantly drops in the Figure 5.5, however, the real scale on the graph shows that only 0.09 % oxygen is consumed after 25 seconds.

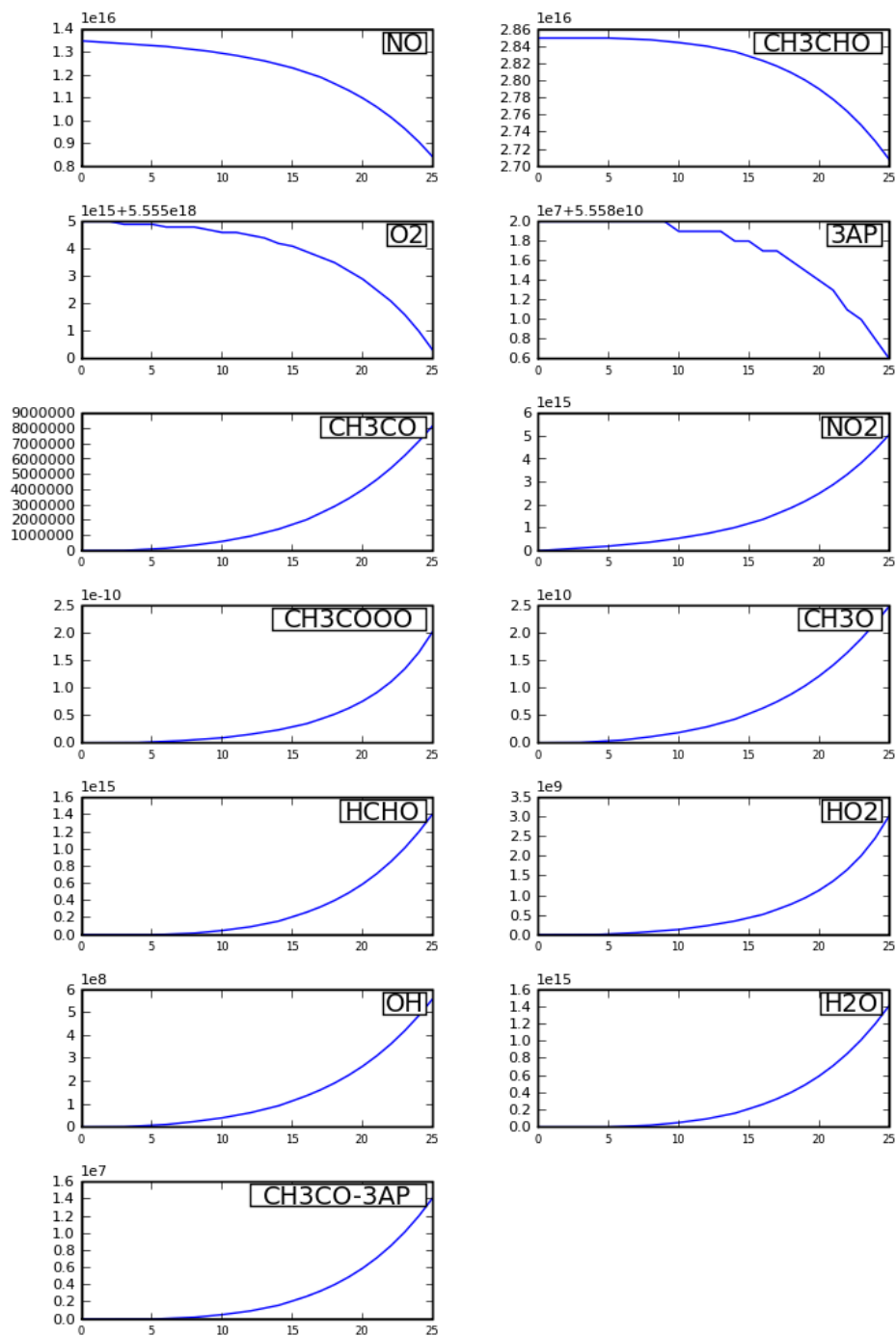


Figure 5.5. MCM simulation by NO/air/CH₃CHO model on the generation of CH₃C(O)-3AP from the 3R4F Kentucky Reference cigarette smoke at 25 s when $k_{3AP}[3AP]/k_{O_2}[O_2]$ equals to 10^{-8} . Concentrations are in molecules/cm³.

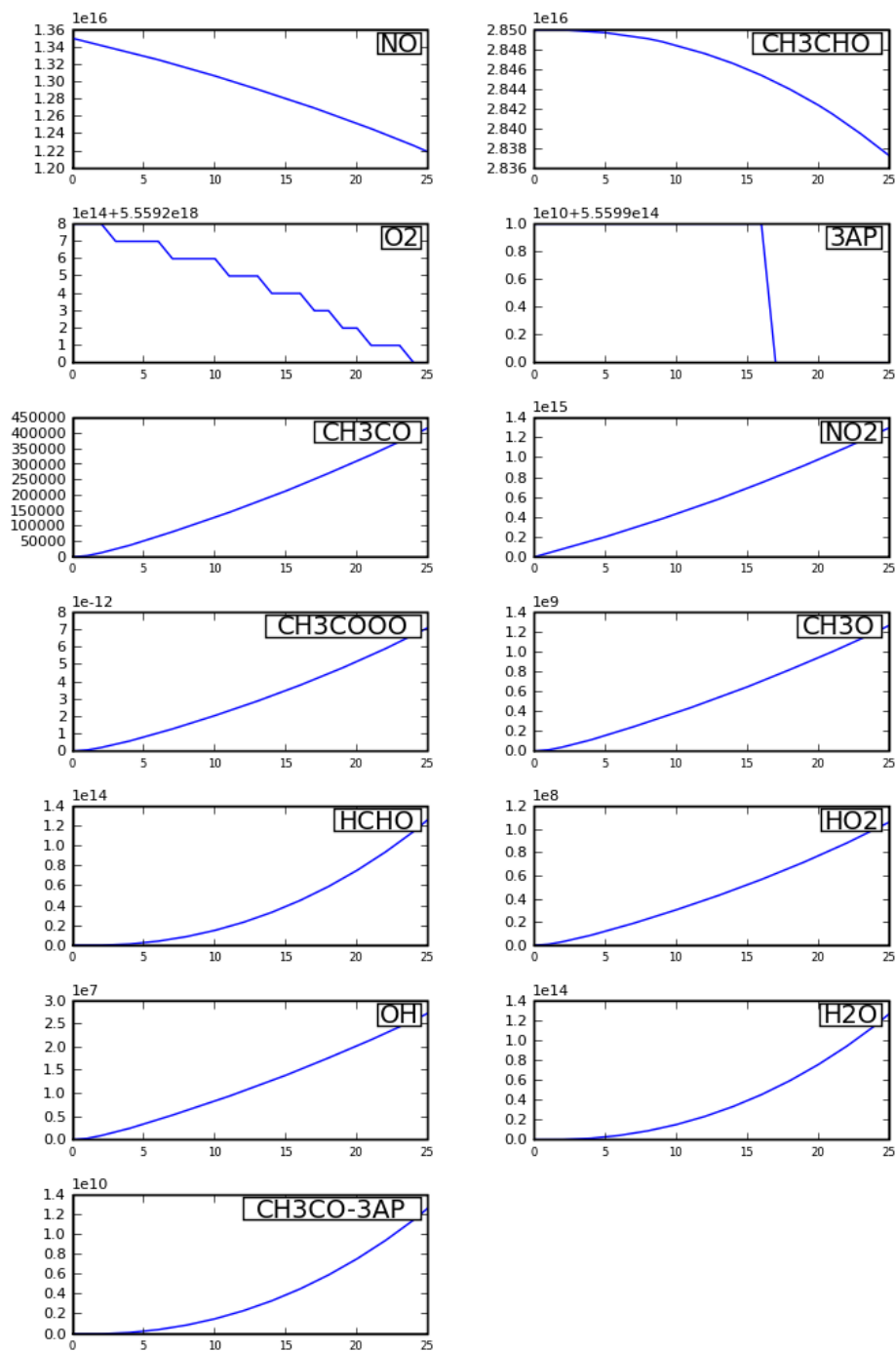


Figure 5.6. MCM simulation by NO/air/CH₃CHO model on the generation of CH₃C(O)-3AP from the 3R4F Kentucky Reference cigarette smoke at 25 s when $k_{3AP}[3AP]/k_{O_2}[O_2]$ equals to 1×10^{-4} . Concentrations are in molecules/cm³.

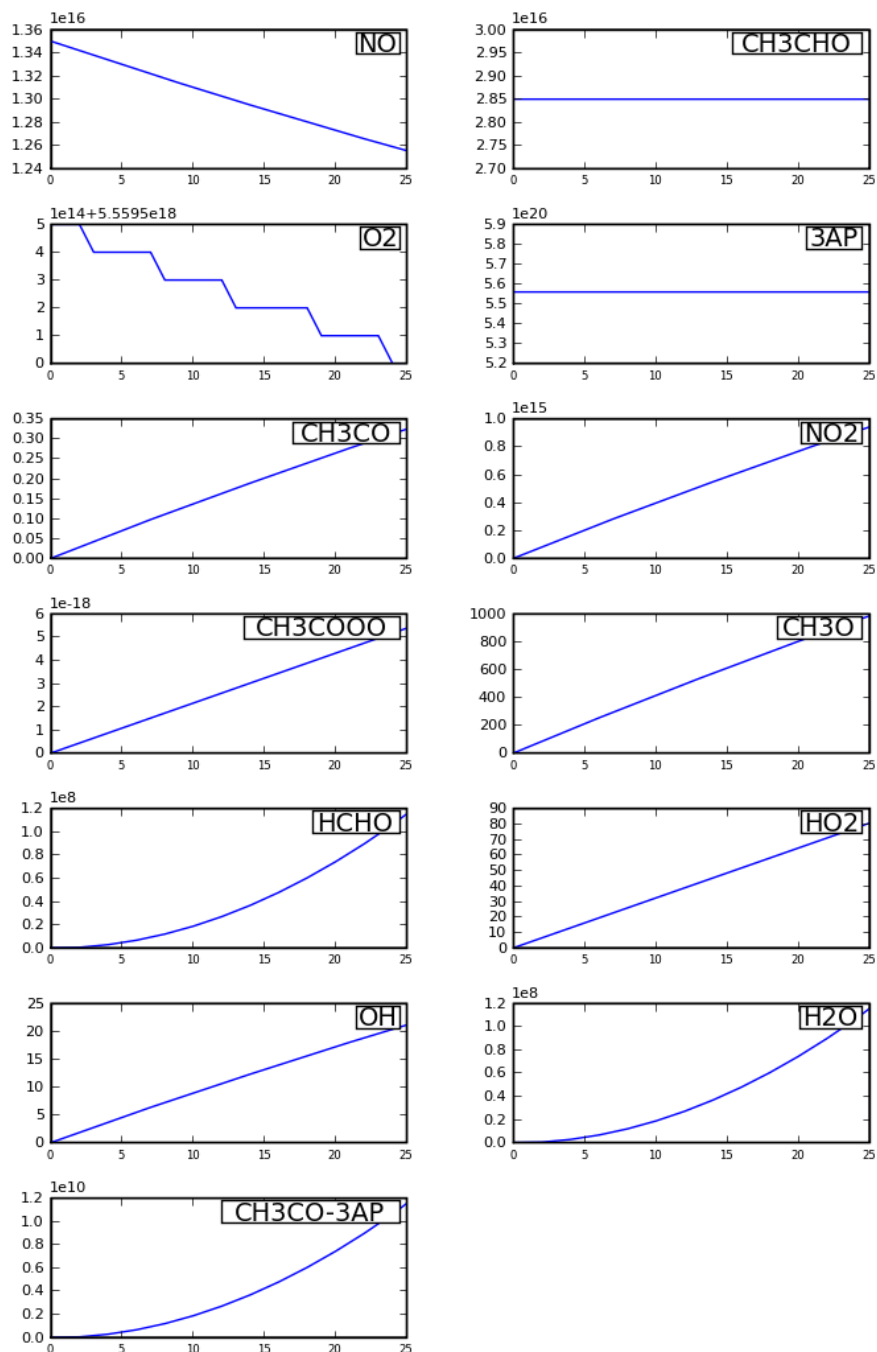


Figure 5.7. MCM simulation by NO/air/CH₃CHO model on the generation of CH₃C(O)-3AP from the 3R4F Kentucky Reference cigarette smoke at 25 s when $k_{3AP}[3AP]/k_{O_2}[O_2]$ equals to 100. Concentrations are in molecules/cm³.

Competitive Effects of 3AP and O₂ on Acetyl Radical Trapping by NO/air/CH₃CHO Model

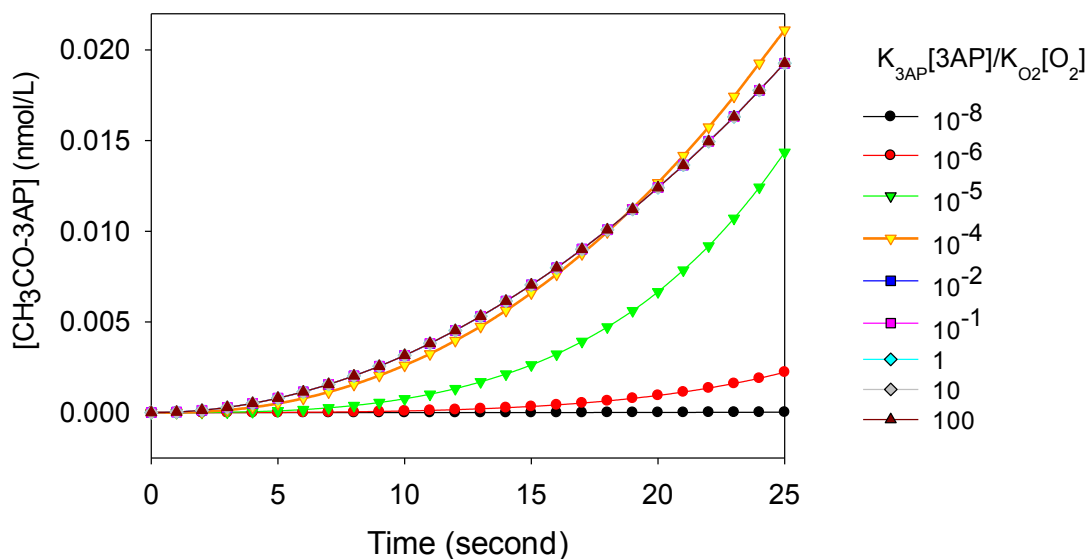


Figure 5.8. MCM simulation by NO/air/CH₃CHO model on the generation of CH₃C(O)-3AP at different $k_{3AP}[3AP]/k_{O_2}[O_2]$. Points from 10^{-2} to 100 are overlapping.

Figure 5.8 shows that the trapped acetyl radical concentration increases with time. It also shows that at 25 s, with the increasing of $k_{3AP}[3AP]/k_{O_2}[O_2]$, the CH₃CO-3AP concentration increases first and then starts to drop at a certain $k_{3AP}[3AP]/k_{O_2}[O_2]$ ratio, and in the end levels off when the ratio is larger than about 10^{-3} .

MCM Simulation of Competitive Effects of 3AP and O₂
on Acetyl Radical Trapping by NO/air/CH₃CHO Model

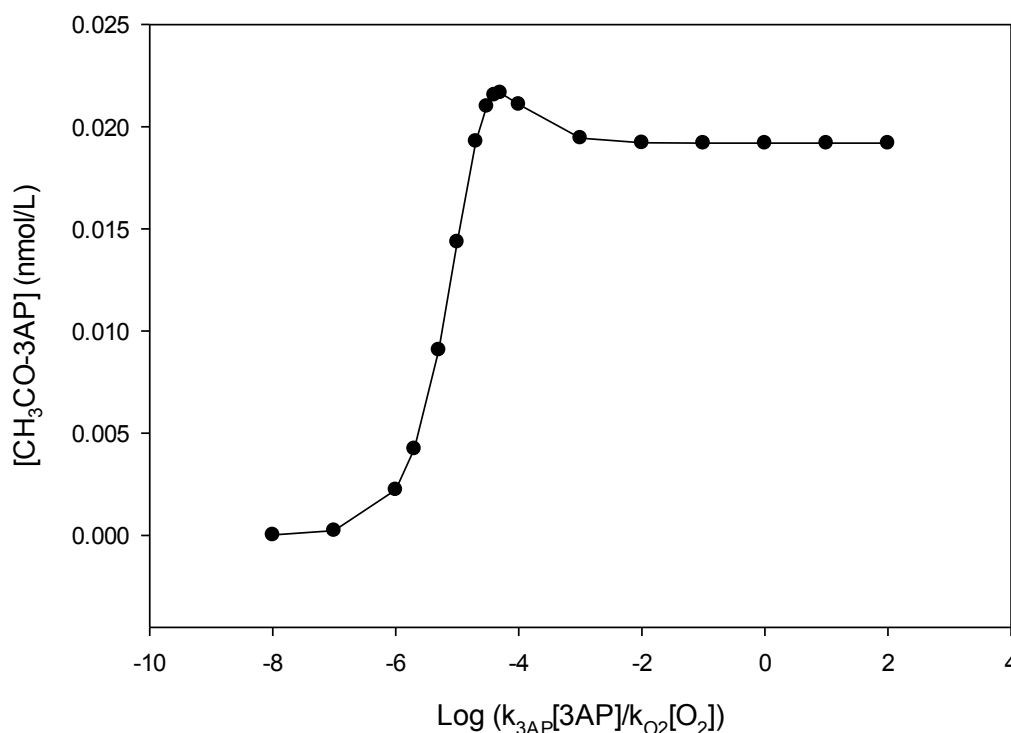


Figure 5.9. MCM simulation by NO/air/CH₃CHO model on the generation of CH₃C(O)-3AP from the 3R4F Kentucky Reference cigarette smoke at 25 s at different $k_{3AP}[3AP]/k_{O_2}[O_2]$ ratios ($k_{O_2}[O_2] = 2.78 \times 10^7 \text{ s}^{-1}$).

As shown in Figure 5.9, the amount of acetyl radical trapped is very sensitive to its relative rate of reaction with O₂ ($k_{O_2}[O_2]$) and the trap (e.g. $k_{3AP}[3AP]$). Surprisingly, as shown in Figure 5.9, in contrast with what Flicker and Green expected, the amount of radicals trapped does not increase continuously with increasing 3AP concentration before it levels off at a maximum value. Instead, the largest amount of acetyl radical is trapped when $k_{3AP}[3AP]/k_{O_2}[O_2]$ equals to 10^{-4} , which shows a bump in the graph. If very small concentrations of 3AP are present,

then most acetyl radicals react with O_2 , and few are trapped; at high 3AP concentrations, all acetyl radicals are trapped as they are formed, so that the chain reaction would be thwarted and the maximum trapped amount is equivalent to values calculated from the simplified Matlab model at the same period of 25 second as shown in Figure 5.10 (0.0195 nmol/L). Hence, below the optimal ratio of $k_{3AP}[3AP]/k_{O_2}[O_2]$, O_2 scavenging reaction plays a major role and the amount of acetyl radical trapped increases with the increasing of 3AP concentration. When it reaches the optimal ratio, O_2 scavenging and 3AP trapping is balanced and a maximum of 0.0220 nmol/L of acetyl radical is obtained. Beyond the optimal ratio, 3AP-trapping reaction plays a major role and the amount of acetyl radical trapped decreases with increasing 3AP concentration until the chain reaction is completely thwarted and the concentration of CH_3CO -3AP levels off. The bump in the graph indicates that an optimal 3AP concentration range is required to achieve the maximum trapping efficiency.

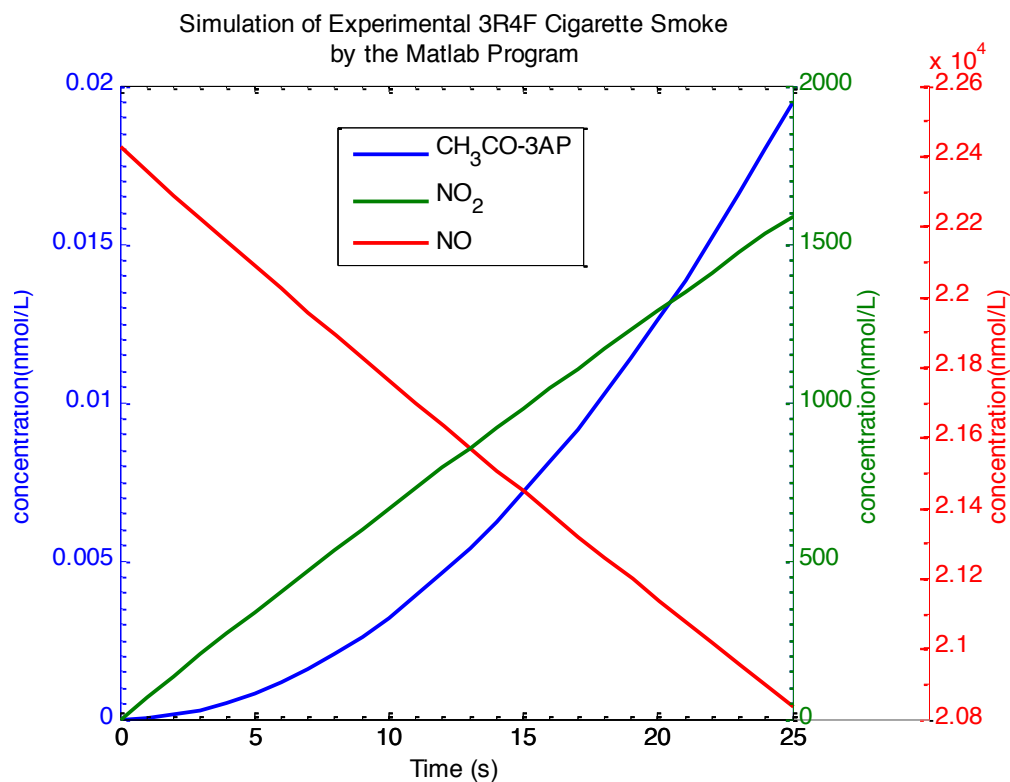


Figure 5.10. Matlab-based kinetic calculation of the production of $\text{CH}_3\text{C}(\text{O})\cdot$ from the 3R4F Kentucky Reference cigarette smoke based on literature reported initial concentrations of CH_3CHO and NO in the smoke. $k_1 = 2.0 \times 10^{-38} \text{ cm}^6/\text{molecule}^2 \cdot \text{s}$ at 298K. $k_2 = 3.36 \times 10^{-23} \text{ cm}^3/\text{molecules} \cdot \text{s}$ at 298K; $[\text{NO}]_0 = 1.35 \times 10^{16} \text{ molecules}/\text{cm}^3$; $[\text{CH}_3\text{CHO}]_0 = 2.85 \times 10^{16} \text{ molecules}/\text{cm}^3$; $[\text{O}_2]_0 = 5.65 \times 10^{18} \text{ molecules}/\text{cm}^3$.

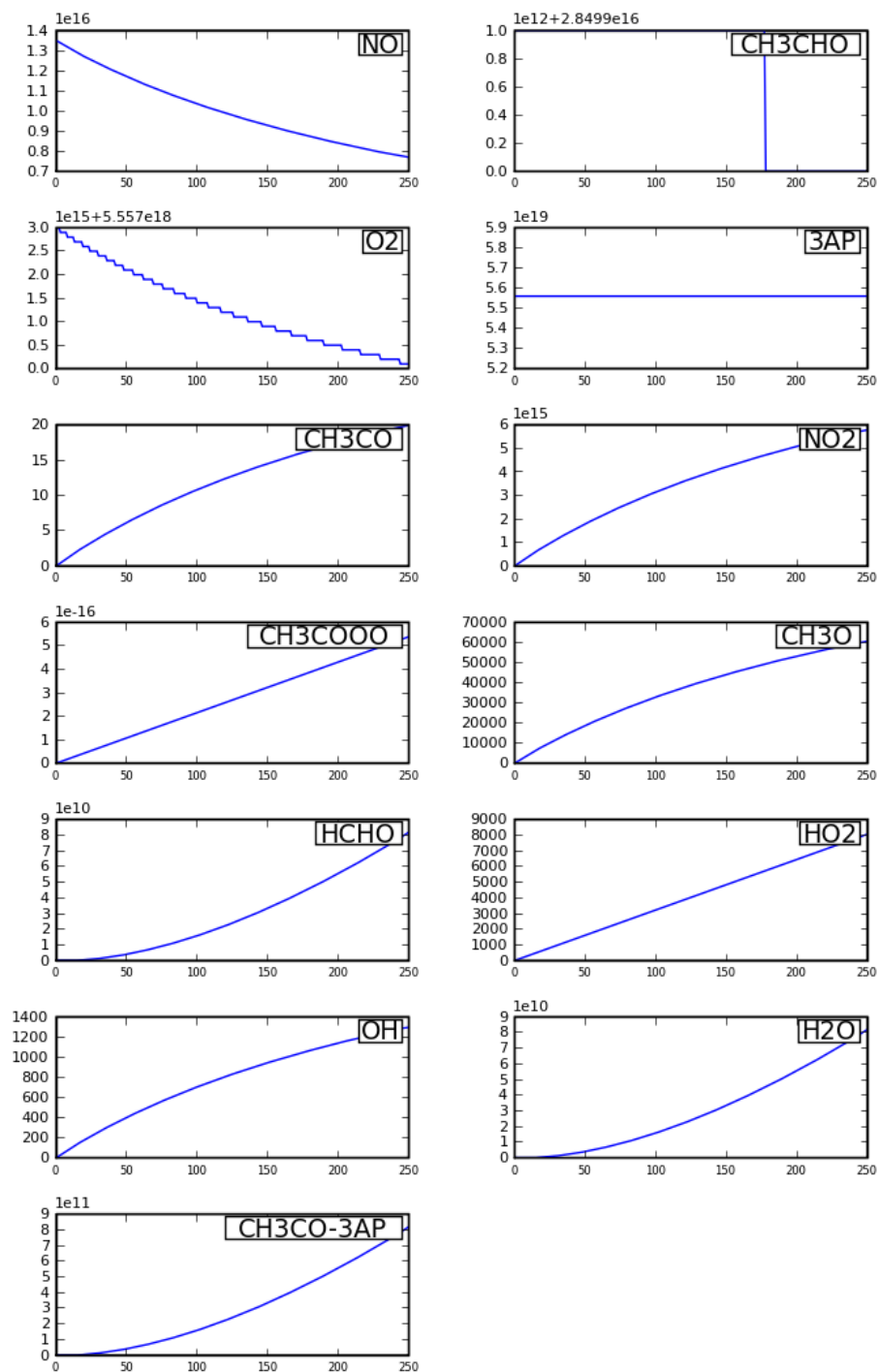


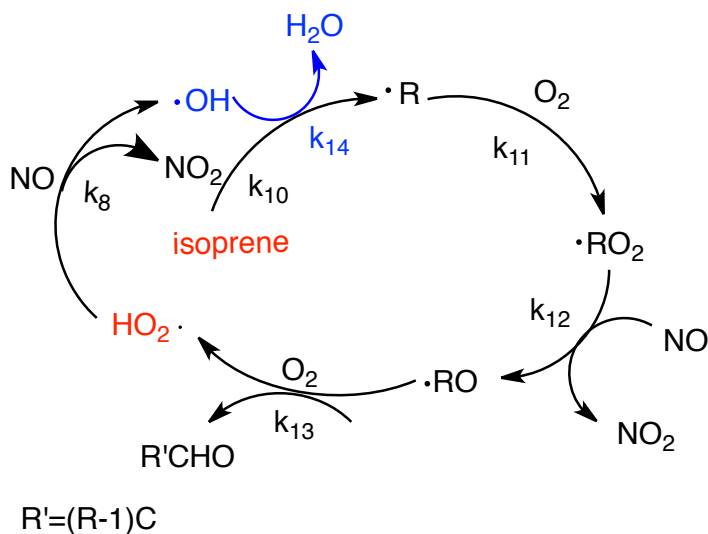
Figure 5.11. MCM simulation by NO/air/CH₃CHO model on the generation of CH₃C(O)-3AP from the 3R4F Kentucky Reference cigarette smoke at 250 s when $k_{3AP}[3AP]/k_{O_2}[O_2]$ equals to 10. Concentrations are in molecules/cm³.

Figure 5.11 shows that with a $k_{3AP}[3AP]/k_{O_2}[O_2]$ ratio of 10, the simulated amount of acetyl radical trapped is only 1.33 nmol/L (or 0.37 nmol/ cigarette), far smaller than we measured experimentally of 50-84 nmol/cigarette . Clearly, the full suite of reactions initiated by NO and acetaldehyde are insufficient to explain the concentration we measured. Thus, an additional constituent in tobacco smoke must contribute to the formation of acetyl radicals in smoke gas phase.

5.3.3. Atmospheric Chain Reactions Model with Isoprene Addition

Investigation by Master of Chemical Mechanisms

As shown in Scheme 5.4, an additional source of radicals initiating radicals could be unsaturated organic compounds such as isoprene, which is a major constituent of tobacco smoke (200-400 $\mu\text{g}/\text{cigarette}$) (Hoffmann et al. 2001). These compounds can undergo radical reactions to generate HO_2 , which can refuel the generation of acetyl radical.



Scheme 5.4. Isoprene chain reactions to generate HO_2 radical in gas phase smoke.

Table 5.5. Compounds and initial concentrations for MCM simulation on 3AP sensitivity by NO/air/CH₃CHO/isoprene model.

| Compounds | Initial Concentration (molecules/cm ³) |
|---|---|
| NO | 1.35×10^{16} |
| CH ₃ CHO | 2.85×10^{16} |
| O ₂ | 5.56×10^{18} |
| 3AP | 5.56×10^{19} |
| C ₅ H ₈ | 1.10×10^{16} |
| CH ₃ CO | 0 |
| NO ₂ | 0 |
| CH ₃ COOO | 0 |
| CH ₃ COO | 0 |
| CH ₃ O | 0 |
| CO | 0 |
| HCHO | 0 |
| HO ₂ | 0 |
| OH | 0 |
| H ₂ O | 0 |
| CH ₃ CO-3AP | 0 |
| C ₅ H ₈ NO ₂ | 0 |
| C ₅ H ₈ NO ₄ | 0 |
| C ₅ H ₈ NO ₃ | 0 |
| C ₄ H ₆ NO ₂ CHO | 0 |
| C ₅ H ₉ O | 0 |

Table 5.6. Proposed reactions for acetyl radical generation in cigarette smoke by NO/air/CH₃CHO/isoprene model.

| No. | Reaction | Reaction rate ^{a,b} |
|------|--|-----------------------------------|
| 5.1 | $2NO + O_2 \rightarrow 2NO_2$ | $k_1 = 2.0 \times 10^{-38}$ |
| 5.2 | $CH_3CHO + NO_2 \rightarrow CH_3C(O) \cdot + HNO_2$ | $k_2 = 3.36 \times 10^{-23}$ |
| 5.3 | $CH_3C(O) \cdot + 3AP \rightarrow CH_3C(O) - 3AP$ | $k_3 = 5.00 \times 10^{-12}$ |
| 5.4 | $CH_3C(O) \cdot + O_2 \rightarrow CH_3C(O)O_2 \cdot$ | $k_4 = 5.00 \times 10^{-12}$ |
| 5.5 | $CH_3C(O)O_2 \cdot + NO + O_2 \rightarrow CH_3O_2 \cdot + NO_2 + CO_2$ | $k_5 = 2.4 \times 10^{-11}$ |
| 5.6 | $CH_3O_2 \cdot + NO \rightarrow CH_3O \cdot + NO_2$ | $k_6 = 8.9 \times 10^{-12}$ |
| 5.7 | $CH_3O \cdot + O_2 \rightarrow HCHO + HO_2 \cdot$ | $k_7 = 1.65 \times 10^{-15}$ |
| 5.8 | $HO_2 \cdot + NO \rightarrow NO_2 + OH \cdot$ | $k_8 = 8.91 \times 10^{-12}$ |
| 5.9 | $CH_3CHO + OH \cdot \rightarrow CH_3C(O) \cdot + H_2O$ | $k_9 = 1.50 \times 10^{-11}$ |
| 5.10 | $NO_2 + C_5H_8 \rightarrow R \cdot$ | $k_{10}^c = 1.81 \times 10^{-19}$ |
| 5.11 | $R \cdot + O_2 \rightarrow RO_2 \cdot$ | $k_{11} = 5.00 \times 10^{-12}$ |
| 5.12 | $RO_2 \cdot + NO \rightarrow RO \cdot + NO_2$ | $k_{12} = 8.9 \times 10^{-12}$ |
| 5.13 | $RO \cdot + O_2 \rightarrow R'CHO + HO_2 \cdot$ | $k_{13} = 1.9 \times 10^{-15}$ |
| 5.14 | $C_5H_8 + OH \cdot \rightarrow R \cdot$ | $k_{14}^d = 1.01 \times 10^{-15}$ |

^a. Units for second order reaction: cm³/molecule s;

Third order third reaction: cm⁶/molecule² s

^b. Reaction rates citations: (Atkinson et al. 2004; Atkinson et al. 1997; Atkinson 2001; Jaffe and Wan 1974; Orlando et al. 2003; Pandis 1998; Paulson et al. 1992)

^{c,d}. R= C₅H₈-NO₂ or C₅H₈-OH

Including isoprene in the MCM model adds reactions 5.10-14 (Table 5.6) and accelerates production of peroxy and hydroxy radicals, as well as NO_2 . Specifically, at 250 s, the levels of OH are over 10,000 times greater while the NO_2 concentration is approximately doubled (Figure 5.12). Adding isoprene-initiated reactions boosts the yield of acetyl radicals to 3002.2 nmol/L, or 840.6 nmol/cigarette, when the $k_{3\text{AP}}[3\text{AP}]/k_{\text{O}_2}[\text{O}_2]$ ratio is 10 at 25 s. Lower ratios are probably more realistic and, according to the sensitivity shown in Figure 5.13, could easily produce the observed experimental range of 50-84 nmol/cigarette of acetyl radical from 3R4F research cigarettes under FTC standard smoking conditions. Approximately 50 nmol/cigarette of acetyl radical was reported by others. (Bartalis et al. 2007; Bartalis et al. 2009; Gerardi and Coleman 2010). This small discrepancy can be accounted for by different trapping efficiencies, nitroxide/oxygen ratios in their experiments, and the nature of the different reference cigarettes (2R4F vs. 3R4F).

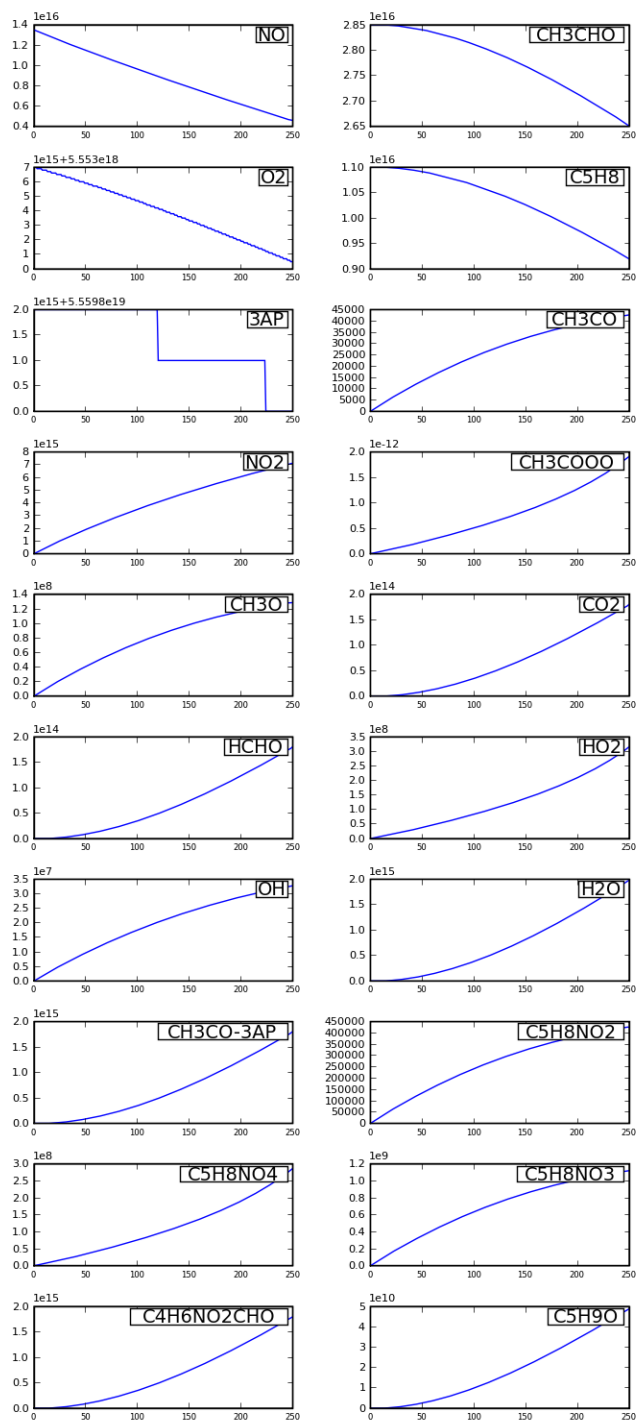


Figure 5.12. MCM simulation by NO/air/CH₃CHO/isoprene model on the generation of CH₃C (O)-3AP from the 3R4F Kentucky Reference cigarette smoke at 250 s when $k_{3AP}[3AP]/k_{O_2}[O_2]$ equals to 10. Concentrations are in molecules/cm³.

MCM Simulation of Competitive Effects of 3AP and O₂
on Acetyl Radical Trapping by NO/air/CH₃CHO/isoprene Model

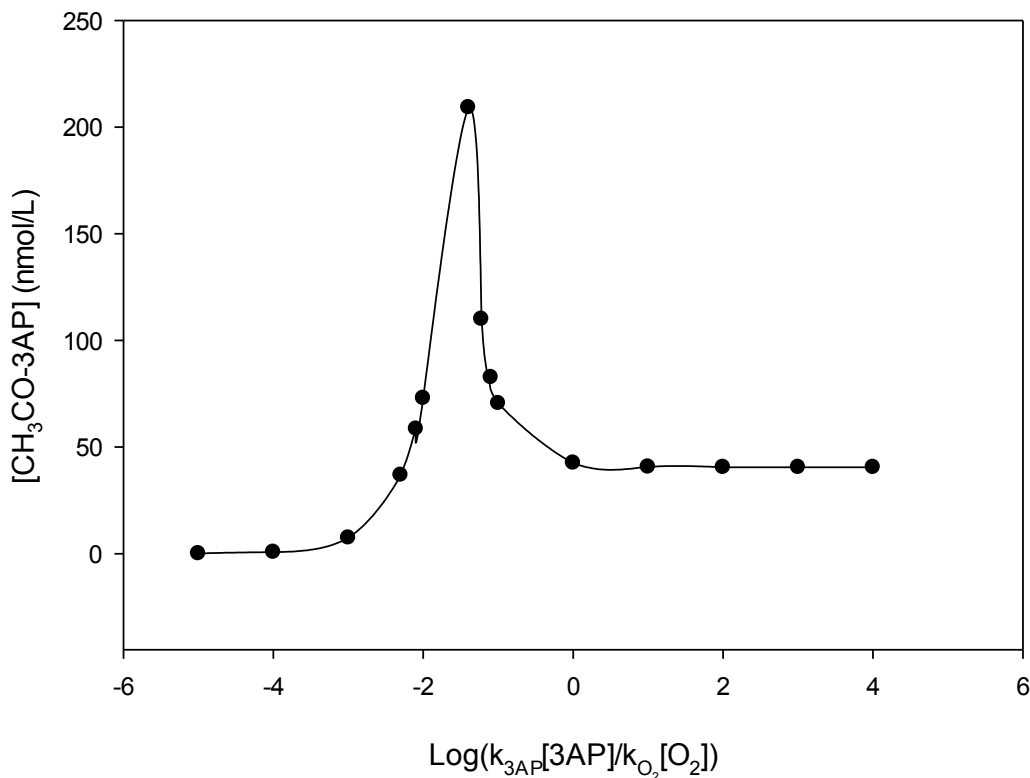


Figure 5.13. MCM simulation by NO/air/CH₃CHO model on the generation of CH₃C(O)-3AP from the 3R4F Kentucky Reference cigarette smoke at 25 s at different $k_{3AP}[3AP]/k_{O_2}[O_2]$ ratios ($k_{O_2}[O_2] = 2.78 \times 10^7 \text{ s}^{-1}$) by NO/air/CH₃CHO/isoprene model.

Similar to results shown in Figure 5.9, the amount of acetyl radical trapped simulated by NO/air/CH₃CHO/isoprene model is also very sensitive to its relative rate of reaction with O₂ ($k_{O_2}[O_2]$) and the trap (e.g. $k_{3AP}[3AP]$).

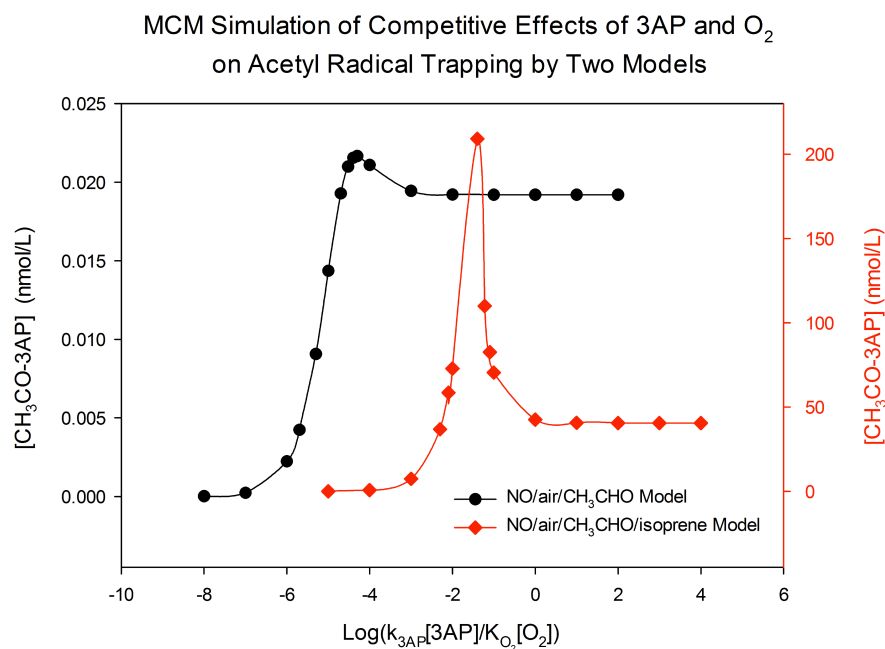


Figure 5.14 Comparison of the competitive effects of 3AP and O₂ on acetyl radical trapping by NO/air/CH₃CHO and NO/air/CH₃CHO/isoprene models.

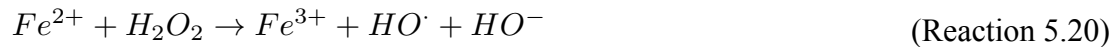
As shown in Figure 5.14, both models show optimal values for $k_{3AP}[3AP]/k_{O_2}[O_2]$ on the acetyl radical trapping. In NO/air/CH₃CHO model, the highest concentration of CH₃CHO-3AP of 0.023 nmol/L is obtained when $k_{3AP}[3AP]/k_{O_2}[O_2]$ is about 10^{-5} ; in NO/air/CH₃CHO/isoprene model, the highest concentration of CH₃CHO-3AP of more than 200 nmol/L is obtained when $k_{3AP}[3AP]/k_{O_2}[O_2]$ is about 10^{-2} . The shift of optimal $k_{3AP}[3AP]/k_{O_2}[O_2]$ in two different models is because more acetyl radical is generated by NO/air/CH₃CHO/isoprene model, it needs more 3AP to trap the radicals. Hence, the optimal $k_{3AP}[3AP]/k_{O_2}[O_2]$ increases from 10^{-4} to 10^{-2} in NO/air/CH₃CHO and NO/air/CH₃CHO/isoprene models.

A direct result demonstrated by Figure 5.14 is that the values of radicals trapped by nitroxides as often reported in the literature should not be considered definitive. Only a small fraction of radicals are trapped, and trapping interrupts further radical generation. Based on different models or reactions, different optimal ratios are suggested. Indeed, in a dynamic system where radicals are continually generated and consumed, the concept of radicals/cigarette isn't well defined and does not provide the full profile of radical generation in gas phase cigarette smoke. Thus, although we have reported radical numbers in units of nmol/cigarette and nmol/L for experimental measurements and computational simulations, respectively, these units are only appropriate to compare results of similar experiments.

In addition to acetaldehyde and isoprene, other aldehydes and alkenes in tobacco smoke could undergo similar reactions and produce acetyl radical in tobacco smoke.

The synergistic effect of tobacco tar is also proposed to be another source for the radicals measured in gas phase smoke. Primary and secondary radicals on TMP can produce OH radicals on the tar, which can greatly promote further reactions. The TMP accumulated on the filter provides tar-deposited long-lived radicals, which can produce superoxide anion ($O_2^{\bullet-}$) and subsequently H_2O_2 and the reactive hydroxyl radical (HO^{\bullet}) as shown in Reaction 5.15-5.23 below (Valavanidis et al. 2009).





As shown in Reaction 5.22, tar can generate OH radicals, which abstract H from acetaldehyde to generate acetyl radicals. Due to their highly reactive and oxidizing nature, OH radicals have a fundamental influence on gas phase free radical generation.

5.4 Conclusion and Future Work

Computational simulations using Matlab and the Master Chemical Mechanism demonstrated that although acetyl radical generation from reactions of CH_3CHO and NO/NO_2 and subsequent chain reactions is feasible, their concentrations in gas phase tobacco smoke cannot account for the amount of acetyl radical detected. However, the addition of isoprene promotes the generation of sufficient hydroxyl and peroxy radicals to accelerate radical generation and accounts for the full amount of acetyl radical detected experimentally.

Simulations also showed that trapping techniques are very sensitive to the relative rates of reaction with the trapping species, 3AP, and oxygen; thus small variations in their concentrations can dramatically change the amount of radical trapped. Caution is advised in comparing numbers of radicals determined from different experiments.

The application of atmospheric models such as MCM to tobacco smoke has been demonstrated. An understanding of the evolution of reactive species within smoke is essential for identifying the origins and fates of toxic components of both mainstream and sidestream smoke.

Future work is needed to understand the components in TPM and mechanisms that may be responsible for the radical formation and stabilization. Aging effect and solubility experiments on tobacco tar are suggested to further understand its mechanism on gas phase radical initiations. It is suspected that transition metal ions play an important role in redox reactions on TPM (Valavanidis et al. 2008).

This observation contributes to the overall understanding of the free radical

generation in gas phase smoke and may have implications on the particle reaction in cigarette smoke. At the same time, we need to point out that although a series of studies have been carried out by different groups for many years, our understanding of this subject is far from complete, and more effort and dedication are needed to unravel complex dynamic interactions among a myriad of smoke components in the future work.

5.5 References

Atkinson R, Baulch DL, Cox RA, Crowley JN, Hampson RF, Hynes RG, et al. 2004. Evaluated kinetic and photochemical data for atmospheric chemistry: Volume I - gas phase reactions of O-x, HOx, NOx and SOx species. *Atmos Chem Phys* 4: 1461-1738.

Atkinson R, Baulch DL, Cox RA, Hampson RF, Kerr JA, Rossi MJ, et al. 1997. Evaluated kinetic, photochemical and heterogeneous data for atmospheric chemistry .5. IUPAC Subcommittee on Gas Kinetic Data Evaluation for Atmospheric Chemistry. *J Phys Chem Ref Data* 26(3): 521-1011.

Atkinson RB, D.L.; Cox, R.A.; Crowley, J.N.; Hampson, R.F, Jr.; Kerr, J.A.; Rossi, M.J.; Troe, J. 2001. Summary of Evaluated Kinetic and Photochemical Data for Atmospheric Chemistry.

Baren RE, Parrish ME, Shafer KH, Harward CN, Quan S, Nelson DD, et al. 2004. Quad quantum cascade laser spectrometer with dual gas cells for the simultaneous analysis of mainstream and sidestream cigarette smoke. *Spectrochim Acta A* 60(14): 3437-3447.

Bartalis J, Chan WG, Wooten JB. 2007. A new look at radicals in cigarette smoke. *Anal Chem* 79(13): 5103-5106.

Bartalis J, Zhao YL, Flora JW, Paine JB, Wooten JB. 2009. Carbon-centered radicals in cigarette smoke: acyl and alkylaminocarbonyl radicals. *Anal Chem* 81(2): 631-641.

Borgerding M, Klus H. 2005. Analysis of complex mixtures - Cigarette smoke. *Experimental and Toxicologic Pathology* 57: 43-73.

Brook D. 2005. Reaction object from online Matlab user library.

Cueto R, Pryor WA. 1994. Cigarette-Smoke Chemistry - Conversion of Nitric-Oxide to Nitrogen-Dioxide and Reactions of Nitrogen-Oxides with Other Smoke Components as Studied by Fourier-Transform Infrared-Spectroscopy. *Vib Spectrosc* 7(1): 97-111.

ERI. 2010. Eigenvector Research Incorporated Dataset. Available: <http://www.eigenvector.com/> [accessed 6 Nov. 2010].

Flicker TM, Green SA. 1998. Detection and separation of gas-phase carbon-centered radicals from cigarette smoke and diesel exhaust. *Analytical Chemistry* 70(9): 2008-2012.

Flicker TM, Green SA. 2001. Comparison of gas-phase free-radical populations in tobacco smoke and model systems by HPLC. *Environ Health Perspect* 109(8): 765-771.

Gerardi AR, Coleman WM. 2010. New Methodologies for Qualitative and Semi-Quantitative Determination of Carbon-Centered Free Radicals in Cigarette Smoke Using Liquid Chromatography-Tandem Mass Spectrometry and Gas Chromatography-Mass Selective Detection. *Beiträge zur Tabakforschung International/Contributions to Tobacco Research* 24(No.2): 58-71.

Hoffmann D, Hoffmann I, El-Bayoumy K. 2001. The less harmful cigarette: a controversial issue. a tribute to Ernst L. Wynder. *Chem Res Toxicol* 14(7): 767-790.

Jaffe S, Wan E. 1974. Thermal and Photochemical Reactions of NO₂ with Butyraldehyde in Gas-Phase. *Environmental Science & Technology* 8(12): 1024-1025.

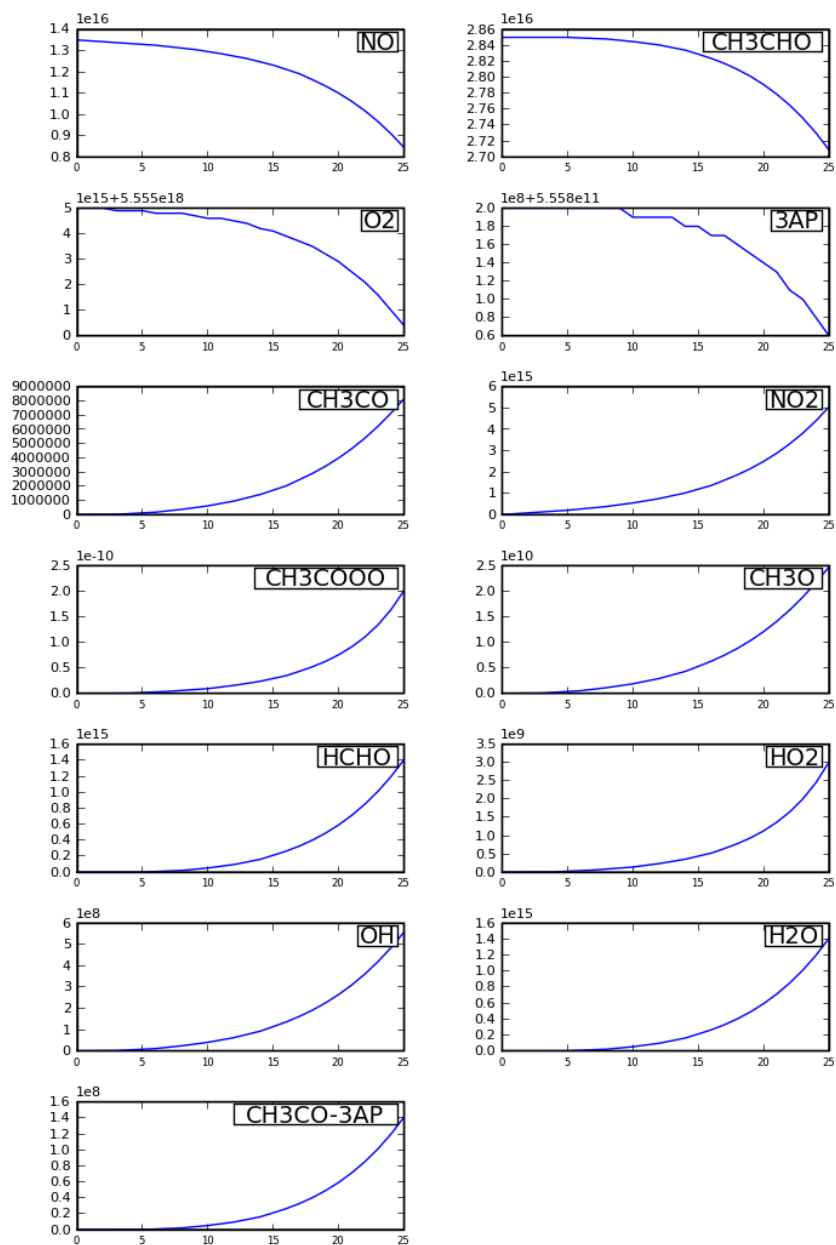
- Jenkin ME, Saunders SM, Pilling MJ. 1997. The tropospheric degradation of volatile organic compounds: A protocol for mechanism development. *Atmos Environ* 31: 81-104.
- Lin P, Yu JZ. 2011. Generation of Reactive Oxygen Species Mediated by Humic-like Substances in Atmospheric Aerosols. *Environmental science & technology*.
- Orlando JJ, Tyndall GS, Wallington TJ. 2003. The atmospheric chemistry of alkoxy radicals. *Chem Rev* 103(12): 4657-4690.
- Pandis JHSSN. 1998. *Atmospheric Chemistry and Physics*.
- Paulson SE, Flagan RC, Seinfeld JH. 1992. Atmospheric Photooxidation of Isoprene .1. The Hydroxyl Radical and Ground-State Atomic Oxygen Reactions. *Int J Chem Kinet* 24(1): 79-101.
- Pryor WA, Hales BJ, Premovic PI, Church DF. 1983a. The radicals in cigarette tar: their nature and suggested physiological implications. *Science* 220(4595): 425-427.
- Pryor WA, Prier DG, Church DF. 1983b. Electron-Spin Resonance Study of Mainstream and Sidestream Cigarette-Smoke - Nature of the Free-Radicals in Gas-Phase Smoke and in Cigarette Tar. *Environ Health Persp* 47(Jan): 345-355.
- Pryor WA, Stone K, Stone K, Cross CE, Machlin L, Packer L. 1993. Oxidants in Cigarette-Smoke - Radicals, Hydrogen-Peroxide, Peroxynitrate, and Peroxynitrite. *Ann Ny Acad Sci* 686: 12-28.
- Saunders SM, Jenkin ME, Derwent RG, Pilling MJ. 1997. World Wide Web site of a Master Chemical Mechanism (MCM) for use in tropospheric chemistry models. *Atmos Environ* 31(8): 1249-1249.

Saunders SM, Jenkin ME, Derwent RG, Pilling MJ. 2003. Protocol for the development of the Master Chemical Mechanism, MCM v3 (Part A): tropospheric degradation of non-aromatic volatile organic compounds. *Atmos Chem Phys* 3: 161-180.

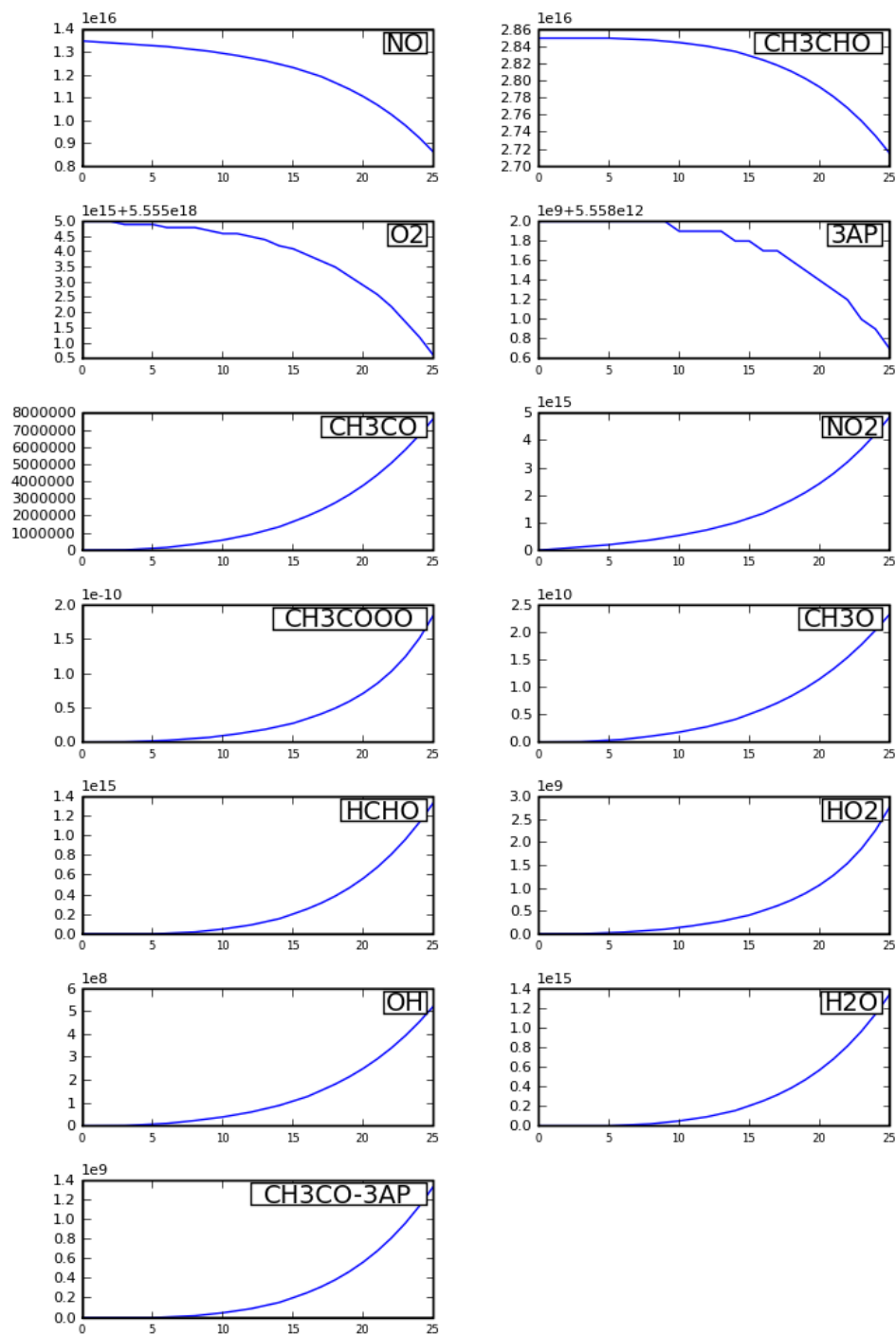
Shorter JH, Nelson DD, Zahniser MS, Parrish ME, Crawford DR, Gee DL. 2006. Measurement of nitrogen dioxide in cigarette smoke using quantum cascade tunable infrared laser differential absorption spectroscopy (TILDAS). *Spectrochim Acta A* 63(5): 994-1001.

Wooten JB. 2011. Gas-phase Radicals in Cigarette Smoke: A Re-evaluation of the Steady-State Model and the Cambridge Filter Pad. *Organic Chemistry*.

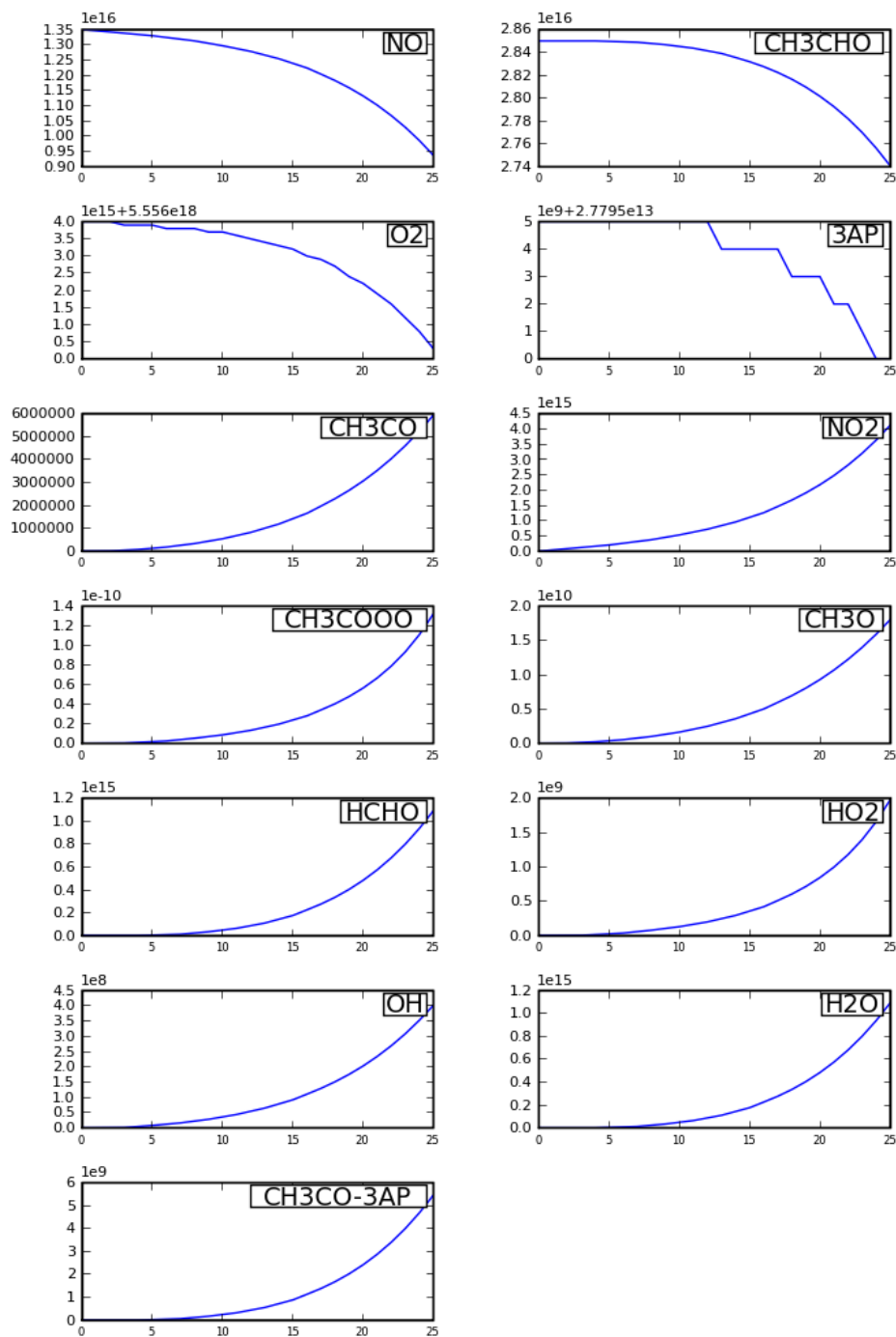
Appendix



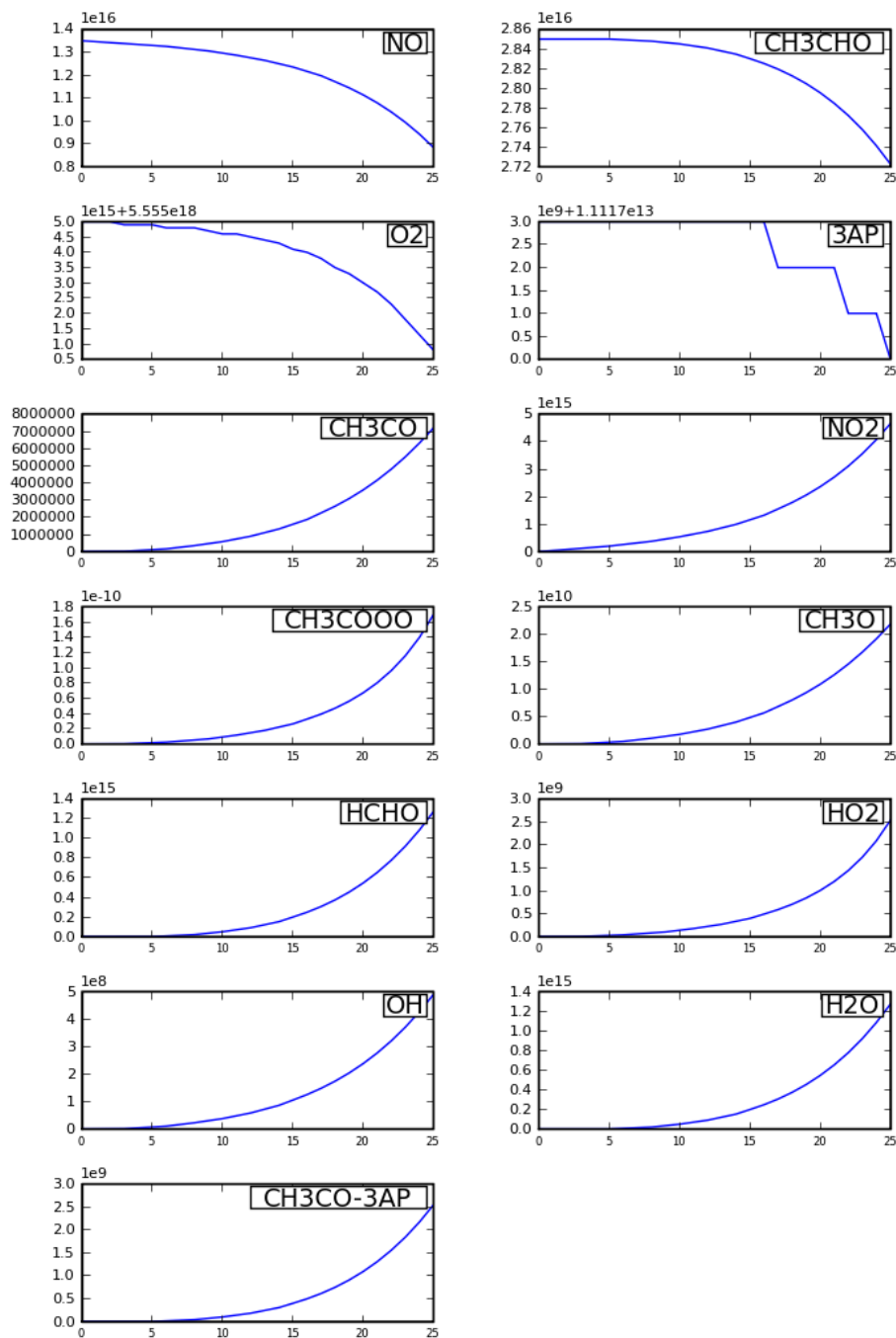
Appendix 1. MCM simulation by NO/air/CH₃CHO model on the generation of CH₃C(O)-3AP from the 3R4F Kentucky Reference cigarette smoke at 25 s when $k_{3AP}[3AP]/k_{O_2}[O_2]$ equals to 10^{-7} . Concentrations are in molecules/cm³.



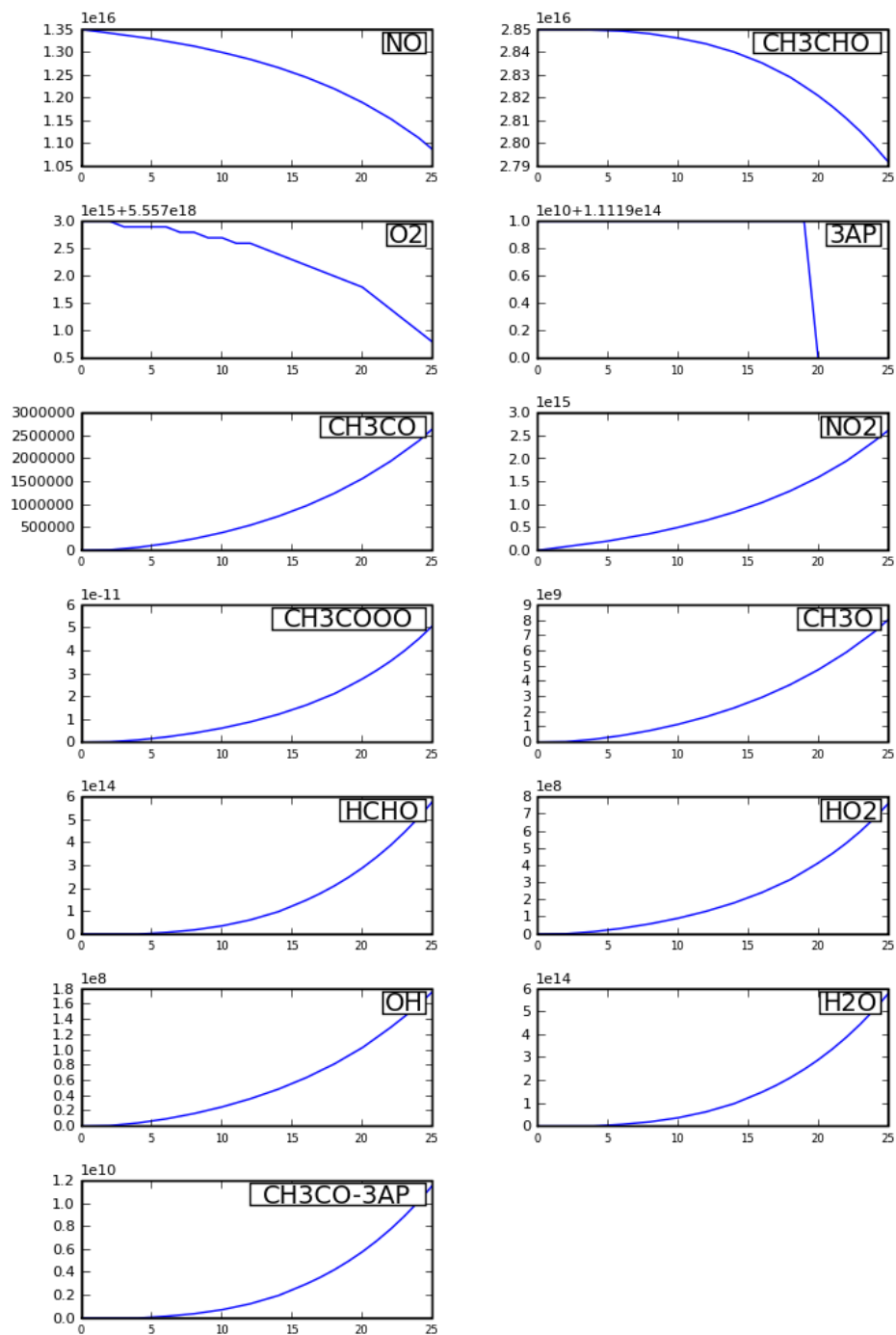
Appendix 2. MCM simulation by NO/air/CH₃CHO model on the generation of CH₃C(O)-3AP from the 3R4F Kentucky Reference cigarette smoke at 25 s when $k_{3AP}[3AP]/k_{O_2}[O_2]$ equals to 10^{-6} . Concentrations are in molecules/cm³.



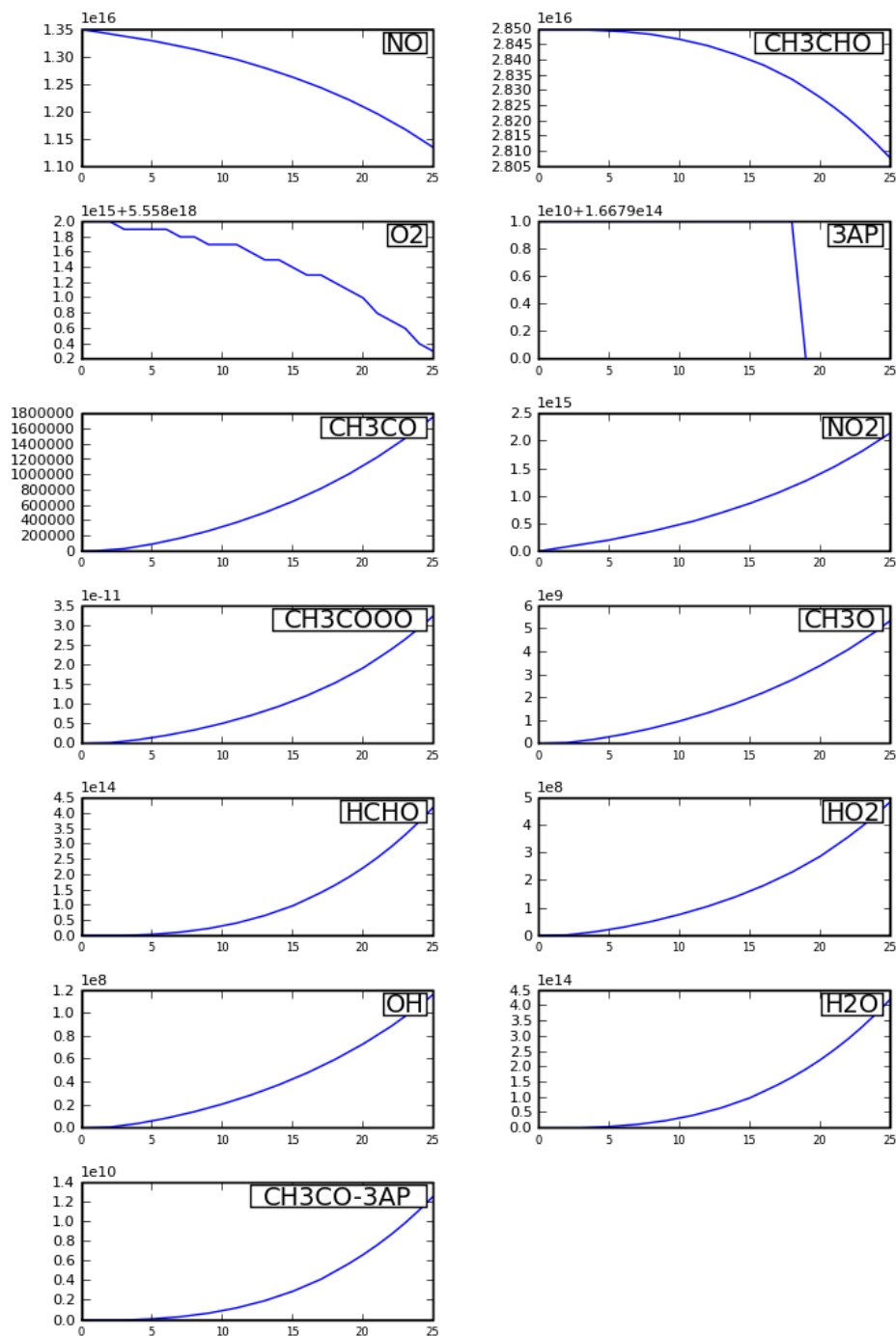
Appendix 3. MCM simulation by NO/air/CH₃CHO model on the generation of CH₃C(O)-3AP from the 3R4F Kentucky Reference cigarette smoke at 25 s when $k_{3AP}[3AP]/k_{O_2}[O_2]$ equals to 5×10^{-6} . Concentrations are in molecules/cm³.



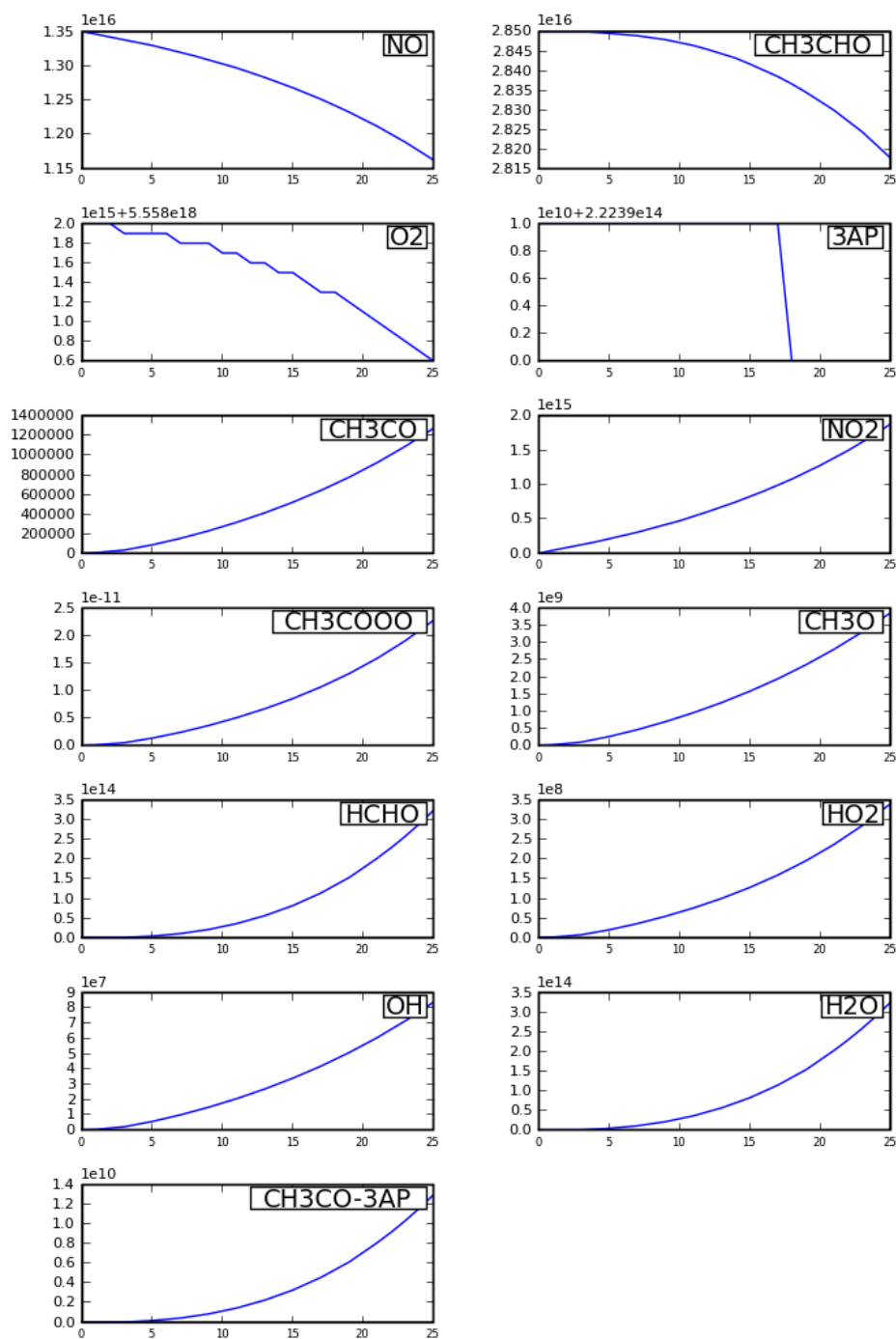
Appendix 4. MCM simulation by NO/air/CH₃CHO model on the generation of CH₃C(O)-3AP from the 3R4F Kentucky Reference cigarette smoke at 25 s when $k_{3AP}[3AP]/k_{O_2}[O_2]$ equals to 2×10^{-6} . Concentrations are in molecules/cm³.



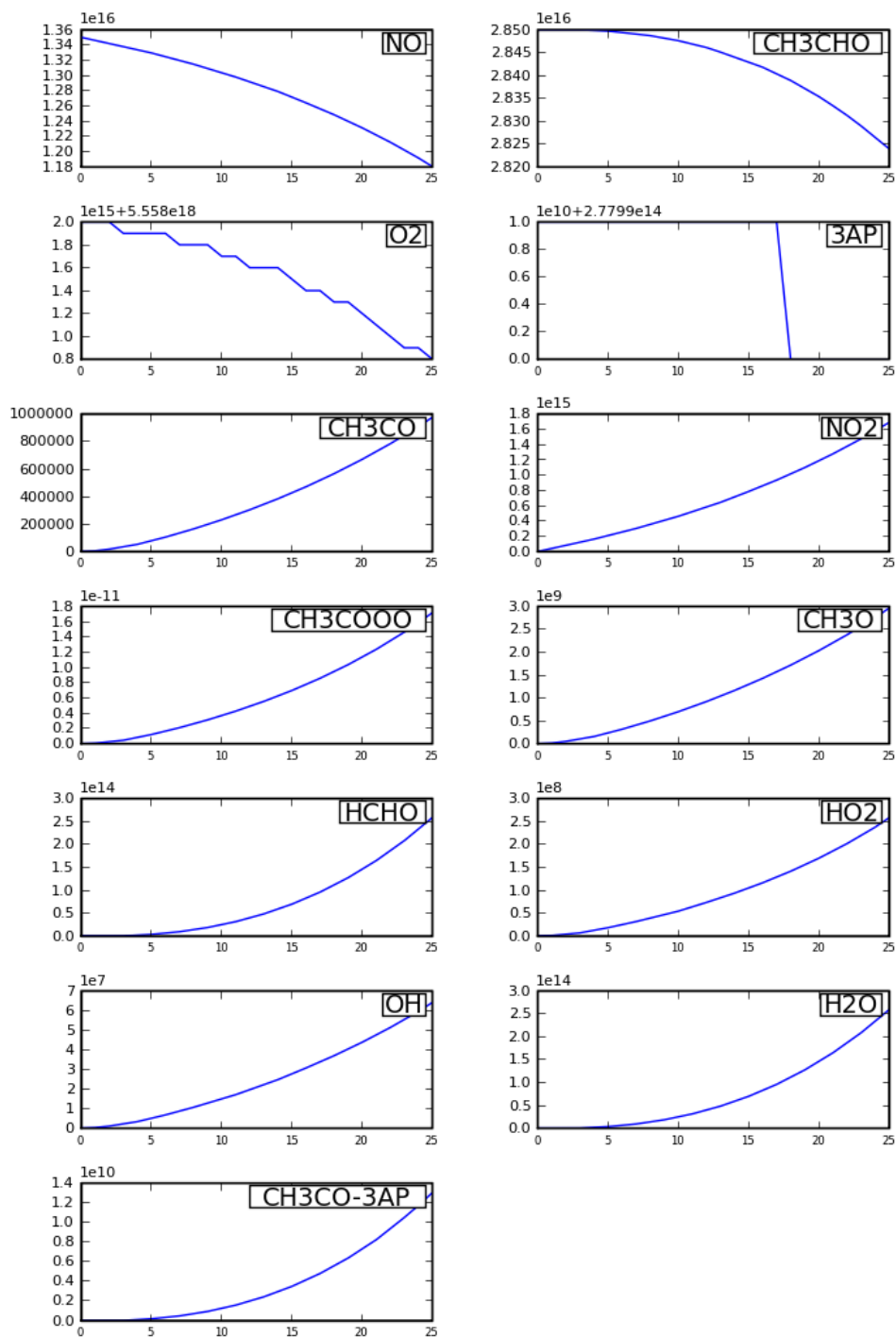
Appendix 5. MCM simulation by NO/air/CH₃CHO model on the generation of CH₃C(O)-3AP from the 3R4F Kentucky Reference cigarette smoke at 25 s when $k_{3AP}[3AP]/k_{O_2}[O_2]$ equals to 2×10^{-5} . Concentrations are in molecules/cm³.



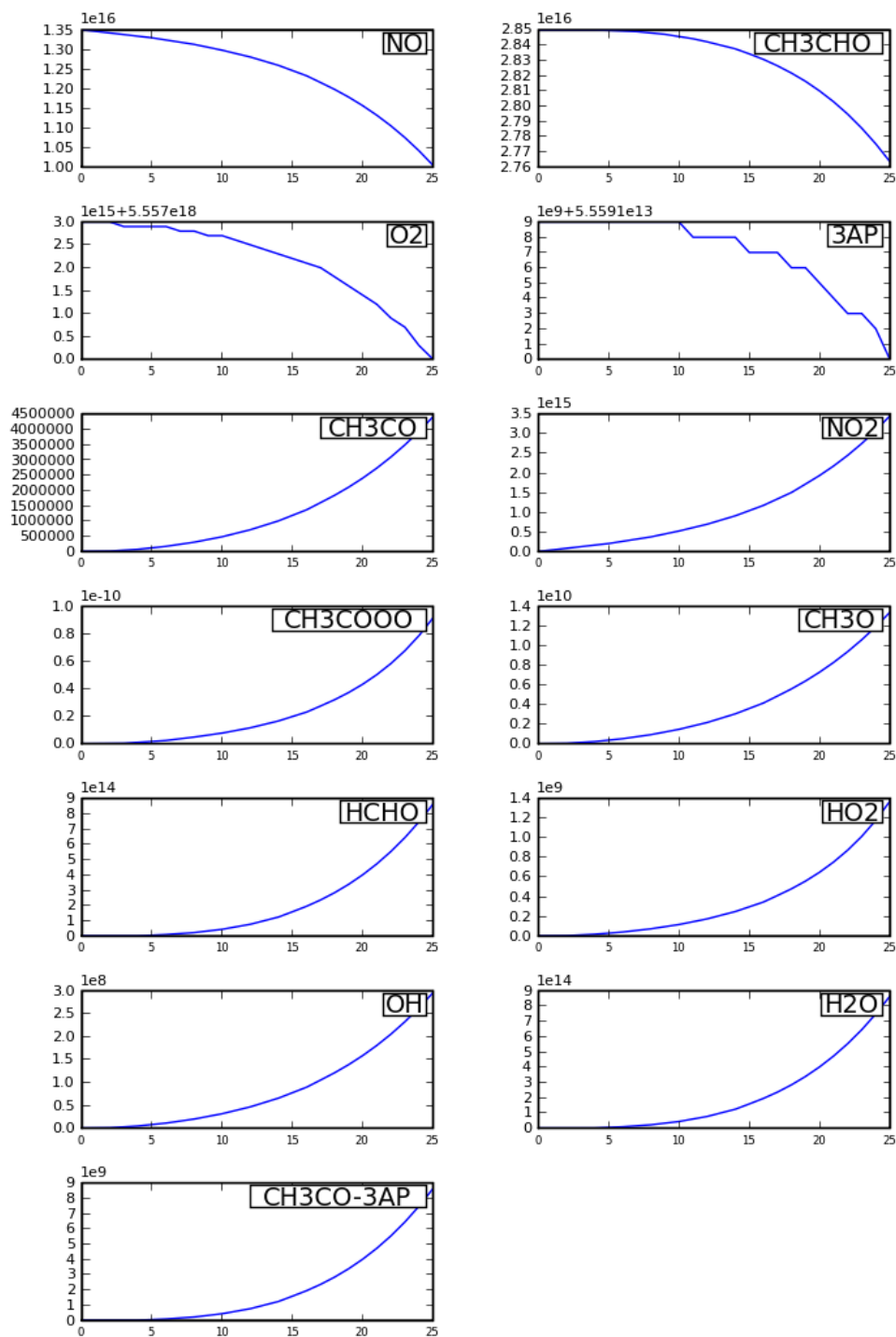
Appendix 6. MCM simulation by NO/air/CH₃CHO model on the generation of CH₃C(O)-3AP from the 3R4F Kentucky Reference cigarette smoke at 25 s when $k_{3AP}[3AP]/k_{O_2}[O_2]$ equals to 3×10^{-5} . Concentrations are in molecules/cm³.



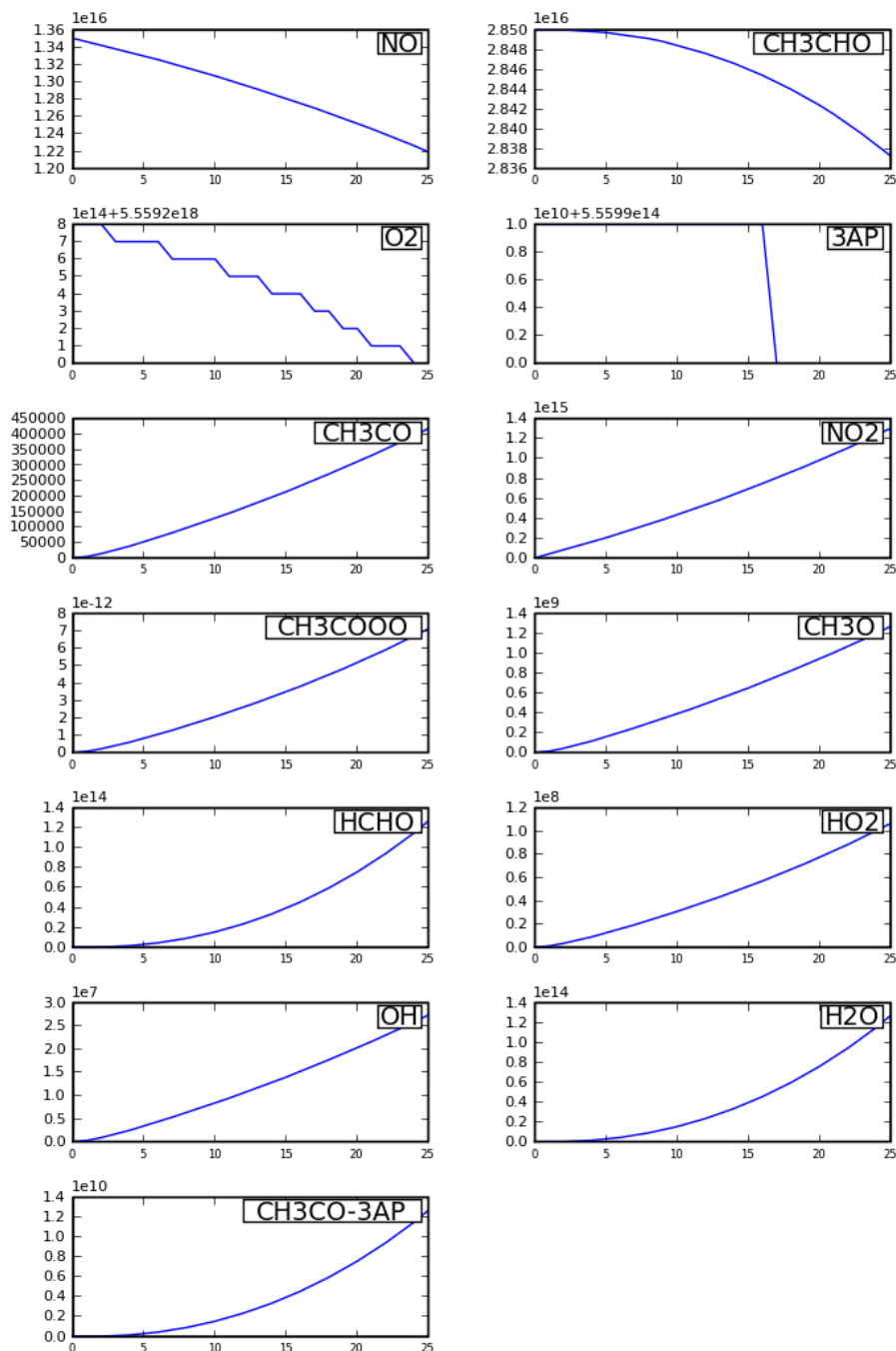
Appendix 7. MCM simulation by NO/air/CH₃CHO model on the generation of CH₃C(O)-3AP from the 3R4F Kentucky Reference cigarette smoke at 25 s when $k_{3AP}[3AP]/k_{O_2}[O_2]$ equals to 4×10^{-5} . Concentrations are in molecules/cm³.



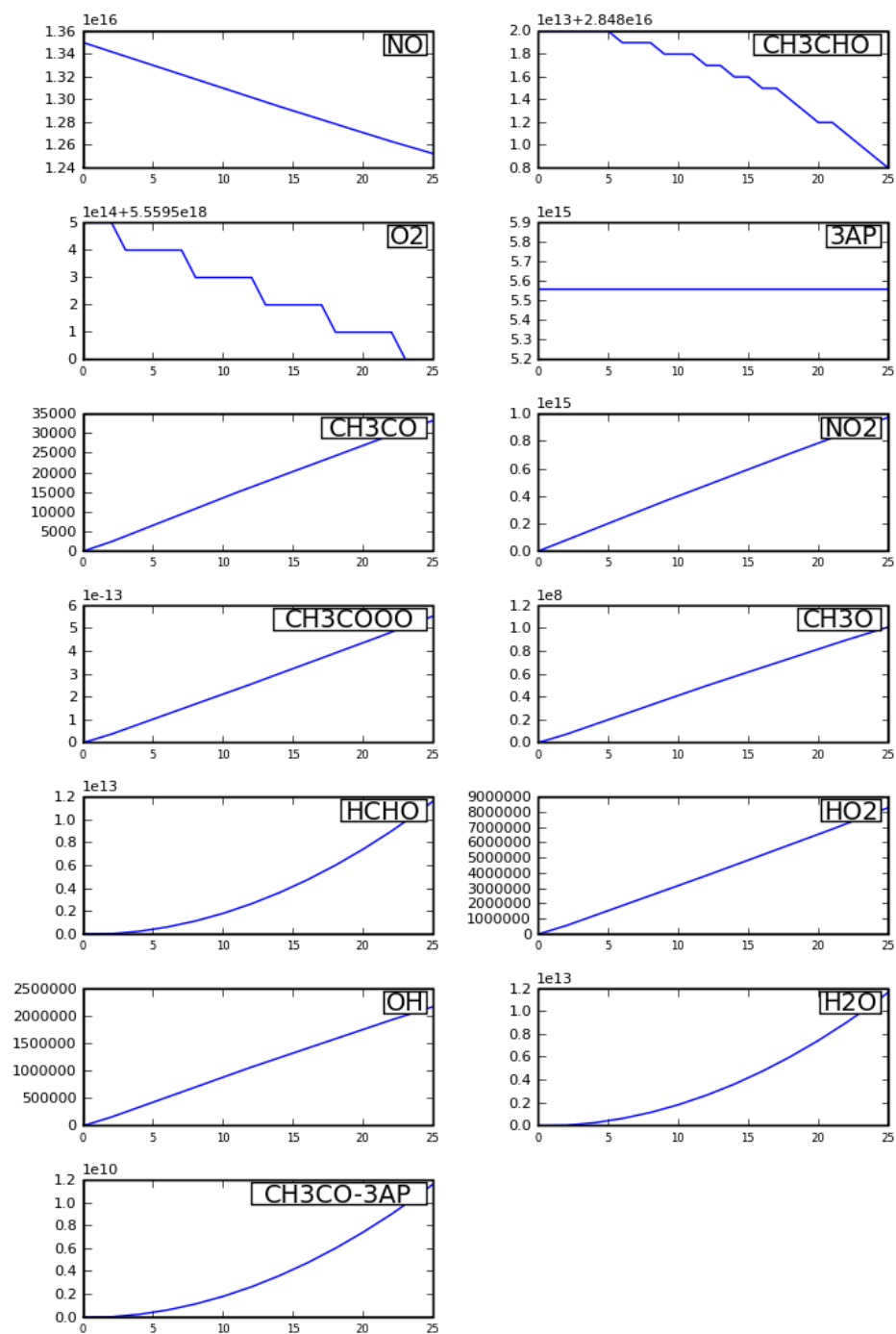
Appendix 8. MCM simulation by NO/air/CH₃CHO model on the generation of CH₃C(O)-3AP from the 3R4F Kentucky Reference cigarette smoke at 25 s when $k_{3AP}[3AP]/k_{O_2}[O_2]$ equals to 5×10^{-5} . Concentrations are in molecules/cm³.



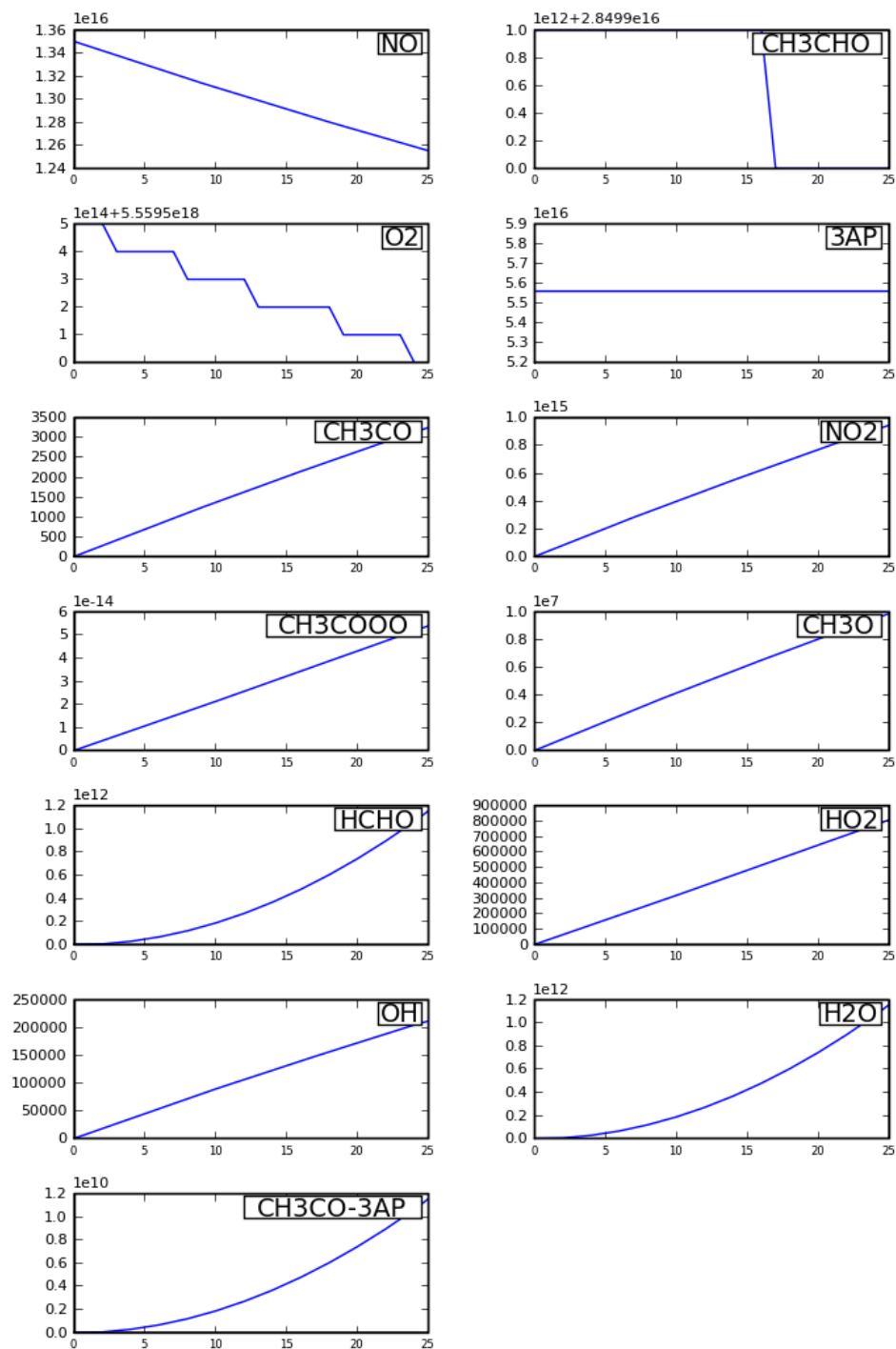
Appendix 9. MCM simulation by NO/air/CH₃CHO model on the generation of CH₃C(O)-3AP from the 3R4F Kentucky Reference cigarette smoke at 25 s when $k_{3AP}[3AP]/k_{O_2}[O_2]$ equals to 1×10^{-5} . Concentrations are in molecules/cm³.



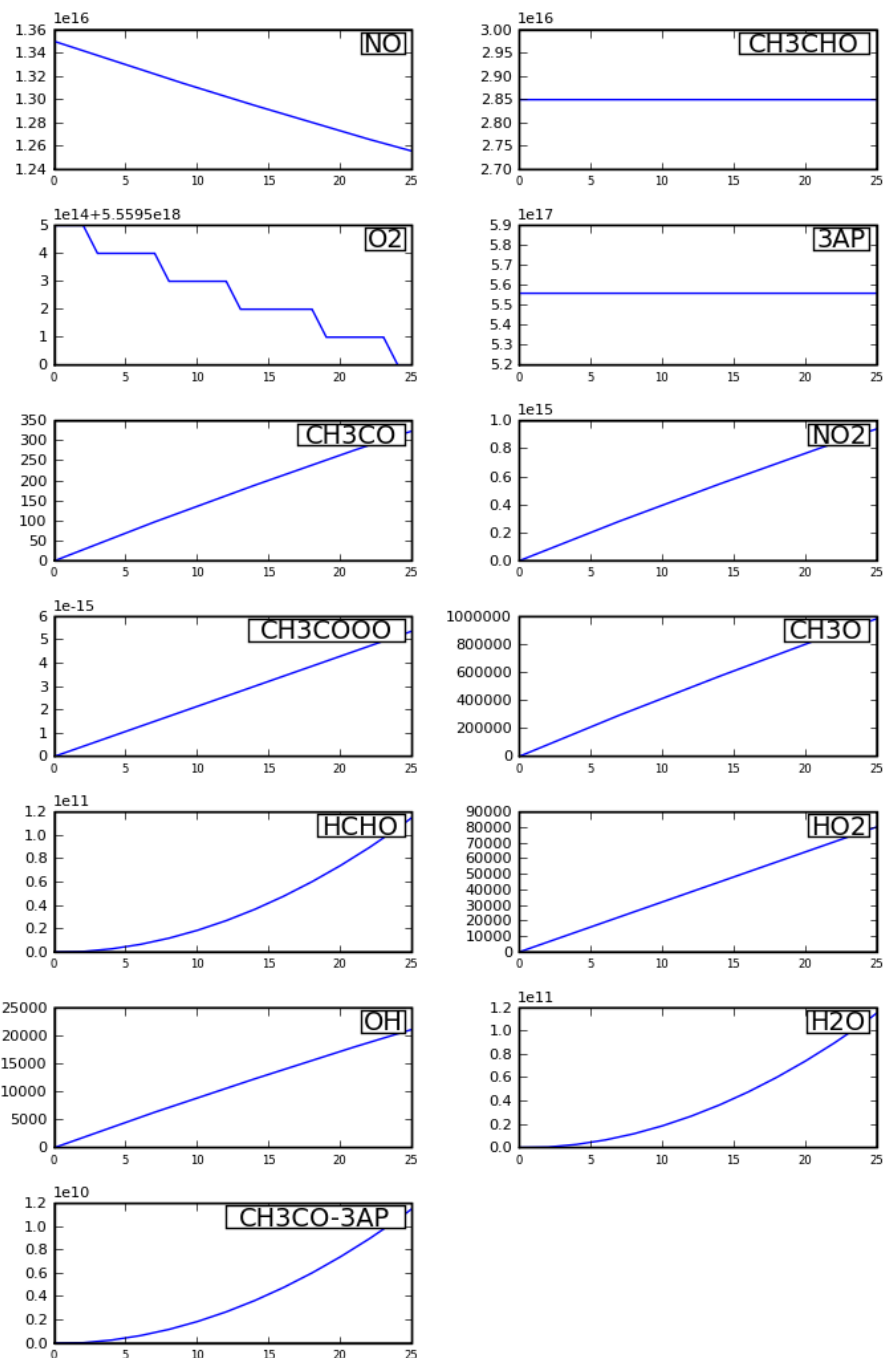
Appendix 10. MCM simulation by NO/air/CH₃CHO model on the generation of CH₃C (O)-3AP from the 3R4F Kentucky Reference cigarette smoke at 25 s when $k_{3AP}[3AP]/k_{O_2}[O_2]$ equals to 1×10^{-4} . Concentrations are in molecules/cm³.



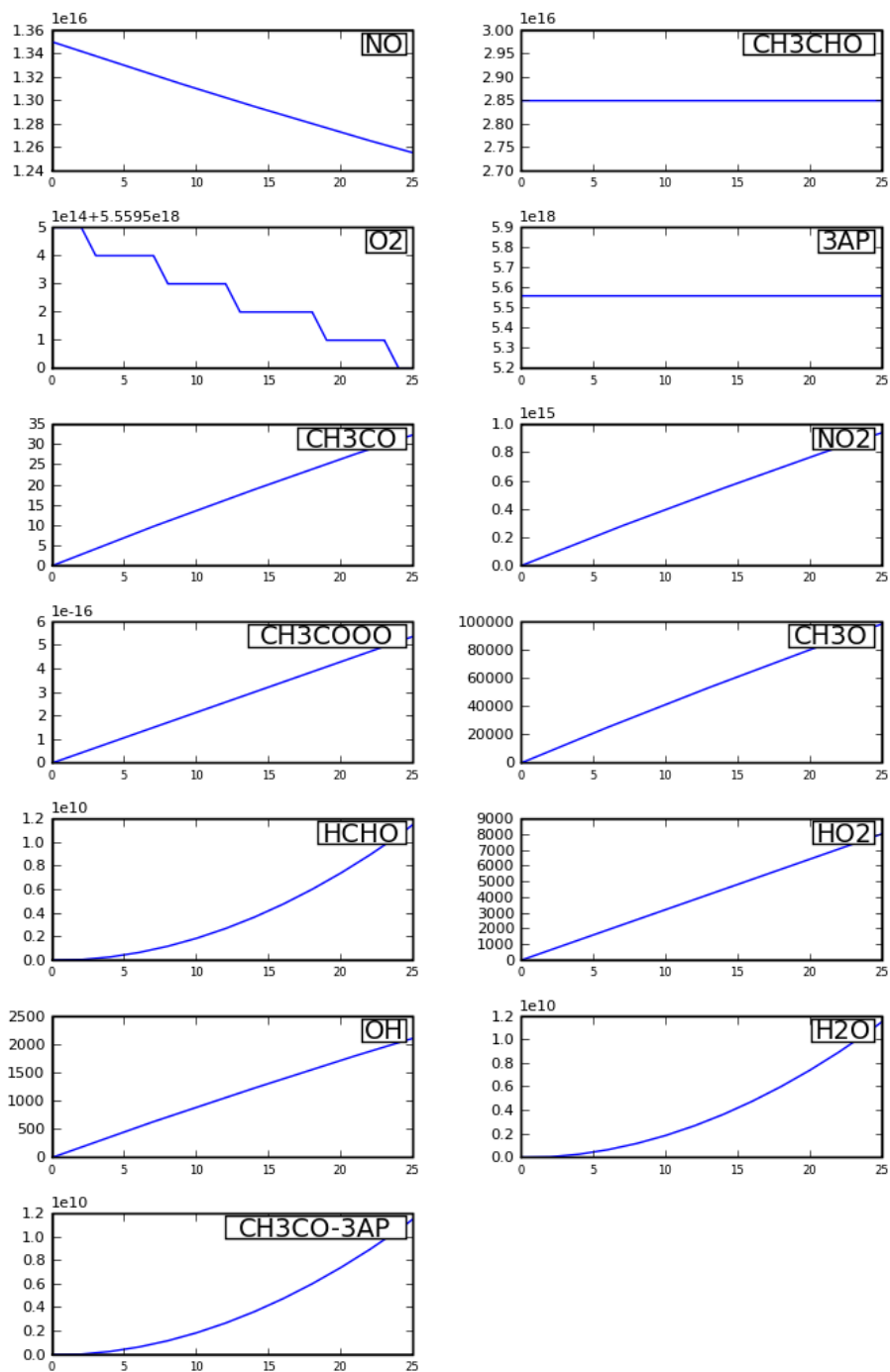
Appendix 11. MCM simulation by NO/air/CH₃CHO model on the generation of CH₃C (O)-3AP from the 3R4F Kentucky Reference cigarette smoke at 25 s when $k_{3AP}[3AP]/k_{O_2}[O_2]$ equals to 1×10^{-3} . Concentrations are in molecules/cm³.



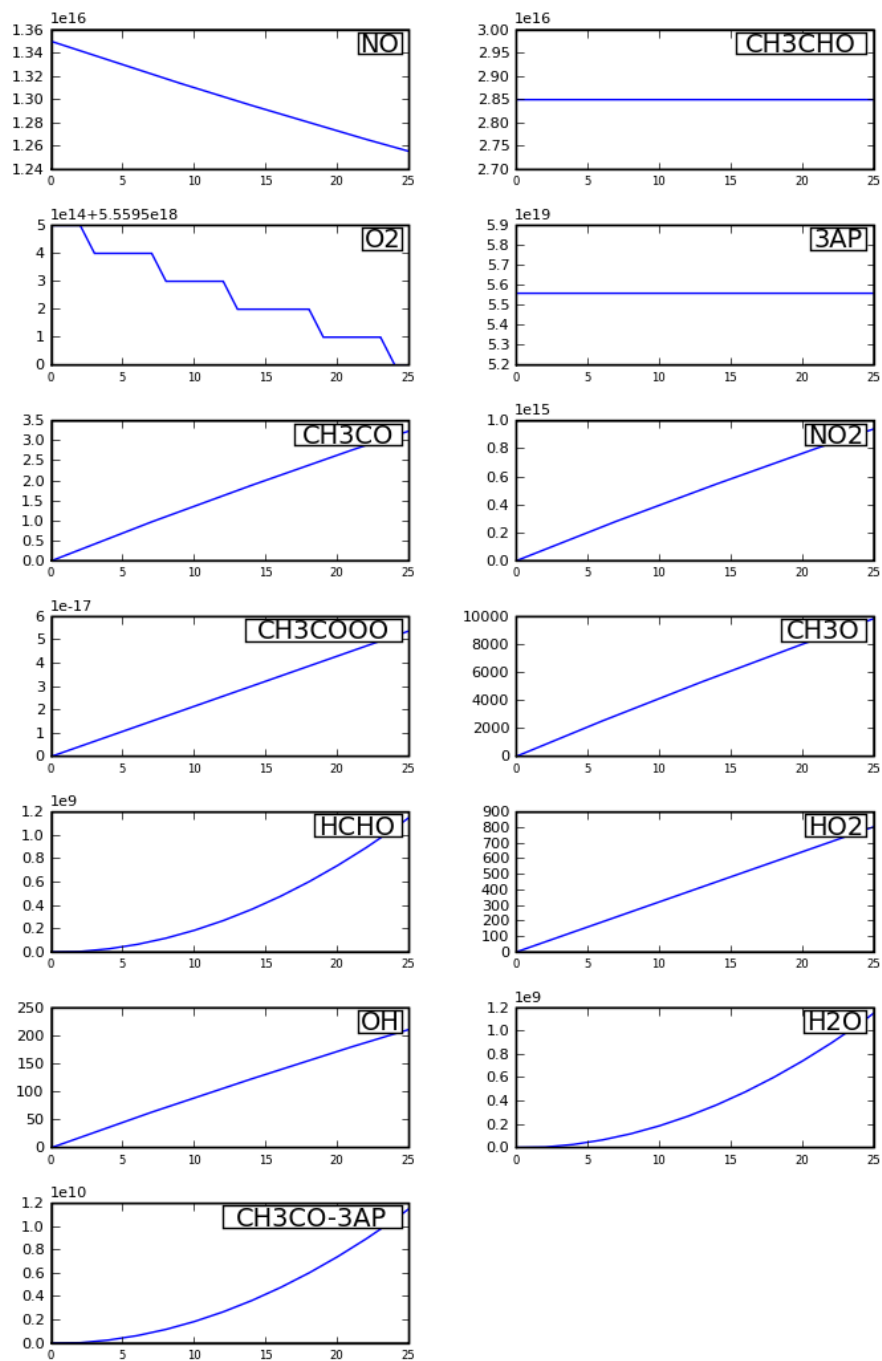
Appendix 12. MCM simulation by NO/air/CH₃CHO model on the generation of CH₃C (O)-3AP from the 3R4F Kentucky Reference cigarette smoke at 25 s when $k_{3AP}[3AP]/k_{O_2}[O_2]$ equals to 1×10^{-2} . Concentrations are in molecules/cm³.



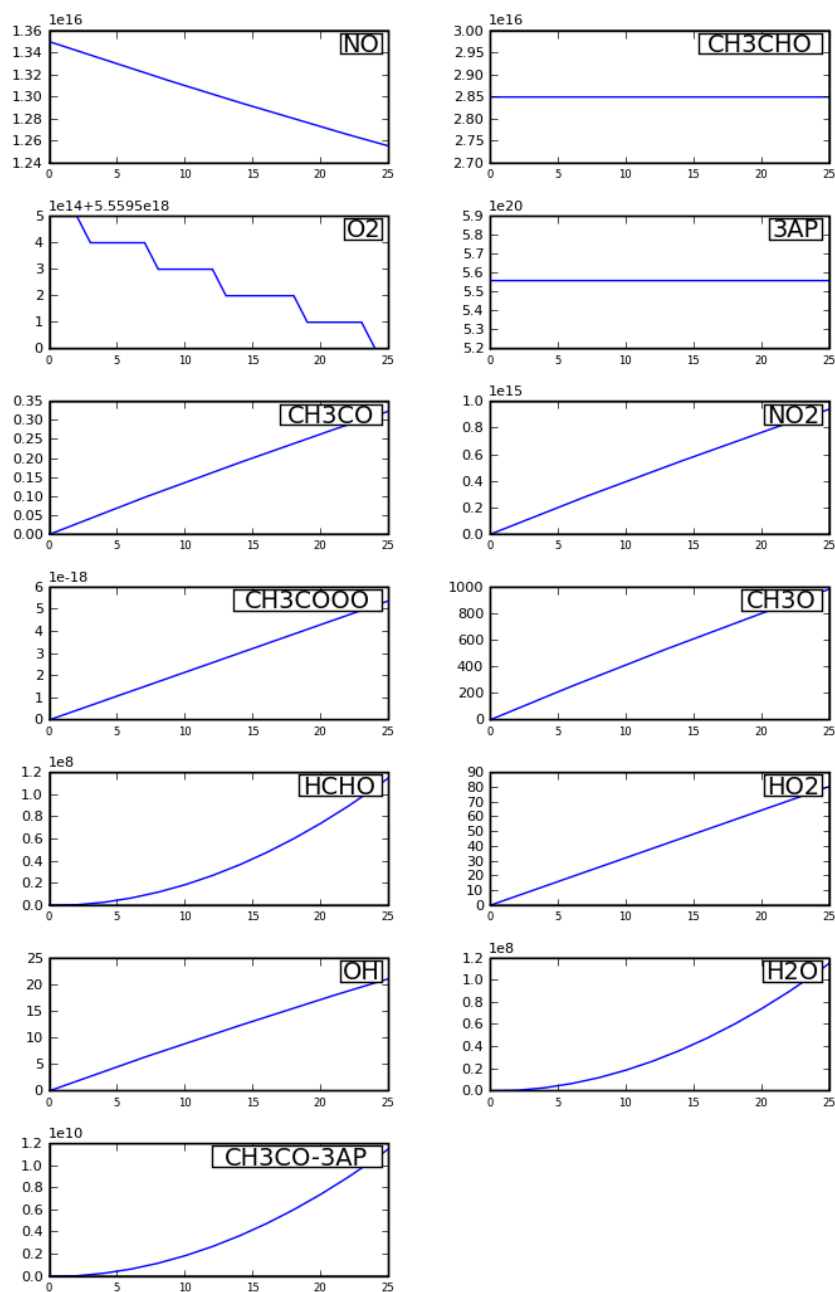
Appendix 13. MCM simulation by NO/air/CH₃CHO model on the generation of CH₃C (O)-3AP from the 3R4F Kentucky Reference cigarette smoke at 25 s when $k_{3AP}[3AP]/k_{O_2}[O_2]$ equals to 0.1. Concentrations are in molecules/cm³.



Appendix 14. MCM simulation by NO/air/CH₃CHO model on the generation of CH₃C (O)-3AP from the 3R4F Kentucky Reference cigarette smoke at 25 s when $k_{3AP}[3AP]/k_{O_2}[O_2]$ equals to 1. Concentrations are in molecules/cm³.



Appendix 15. MCM simulation by NO/air/CH₃CHO model on the generation of CH₃C (O)-3AP from the 3R4F Kentucky Reference cigarette smoke at 25 s when $k_{3AP}[3AP]/k_{O_2}[O_2]$ equals to 10. Concentrations are in molecules/cm³.



Appendix 16. MCM simulation by NO/air/CH₃CHO model on the generation of CH₃C (O)-3AP from the 3R4F Kentucky Reference cigarette smoke at 25 s when $k_{3AP}[3AP]/k_{O_2}[O_2]$ equals to 100. Concentrations are in molecules/cm³.

Coding sample for Figure 5.3.

```
reag1={'NO', 'O2', 'NO2'};

stoich1 = [-2 -1 2];

rate1 = [2e-38];

equil1= [inf];

rxn1=reaction(reag1, stoich1, rate1, equil1);

reag2={'NO2', 'CH3CHO', 'CH3CO', 'HNO2'};

stoich2 = [-1 -1 1 1];

rate2 = [3.36e-23];

equil2= [inf];

rxn2=reaction(reag2, stoich2, rate2, equil2);

rxn1_2=vertcat(rxn1, rxn2);

times = [0: 1:8000];

C0= [ 2.44e19 0 0 2.47e16 0 5.65e18];

data1_2 = concentration(rxn1_2, times, C0);

data1_2.data;

A=data1_2.data;

A(:,2);

A(:,5);

A(:,4);

[CH3CHO]=A(:,1)/6.02e11

[CH3CO]=A(:,2)/6.02e11

[NO2]=A(:,5)/6.02e11
```

```

[NO]=A(:,4)/6.02e11
plot(times,[CH3CO],times,[NO2], times,[NO],'linewidth',2);
legend('CH_3CO^.', 'NO_2', 'NO');
title({'Simulation of Experimental Gas Mixture'});
xlabel('Time (s)');
ylabel('concentration (nmol/L)');

```

Coding Sample For Figure 5.4.

```
reag1={'NO', 'O2', 'NO2'};
stoich1 = [-2 -1 2];
rate1 = [2e-38]; equil1= [inf];
rxn1=reaction(reag1, stoich1, rate1, equil1);
reag2={'NO2', 'CH3CHO', 'CH3CO', 'HNO2'};
stoich2 = [-1 -1 1 1];
rate2 = [3.36e-23];
equil2= [inf];
rxn2=reaction(reag2, stoich2, rate2, equil2);
rxn1_2=vertcat(rxn1, rxn2)
times = [0: 1:25];
C0= [2.85e16 0 0 1.35e16 0 5.65e18];
data1_2= concentration(rxn1_2, times, C0);
data1_2.data;
A=data1_2.data;
[CH3CO]=A(:,2)/6.02e11
[NO]=A(:,4)/6.02e11;
[NO2]=A(:,5)/6.02e11;
ylabel{1}='concentration(nmol/L)'
ylabel{2}='concentration(nmol/L)'
ylabel{3}='concentration(nmol/L)'
[ax,hlines] = plotyyy(times,[CH3CO],times,[NO2],times,[NO],ylabel);
```

```
set(hlines(1),'linewidth',2);  
set(hlines(2),'linewidth',2);  
set(hlines(3),'linewidth',2);  
legend(hlines, 'CH_3CO-3AP','NO_2','NO')  
title('Simulation of Experimental 3R4F Cigarette Smoke by the Matlab Program');  
xlabel('Time (s)');  
ylabel('concentrationmol/L');
```